DESIGN CONSIDERATIONS

OF

A PLANAR CROSS CHANNEL OPTICAL DEMULTIPLEXER

by

Jian-yao Chen

Department of Electrical Engineering
McGill University
Montreal, Quebec
December, 1991

A Thesis submitted to the Faculty of Graduate Studies and Research in partial fulfillment of the requirements for the degree of Master of Engineering

ABSTRACT

In this thesis, several simple and accurate techniques applicable to the analyses of diffused slab and channel optical waveguide are discussed. A zero-gap coupler type single-mode optical wavelength division demultiplexer by K^+-ion exchange in glass is proposed. The detailed device property studies based upon our own characterization results on soda-lime glass materials are carried out by the effective index method (EIM) and beam propagation method (BPM). To overcome the fabrication difficulties under the present state of art, some improved device structures are also discussed.

RESUME

Cette thèse contient d'abord la description de plusieurs methodes simples permettant l'analyse de guides d'ondes optiques aux frontières diffuses. Une structure de coupleur monomode sans espacement obtenue par échange d'ions potassium-positifs dans le verre est ensuite proposee comme démultiplexeur à déphasage. L'étude des proprietes de ce demultiplexeur, basée sur nos propres données de characterisation des verres soda-calcique, est entreprise à l'aide des methodes d'index effectif et de propagation par rayon (BPM). Finalement, quelques améliorations à la structure proposée sont discutées dans le but de réduire les difficultés de fabrication.

ACKNOWLEDGEMENTS

I would like to express my gratitude to my supervisor, Professor Gar Lam Yip, for his patience, guidance, encouragements and much personal assistance during my studies.

I am also especially grateful to Dr. Kiyoshi Kishioka, now with Osaka Electro Communication University, Japan, for his guidance, encouragement and teaching me the ion-exchange and device fabrication techniques experimentally.

I would like to thank Mr. K. Fraser for giving me access to the micro-VAX computers in the Undergraduate Computer Laboratory, which were used to do the horrendous amount of 'number crunching' required for the BPM simulations.

I must also thank my fellow students for their encouragement and fruitful discussions. In particular, the contributions from Michael A. Sekerka-Bajbus, Peter C. Noutsios, John Nikolopoulos, Feng Xiang, Dennis Kan and Phillippe G Allard are gratefully acknowledged.

Both the technical and secretarial staff provided me with their always friendly services and helped solve the ever occurring administrative problems.

This research was supported financially by a Chinese government scholarship for one year (1988-9), a NSERC operating grant, a tuition waive from the Graduate Faculty at McGill and two summer research stipend from the Department of Electrical Engineering (1990, 1991).

CONTENTS

CHAPTER I

INTRODUCTION

I-1. Overview of the Integrated Optics

The term "integrated optics" (IO) was first coined by Stewart E. Miller [1] in 1969 to describe the optics of miniaturized optical circuits in which light signals are generated, guided and processed by related effects before finally being detected. The feasibility of this technology is due to the fact that light can be guided in a thin film. Since the invention of optical fiber during 1960's, to achieve the full promise of optical fiber communication link, many discrete functional components, such as laser diodes, photodiodes, couplers, modulators, switches as well as transmitter and receiver electronics have been developed [2]. Currently, increasing efforts are also being applied in achieving a synthesis of electronic and optical components into an integrated optoelectronics format which is expected to provide a wide range of systems with miniaturized, high speed, broad-band, reliable and cost-effective components for telecommunication data processing, optical computing and other applications in the near and distant future [3].

There are many types of materials currently studied in integrated optical applications. e.g. glass, lithium niobate ($LiNbO_3$) and III-V semiconductors. Since the advantages of their compatibility with optical fibers, low cost, low propagation losses, and ease of their integration into the system, glass waveguides made by the ion-exchange technique are considered to be prime candidates for the passive integrated optical components [2]. By virtue of its high electro-optic coefficient, lithium niobate usually is the premier material for the integrated electrooptic components and the Ti indiffused waveguide fabrication technology for this type of substrates has been most extensively developed [4]. Many high performance modulators [5] and switches [6] have been envisaged and even commercialized. However, glass and lithium niobate are all passive materials so that lasers and detectors can not yet be fabricated on the same substrate By contrast, semiconductors can be used for constructing both the passive and active devices so that a monolithic integration in which all devices are made in a single substrate can be realized [3]. But the higher loss and low electro-optic coefficient make the semiconductor materials less effective for guiding and modulating purpose Great efforts have been made to improve the optical properties of semiconductors and an InP/GaInAsP rib waveguide with loss as low as $0.18dB/cm$ has been reported [7].

Since integrated optics is still a thin film technology, the implementation of the proposed devices requires almost the same thin-film processing techniques as used in the semiconductor technology. However, main differences arise in the materials and substrates used. Using glass as a substrate, ion-exchange is the most favorable technique used to form optical waveguides [8]. Sputtering, plasma etching or ion-beam milling are also applied to fabricate the ridge type waveguides [9] For the $LiNbO_3$ material, the most widely employed is the diffusion of titanium into $LiNbO_3$ [4]. Also, a proton exchange technique has been developed [9] In the cases of semiconductor materials like GaAs and InP, the waveguides are formed by methods like liquid phase epitaxy (LPE), metal organic chemical vapor deposition (MOCVD), and molecular beam epitaxy (MBE) or ion implantation [10]. Although the packing density of integrated optics is many times less than in microelectronics, the required pattern accuracy is sometimes considerably greater [11].

I-2. Wavelength-Division-Multiplexing Technology

The advantages of the optical fiber Wavelength Division

Multiplexing (WDM) communication systems are transmission capacity increase per fiber, system cost reduction, simultaneous transmission of signals modulated with different schemes, and service channel expandability after fiber installation. Therefore, it is a useful means of fully using the large bandwidth provided by low-loss optical fibers and expected to be broadly applicable to systems in various field of communications [12].

In WDM transmission systems, wavelength multiplexers and demultiplexers (MUX/DEMUX) are the essential components employed to combine and separate wavelengths carrying different information The realization of single-mode MUX/DEMUX's has been accomplished by using wavelength dispersive elements like optical interference filter, optical diffraction gratings, and wavelength selective coupling between two adjacent waveguides In Table I-1, typical performance characteristics of these classes of multi- /demultiplexers are listed [12].

The optical interference filter type MUX/DEMUX's have been experimentally demonstrated by using fiber-optics and microoptics, where GRIN-lenses [13] or ball lenses [14] have been implemented as beam collimators. These devices are considered to be of practical importance, if the transmission system does not require more than about six channels with a spacing in the order of *30nm*. A greater number of channels, e g , *N=20* [15], with a much narrower channel spacing, e g , *1.35nm* [16], can be multiplexed by grating components. Here, microoptic techniques using GRIN-lenses and guided wave approaches with gratings, waveguides, and photodetectors, integrated on one substrate, have been applied [15, 17] The wavelength-selective coupling has been utilized in all fiber [18] and integrated optic [19] directional couplers Due to the symmetry of the coupler, this type MUX/DEMUX device can have a periodic wavelength transmission curve [18] or exhibit a band-pass behavior [19-20] Besides, a Y-branch type structure behaving as pass filter either for the longer or the shorter wavelengths was proposed in the literature [21].

From the considered fabrication technologies, integrated optics offers the greatest potential of building compact multi/demultiplexers in a stable rugged structure with simplified assembly. Recently, to overcome the sensitivity of asymmetry to the individual waveguides of directional coupler, a new structure based on the wavelength dependence of the two-mode interference (TMI) has also been proposed and experimentally demonstrated [22]. This type of structure, as so called X-branch type single mode demultiplexer, is more compact and fabrication tolerant so that it provides a powerful alternative to directional coupler structure applied to various applications. Previously, most people only tried the configuration in the $LiNbO_3$ substrate material. For the sake of lower cost, a lower refractive index and simpler fabrication techniques, it is also beneficial to apply the same configuration by ion-exchange technique on soda-lime glass substrates which is also the main purpose of this thesis work.

I-3. Chapter Description

In the following chapters, we first discuss some analytical techniques applied in analyzing the diffused slab and channel optical waveguides in Chapter II, which is prepared for further integrated optical device design applications. Chapter III presents a detailed analysis for the X-branch type optical wavelength division demultiplexer properties and design considerations by the effective index method. In order to verify our analysis by the effective index approach, Chapter IV applied the beam propagation method to simulate the X-branch type demultiplexer functions and discuss the Y-branching angle effects on the scattering loss

References:

[1] S E. Miller, "Integrated optics: an introduction", Bell System Tech. J., No. 48, pp. 2059-2069, 1969.

[2] W. J. Tomlinson and C. A. Brackett, "Telecommunications applications of integrated optics and optoelectronics", Proc IEEE, vol. 75, No. 11, pp 1512-1523, 1987.

[3] S. R. Forrest, "Optoelectronic Integrated Circuits", Proc IEEE, vol 75, No. 11, Nov. 1987.

[4] E. Voges and A. Neyer, "Integrated-optic devices on $LiNbO_3$ for optical communication", J. Lightwave Technol., vol LT-5, pp 1229-1238, 1987.

[5] F. Koyma and K. Iga, "Frequency chirping of external modulation and its reduction", Electron. Lett., vol. 21, pp 1065-1066, 1985

[6] P. Granestrand, B. Stoltz, L. Bergvall, W. Doldissen, H. Heidrich and D Hoffman, "Strictly nonblocking 8×8 integrated-optic switch matrix", Electro. Lett., vol. 22, pp. 816-817, 1986.

[7] J. H. Angenent, M. Ermam, J. M. Auger and R. Gamonal, "Extremely low loss InP/GaInAsP rib waveguides", Electron. Lett, vol 25, No. 10, pp. 628-629, 1989

[8] T. Findakly, "Glass waveguides by ion exchange: a review", Opt Eng., vol. 24, pp. 244-250, 1985.

[9] H. Nishihara, M. Haruna and T. Suhara, "Optical Integrated Circuits", New York: McGraw-Hill, 1989.

[10] D. H. Lee, "Electromagnetic Theory of Integrated Optics", New York, Academic Press, 1986.

[11] F. Auracher, H. F. Mahlein and G. Winzer, "Development Trends in Integrated Optics", Telecom Report 10, No. 4, pp. 148-156, 1987

[12] O. E. Delange, "Wideband optical communication systems: part II-frequency division multiplexing", Proc. IEEE, vol. 58, pp 1683, 1970.

[13] Y. Fujii, J. Minova and T. Kanada, "Practical two-wavelength multi-/demultiplexer: design and performance", Appl. Opt., vol 22, pp. 3090-3097, 1983.

[14] Y. Tamura, H. Maeda, N. Satoh and K. Katoh, "Single-mode fiber WDM in the *1.2-1.3* μm wavelength region", J. Lightwave Technol., vol. LT-4, pp. 841-845, 1986.

[15] M. Seki, K. Kobayashi, Y. Odagiri, M. Shikada, T. Tangigawa and R. Ishikawa, "20-channel microoptic grating demultiplexer for *1.1-1.6*

μm band using a small focusing parameter graded- index rod lens", Electron. Lett., vol. 18, pp. 257-258, 1982.

[16] J. Hegarty, S. D. Poulsen, K. A. Jackson and I. P. Kaminow, "Low-loss single mode wavelength division multiplexing with etched fiber arrays", Electron. Lett., vol 20, pp. 685-686, 1984.

[17] T. Suhara and H. Nishihara, "Integrated optics components and devices using periodic structures", IEEE J. Quantum Electron., vol. QE-22, pp 845-865, 1986.

[18] M. Digonnet and H. J. Shaw, "Wavelengths multiplexing in single-mode fiber couplers", Appl. Opt., vol. 22, pp. 484-491, 1983.

[19] R C. Alferness and R. V. Schmidt, "Tunable optical waveguide directional coupler filter", Appl. Phys. Lett., vol. 33, pp 161-163, 1978.

[20] R Zengerle and Leminger, "Narrow-band wavelength-selective directional couplers made of dissimilar single-mode fibers", in Proc. OFS/IOOC 1987 (Reno, NV), pap. THB2.

[21] N. Goto. and G. L. Yip, "Y-branch wavelength multi/demulti- plexer for λ=1.30 and 1.55 μm", Electron. Lett., vol. 26, pp. 102-103, 1990.

[22] F. Rottmann, A. Neyer, W. Mevenkamp and E. Voges, "Integrated -optic wavelength multiplexers on lithium niobate based on two-mode interference", J. Lightwave Technol., vol. LT-6. pp. 946-952, 1988.

Table I-1. Typical Performance Characteristics of Different Classes of Wavelength Multi-/Demultiplexers

	Interference filter	Grating	Directional Coupler
Number of channels	*2-6*	*3-20*	*2-8*
Insertion loss	*0.5-5dB*	*1-4dB*	*0.6-2dB*
Channel spacing	*30-100nm*	*1-40nm*	*40-200nm*
Far-end crosstalk	*20-70dB*	*20-30dB*	*10-13dB*

CHAPTER II

METHODS OF ANALYSIS FOR DIFFUSED OPTICAL WAVEGUIDES

II-1. Introduction

Ion-exchange is the prime candidate for fabricating passive optical waveguides in glass substrates [1]. Usually, the refractive index increment formed in the substrate by this technique is distributed. Fig. II-1 shows four of typical glass channel waveguides by the diffusion processes, in which a step index cladding is deposited onto the waveguides by RF-sputtering to increase the waveguide's effective index in order to enhance waveguide field confinement abilities and/or adjust waveguide dispersion properties. The characteristics of the propagating mode in such waveguides are obtained by solving Maxwell's equations for the corresponding boundary-value problem. Due to the vectorial nature of the electromagnetic field, the geometrical shape and/or the refractive index distribution of the guides, and the infinite domain of the cross section, the fully analytical solutions for the vectorial electromagnetic fields are usually not obtainable for most of the practical waveguides. Therefore, using some approximate or numerical methods applicable to the studies of dispersion properties of optical waveguides with arbitrary index distribution is necessary and important for engineering device designs and fabrications [2-5].

In this Chapter, we first derive the transverse vector wave equations from the Maxwell's equations and briefly discuss the classification of propagating modes in the optical waveguides under a weak guidance condition in the Section II-2. To analyze optical waveguides with one dimensional arbitrary (step and graded) index profile, the WKB and transverse resonance methods are presented and discussed in Section II-3 and II-4, respectively. Also, the effective index modelling and scalar variational technique to study the characteristics of two-dimensional diffused channel optical waveguides are discussed in Section II-5 and II-6, respectively.

II-2. Wave Equations

For a general graded-index optical waveguide, Maxwell's equations may be written as

$$\nabla \times \mathbf{H} = n^2(x,y)\varepsilon_o \frac{d\mathbf{E}}{dt} \tag{II-1}$$

$$\nabla \times \mathbf{E} = -\mu_o \frac{d\mathbf{H}}{dt} \tag{II-2}$$

$$\nabla \cdot [n^2(x,y)\varepsilon_o \mathbf{E}] = 0 \tag{II-3}$$

$$\nabla \cdot \mathbf{H} = 0 \tag{II-4}$$

If we apply the curl operator to equation (II-2), we find

$$\nabla \times (\nabla \times \mathbf{E}) = -\mu_o \nabla \times \frac{d\mathbf{H}}{dt} = -\mu_o \varepsilon_o n^2(x,y) \frac{d\mathbf{E}}{dt} \tag{II-5}$$

where equation (II-1) was used to eliminate **H**. Using the vector indentity

$$\nabla \times (\nabla \times \mathbf{E}) = \nabla(\nabla \cdot \mathbf{E}) - \nabla^2 \mathbf{E} \tag{II-6}$$

together with equation (II-3), equation (II-5) becomes:

$$\nabla^2 \mathbf{E} + \nabla \left(\frac{\mathbf{E} \cdot \nabla n^2(x,y)}{n^2(x,y)} \right) + k_o^2 n^2(x,y) \mathbf{E} = 0 \tag{II-7}$$

where the time dependence $exp(-j\omega t)$ of **E** has been assumed and the conventional notation $k_o^2 = \omega^2 \mu_o \varepsilon_o$ has been used. Equation (II-7) is the vector wave equation satisfied by the electric field **E**.

Similarly, the corresponding wave equation for the magnetic field **H** can be derived from the equations (II-1) to (II-4) as:

$$\nabla^2 \mathbf{H} + \frac{\nabla n^2(x,y)}{n^2(x,y)} \times (\nabla \times \mathbf{H}) + k_o^2 n^2(x,y)\mathbf{H} = 0 \qquad \text{(II-8)}$$

Since the fact that $n(x,y)$ is the function of transverse coordinate x and y only, the vector wave equations just for the transverse field components can be separated from the equations (II-7) and (II-8) as

$$\nabla_\perp^2 \mathbf{E}_t + \nabla_\perp \left(\frac{\mathbf{E}_t \cdot \nabla_\perp n^2(x,y)}{n^2(x,y)} \right) + [k_o^2 n^2(x,y) - \beta^2]\mathbf{E}_t = 0$$

$$\text{(II-9)}$$

$$\nabla_\perp^2 \mathbf{H}_t + \frac{\nabla_\perp n^2(x,y)}{n^2(x,y)} \times (\nabla_\perp \times \mathbf{H}_t) + [k_o^2 n^2(x,y) - \beta^2]\mathbf{H}_t = 0$$

$$\text{(II-10)}$$

where a z-dependence as $exp(j\beta z)$ is assumed and $\nabla_\perp = \partial^2/\partial x^2 + \partial^2/\partial y^2$.

From the above equations, we know the vectorial properties of the propagating modes in the optical waveguides arise from the terms with $\nabla_\perp ln[n^2(x,y)]$. For the piecewise uniform medium, it lies in the discontinuities of $\nabla_\perp ln[n^2(x,y)]$ across the boundaries between different refractive indices. For the glass optical waveguides, the refractive index of the waveguide does not vary rapidly in the cross-sectional plane and/or differs only a little across the index discontinuities. Under this condition, the propagating modes are almost linearly polarized and can be classified into two groups as TE-like and TM-like modes for the strong **E** field components are parallel and perpendicular to the waveguide surface, respectively. The corresponding transverse vector wave equation approximately becomes

$$\frac{\partial^2 E_x}{\partial x^2} + \frac{\partial^2 E_x}{\partial y^2} + \frac{\partial}{\partial x}\left\{ E_x \frac{\partial}{\partial x} ln[n^2(x,y)] \right\} + [k_o^2 n^2(x,y) - \beta^2]E_x = 0$$

$$\text{(II-11)}$$

$$\frac{\partial^2 H_y}{\partial x^2} + \frac{\partial^2 H_y}{\partial y^2} - \frac{\partial}{\partial x} ln[n^2(x,y)] \frac{\partial H_y}{\partial x} + [k_o^2 n^2(x,y) - \beta^2]H_y = 0$$

(II-12)

for the TM-like modes, and

$$\frac{\partial^2 E_y}{\partial x^2} + \frac{\partial^2 E_y}{\partial y^2} + \frac{\partial}{\partial y}\left\{E_y \frac{\partial}{\partial y} ln[n^2(x,y)]\right\} + [k_o^2 n^2(x,y) - \beta^2]E_y = 0$$

(II-13)

$$\frac{\partial^2 H_x}{\partial x^2} + \frac{\partial^2 H_x}{\partial y^2} - \frac{\partial}{\partial y} ln[n^2(x,y)] \frac{\partial H_x}{\partial y} + [k_o^2 n^2(x,y) - \beta^2]H_x = 0$$

(II-14)

for the TE-like modes.

The extreme case is the slab waveguides. Since $\frac{\partial}{\partial y} = 0$, the propagating modes can be rigorously distinguished as TM modes with

$$E_y = H_x = H_z = 0; \quad E_x = \frac{\beta^2}{\omega\varepsilon_o n^2(x)} H_y; \quad E_z = \frac{J}{\omega\varepsilon_o n^2(x)} \frac{dH_y}{dx}$$

and TE modes with

$$E_x = H_y = E_z = 0; \quad H_x = -\frac{\beta}{\omega\mu_o} E_y; \quad H_z = -\frac{J}{\omega\mu_o} \frac{dE_y}{dx}$$

The equations (II-11) to (II-14) are simplified to become

$$\frac{\partial^2 E_x}{\partial x^2} + \frac{\partial}{\partial x}\left\{E_x \frac{\partial}{\partial x} ln[n^2(x)]\right\} + [k_o^2 n^2(x) - \beta^2]E_x = 0$$

(II-15)

$$\frac{\partial^2 H_y}{\partial x^2} - \frac{\partial}{\partial x} ln[n^2(x)] \frac{\partial H_y}{\partial x} + [k_o^2 n^2(x) - \beta^2]H_y = 0$$

(II-16)

for TM modes and

$$\frac{\partial^2 E_y}{\partial x^2} + [k_o^2 n^2(x) - \beta^2]E_y = 0 \quad \text{(II-17)}$$

$$\frac{\partial^2 H_x}{\partial x^2} + [k_o^2 n^2(x) - \beta^2]H_x = 0 \quad \text{(II-18)}$$

for TE modes.

From the above derivations, we know, under the weak-guidance condition, glass optical waveguide analysis is possible under certain approximations. In the following sections, starting from the one-dimensional problems, we are going to discuss some approximate or numerical methods which are practical for studying arbitrary index distribution waveguide problems.

II-3. The WKB Approximation

In optical waveguide theory, although the ray optics approach and the WKB approximation have a similar range of applicability, both being suitable for use only when the variation of index is small in distances of the order of the wavelength, it is believed usually that, in analyzing surface diffused optical waveguides, the ray theory can provide a better level of approximation than the WKB theory for being capable of accounting for the phase changes occurring on reflection from a dielectric discontinuity. However, this advantage is difficult to be extended to the analysis of the multilayer waveguide problems. In this section, we shall see, if the field solutions are matched properly at the dielectric discontinuities, the first-order WKB approximation can yield not only identical results with the ray optics approach, but also can be used to analyze the piecewise graded-index optical waveguide problems, such as a diffused surface optical waveguide with a cladding.

For the planar diffused optical waveguides, the scalar wave equation is

$$\frac{\partial^2 \phi}{\partial x^2} + [k_o^2 n^2(x) - \beta^2]\phi = 0 \qquad \text{(II-19)}$$

where $\phi = E_y$ or H_y for TE and TM modes, respectively. Since the value of $\frac{\partial}{\partial x} ln[n^2(x)]$ is very small in the graded-index region, we neglected the term for TM modes. In fact, for the diffused surface waveguides, the polarization discrepancy of the propagating modes are due to the waveguide surface step-index change mainly. Therefore, different polarization modes can be determined by the corresponding boundary conditions as $\phi(x_1^-) = \phi(x_1^+)$ and $\phi'(x_1^-) = \phi'(x_1^+)$ for TE modes; $\dfrac{\phi'(x_1^-)}{n^2(x_1^-)} = \dfrac{\phi'(x_1^+)}{n^2(x_1^+)}$ for TM modes respectively at the dielectric discontinuity position $x=x_1$.

According to the WKB theory [6], the first order approximate solutions are given

$$\phi(x) \propto \frac{C_1}{\sqrt{Q(x)}} \exp\left[\pm j\int Q(x)dx\right] \qquad \text{for regions } k_o n(x) > \beta \tag{II-20}$$

$$\phi(x) \propto \frac{C_2}{\sqrt{P(x)}} \exp\left[\pm\int P(x)dx\right] \qquad \text{for regions } k_o n(x) < \beta \tag{II-21}$$

where $P^2=-Q^2=\beta^2-k_o^2n^2(x)$. Although these solutions diverge at the turning point, two sets of independent connection formulas relating the fields on either side of the turning point can be obtained by the asymptotic solutions of the wave equation as

$$P^{-1/2}exp\left(-\int_x^{x_1} Pdx\right) \longleftrightarrow 2Q^{-1/2}sin\left(\int_{x_1}^{x} Qdx + \frac{\pi}{4}\right) \tag{II-22}$$

$$P^{-1/2}exp\left(\int_x^{x_1} Pdx\right) \longleftrightarrow Q^{-1/2}cos\left(\int_{x_1}^{x} Qdx + \frac{\pi}{4}\right) \tag{II-23}$$

for Fig. II-2(a), and

$$2Q^{-1/2}sin\left(\int_x^{x_2} Qdx + \frac{\pi}{4}\right) \longleftrightarrow P^{-1/2}exp\left(-\int_{x_2}^{x} Pdx\right) \tag{II-24}$$

$$Q^{-1/2}\cos\left(\int_{x}^{x_2} Q dx + \frac{\pi}{4}\right) \longleftrightarrow P^{-1/2}\exp\left(\int_{x_2}^{x} P dx\right)$$

(II-25)

for Fig. II-2(b) respectively, where the upper bounds of the integral are always greater than the lower bounds.

A general index profile of the diffused surface optical waveguides is shown in the Fig. II-3. According to the WKB approximation, the scalar fields on either side of the discontinuity can be expressed as

$$\phi \propto P^{-1/2}\exp\left(-\int_{0^+}^{x} P dx\right) \qquad \text{in the region } x > 0^+$$

(II-26)

$$\phi \propto Q^{-1/2}\cos\left(\int_{x_1}^{x} Q dx - \frac{\pi}{4}\right) \qquad \text{in the region } x_1 < x < 0^-$$

(II-27)

In order to match the fields and their derivatives at $x=0$, we can have

$$\frac{C_1}{\sqrt{Q(0^-)}}\cos\left(\int_{x_1}^{0} Q dx - \frac{\pi}{4}\right) = \frac{C_2}{\sqrt{P(0^+)}}$$

(II-28)

$$C_1\frac{\sqrt{Q(0^-)}}{n^p(0^-)}\sin\left(\int_{x_1}^{0} Q dx - \frac{\pi}{4}\right) = C_2\frac{\sqrt{P(0^+)}}{n^p(0^+)}$$

(II-29)

where $p=0$ or 2 for TE and TM modes, respectively. It is worth noting that the derivatives in (II-28) and (II-29) only include the terms from the argument of the trigonometric or exponential functions. Since the derivatives of the coefficients would be of higher order in the WKB expansion, then it is best not to differentiate these terms [6].

Combining equations (II-28) and (II-29) gives the eigenvalue equation for modes of N as

$$\int_{x_1}^{0} Qdx - \frac{\pi}{4} = N\pi + \tan^{-1}\left[\frac{n^P(0^-)}{n^P(0^+)}\,\frac{P(0^+)}{Q(0^-)}\right] \qquad (N=0,1,2,\ldots)$$

$$= N\pi + \tan^{-1}\left[\frac{n^P(0^-)}{n^P(0^+)}\,\frac{[\beta^2-k_o^2n^2(0^+)]^{1/2}}{[k_o^2n^2(0^-)-\beta^2]^{1/2}}\right]$$

(II-30)

It is clear that this result is the same as the one given by a rigorous application of the ray optics theory [7]. Therefore, with the proper treatment on derivatives, the first-order WKB approximation can yield identical results with the ray optics approach. In principle, we can extend this method to the analysis of the piecewice graded-index optical waveguide problems where the geometrical optics theory cannot be applied.

Fig. II-4 shows a very practical optical waveguide, cladded diffused surface waveguide, index profile. Similar to the last waveguide problem, the fields in each region can be written as

$$\phi \propto Q^{-1/2}\cos\left(\int_{x_1}^{x} Qdx - \frac{\pi}{4}\right) \qquad \text{for} \quad x_1 > x > 0^-$$

(II-31)

$$\phi \propto C_1P^{-1/2}\exp\left(\int_{0^+}^{x} Pdx\right)+C_2P^{-1/2}\exp\left(-\int_{0^+}^{x} Pdx\right) \qquad \text{for} \quad t > x > 0^+$$

(II-32)

$$\phi \propto C_3P^{-1/2}\exp\left(-\int_{t}^{x} Pdx\right) \qquad \text{for} \quad x > t$$

(II-33)

In order to match the fields and their derivatives at the discontinuity $x=0$, we let

$$\frac{1}{\sqrt{Q(0^-)}}\cos\left(\int_{x_1}^{0} Qdx - \frac{\pi}{4}\right) = \frac{1}{\sqrt{P(0^+)}}\left[C_1 + C_2\right]$$

(II-34)

$$-\frac{\sqrt{Q(0^-)}}{n^P(0^-)}\sin\left(\int_{x_1}^{0} Qdx - \frac{\pi}{4}\right) = \frac{\sqrt{P(0^+)}}{n^P(0^+)}\left[C_1 - C_2\right]$$

(II-35)

Therefore, the coefficient C_1 and C_2 can be solved from this linear equations as

$$C_1=\frac{1}{2}\left\{\frac{\sqrt{P(0^+)}}{\sqrt{Q(0^-)}}\cos\left(\int_{x_1}^{0} Qdx-\frac{\pi}{4}\right)-\frac{n^p(0^+)\sqrt{Q(0^-)}}{n^p(0^-)\sqrt{P(0^+)}}\sin\left(\int_{x_1}^{0} Qdx-\frac{\pi}{4}\right)\right\}$$

(II-36)

$$C_2=\frac{1}{2}\left\{\frac{\sqrt{P(0^+)}}{\sqrt{Q(0^-)}}\cos\left(\int_{x_1}^{0} Qdx-\frac{\pi}{4}\right)+\frac{n^p(0^+)\sqrt{Q(0^-)}}{n^p(0^-)\sqrt{P(0^+)}}\sin\left(\int_{x_1}^{0} Qdx-\frac{\pi}{4}\right)\right\}$$

(II-37)

Again we match the fields and their derivatives at $x=t$ as

$$\frac{1}{\sqrt{P(t^-)}}\left\{C_1 exp\left(\int_0^t Pdx\right)+C_2 exp\left(-\int_0^t Pdx\right)\right\} = \frac{C_3}{\sqrt{P(t^+)}}$$

(II-38)

$$\frac{\sqrt{P(t^-)}}{n^p(t^-)}\left\{C_1 exp\left(\int_0^t Pdx\right)-C_2 exp\left(-\int_0^t Pdx\right)\right\} = -C_3\frac{\sqrt{P(t^+)}}{n^p(t^+)}$$

(II-39)

Substituting formulas (II-36) and (II-37) into the above equations and combining them with some algebraic manipulations, we can derive the eigenvalue equation for the cladded surface diffused optical waveguides under first-order WKB approximation

$$\frac{B_1+ tg(A)}{B_1- tg(A)} = exp[-2t(\beta^2-k_o^2n_c^2)^{1/2}]\frac{1 - B_2}{1 + B_2}$$

(II-40)

where $A=\frac{\pi}{4} - \int_{x_1}^{0}[k_o^2n^2(x)-\beta^2]^{1/2}dx$, $B_1=\frac{n^p(0^-)}{n^p(0^+)}\frac{[\beta^2-k_o^2n^2(0^+)]^{1/2}}{[k_o^2n^2(0^-)-\beta^2]^{1/2}}$ and $B_2=\frac{n_c^p}{n_a^p}\frac{[\beta^2-k_o^2n_a^2]^{1/2}}{[\beta^2-k_o^2n_c^2]^{1/2}}$; $p=0, 2$ for TE and TM modes, respectively. With this eigenvalue equation, the dispersion properties of the propagating modes in such waveguides can be solved by root-searching techniques. By assuming the index profile in the graded index region as

$$n^2(x) = n_b^2 + 2\Delta nn_b exp(-x^2/d_x^2) \qquad x < 0 \qquad \text{(II-41)}$$

where Δn is the index change at $x=0$ and d_x is the effective diffsion depth, Table II-1 and 2 give two calculation examples to demonstrate that the eigen-equation provides quite accurate results, in which the exact values are provided by the transverse resonance method (TRM, see next section) From these we know that, as the cladding thickness changes, the errors introduced by the WKB first-order approximation for the cladded diffused surface waveguides are minimal And, for the fixed diffusion depth waveguides, by increasing the $n_c<n_b$ cladding thickness, the propagation constant will tend to a constant. Comparing with the numerical TRM method, the WKB approach produces results faster. However, it systematically underestimates the effective indices.

Although we only discuss the case of $n_c<n_b$ here, for the other cases, such as $n_c>\beta/k_o$, the corresponding eigenvalue equations can also be derived by repeating the similar procedure.

II-4. Transverse Resonance Method

In planar waveguides, the propagating modes can be rigorously classified into TE and TM types of modes. Therefore, the transverse resonance method can be applied to study the waveguide dispersion properties since the transverse impedances and admittances can be uniquely defined. However, in the conventional optical waveguide theory, only the uniform transmission line theory is applied to study those multi-layer homogeneous waveguide problems. In this section, we extend the transverse resonance method to the studies of diffused (inhomogeneous) planar waveguide problems By this development, not only the dispersion properties of the waveguides with an arbitrary index profile can be investigated with any desired accuracy, but also the inhomogeneous and homogeneous planar waveguides can be treated in the same fashion thoroughly without considering the modal fields or the turning points as in the WKB theory.

According to the uniform transmission line theory [8], for the graded characteristic impedance transmission lines, the impedance transformation formula becomes (see Fig II-5)

$$Z(x) + dZ = Z_c(x)\frac{Z(x) + Z_c(x)tanh(j\beta+\alpha)dx}{Z_c(x) + Z(x)tanh(j\beta+\alpha)dx}$$

$$\sim \frac{Z(x) + Z_c(x)(j\beta+\alpha)dx}{1 + [Z(x)/Z_c(x)](j\beta+\alpha)dx}$$

$$\approx \left[Z(x) + Z_c(x)(j\beta+\alpha)dx\right]\left[1 - Z(x)/Z_c(x)(j\beta+\alpha)dx\right]$$

$$\approx Z(x) + \left[Z_c(x) - Z^2(x)/Z_c(x)\right](j\beta+\alpha)dx \tag{II-42}$$

where $Z_c(x)$ is the characteristic impedance of the graded transmission line. Therefore, the impedance transform formula for the graded transmission lines is a nonlinear ordinary differential equation as given by

$$\frac{dZ}{dx} = -(j\beta+\alpha)\frac{Z^2(x)-Z_c^2(x)}{Z_c(x)} \tag{II-43}$$

In the planar waveguides, we can define the local transverse impedances as $Z_{cTE}=\frac{E_y}{H_z}=j\frac{\omega\mu_o}{k_x}$ and $Z_{cTM}=-\frac{E_z}{H_y}=j\frac{k_x}{\omega\varepsilon_o n^2}$ for TE and TM modes respectively, where $k_x=j[k_o^2n^2(x)-\beta^2]^{1/2}$ as $n(x) > \beta/k_o$ and $k_x=[\beta^2-k_o^2n^2(x)]^{1/2}$ as $n(x) < \beta/k_o$. Substitute these into the equation (II-41) and let $Z'_{cTE}=Z_{cTE}/j\omega\mu_o$; $Z'_{TE}=Z_{TE}/j\omega\mu_o$ for TE modes and $Z'_{cTM}=j\omega\varepsilon_o Z_{cTM}$; $Z'_{TM}=j\omega\varepsilon_o Z_{TM}$ for TM modes, we can have

$$\frac{dZ'_{TE}}{dx} = -k_x\frac{Z'^2_{TE} - Z'^2_c}{Z'_c} = -k_x\frac{Z'^2_{TE} - k_x^{-2}}{1/k_x} = -[\beta^2-k_o^2n^2(x)]Z'^2_{TE} + 1$$

$$\frac{dZ'_{TM}}{dx} = -k_x\frac{Z'^2_{TM} - Z'^2_c}{Z'_c} = -k_x\frac{Z'^2_{TM} - k_x^2/n^4}{k_x/n^2} \tag{II-44}$$

$$= [\beta^2 - k_o^2 n^2(x)]/n^2(x) - n^2(x) Z'^2_{TM} \tag{II-45}$$

Actually, similar results can be derived directly from the wave equations (II-16) and (II-17) [9]. From these, we have

$$\frac{1}{E_y}\frac{d^2E_y}{dx^2} = -[k_o^2 n^2(x) - \beta^2] \tag{II-46}$$

$$\frac{1}{H_y}\frac{d^2H_y}{dx^2} = -[k_o^2 n^2(x) - \beta^2] + \left[\frac{dn^2(x)}{dx}\Big/n^2(x)\right]\frac{dH_y}{dx}\Big/H_y \tag{II-47}$$

for TE and TM modes, respectively. Therefore, if we define the transverse impedances as

$$Z_{TE} = \frac{E_y}{H_z} = j\omega\mu_o E_y\Big/\frac{dE_y}{dx} \quad \text{or} \quad Z'_{TE} = Z_{TE}/j\omega\mu_o = E_y\Big/\frac{dE_y}{dx} \tag{II-48}$$

$$Z_{TM} = -\frac{E_z}{H_y} = \frac{1}{j\omega\varepsilon_o n^2(x)}\frac{dH_y}{dx}\Big/H_y \quad \text{or} \quad Z'_{TM} = j\omega\varepsilon_o Z_{TM} = \frac{1}{n^2(x)}\frac{dH_y}{dx}\Big/H_y \tag{II-49}$$

Then, by differentiating them, we can obtain

$$\frac{dZ'_{TE}}{dx} = 1 - \frac{d^2E_y}{dx^2}E_y\Big/\left[\frac{dE_y}{dx}\right]^2 = 1 + [k_o^2 n^2(x) - \beta^2] Z'^2_{TE} \tag{II-50}$$

$$\frac{dZ'_{TM}}{dx} = -\frac{1}{n^4(x)}\frac{dn^2(x)}{dx}\frac{dH_y}{dx}\Big/H_y - n^2(x)\left[\frac{1}{n^2(x)H_y}\frac{dH_y}{dx}\right]^2 + \frac{1}{n^2(x)}\frac{1}{H_y}\frac{d^2H_y}{dx^2}$$

$$= [\beta^2 - k_o^2 n^2(x)]/n^2(x) - n^2(x) Z'^2_{TM} \tag{II-51}$$

These results are identical to equations (II-43) and (II-44). Therefore, after we obtain the distributed transverse impedance $Z'(x)$, the corresponding transverse modal field E_y or H_y as function of x can be deduced by the integrals

$$E_y = exp\left(\int_0^x 1/Z'_{TE}(x)dx\right) \qquad \text{and} \qquad H_y = exp\left(\int_0^x n^2(x)Z'_{TM}(x)dx\right) \tag{II-52}$$

for TE and TM mode, respectively, where we assume the field to be unity at the air-guide interface $x=0$.

For the guided modes, β/k_o is always greater than the index value $n(x)$ at $x=\infty$, therefore, the initial values

$$Z'(\infty)=Z'_c(\infty)=1/[\beta^2-k_o^2n^2(\infty)]^{1/2} \qquad \text{for TE modes}$$
$$Z'(\infty)=Z'_c(\infty)=[\beta^2-k_o^2n^2(\infty)]^{1/2}/n^2(\infty) \qquad \text{for TM modes}$$

are purely real generally. Since all variables involved in the differential equations are also real, $Z'(x)$ will remain purely real, or in another words, $Z(x)$ is imaginary as x changes along this whole graded transmission line. This coincides with a conclusion in the uniform transmission line theory that, when the load is a reactance, the impedance will be invariably imaginary with open and short circuits alternatively appearing along the transmission line. Similarly, for the graded transmission lines, there will be some poles (open circuits) appearing which would cause an overflow in the calculations for high order modes. To avoid them, we can make a transformation by setting $Z'_{TE}=tan\theta$ and $Z'_{TM}=ctan\theta$. Then the equations become

$$\frac{d\theta}{dx} = cos^2\theta + sin^2\theta[k_o^2n^2(x)-\beta^2] \tag{II-53}$$

for TE modes

$$\frac{d\theta}{dx} = n^2(x)cos^2\theta + sin^2\theta[k_o^2n^2(x)-\beta^2]/n^2(x) \tag{II-54}$$

for TM modes, respectively.

To solve these nonlinear differential equations, we use a fourth order Runge-Kutta method [10] as follows

$$\theta_{n+1} = \theta_n + (k_1+2k_2+2k_3+k_4)/6 \tag{II-55}$$

with

$$
\begin{aligned}
k_1 &= hF(x_n, \theta_n) \\
k_2 &= hF(x_n+h/2,\ \theta_n+k_1/2) \\
k_3 &= hF(x_n+h/2,\ \theta_n+k_2/2) \\
k_4 &= hF(x_n+h,\ \theta_n+k_3)
\end{aligned}
\tag{II-56}
$$

where $F(x,\theta)$ represents the right hand side of the differential equations. The associated truncation error is $R=O(h^5)$ and, for $h=0.005$, one expects accuracy of seven or eight decimal places. To compare the numerical results with the WKB theory, Fig. II-6 (a)-(b) shows two samples of the calculated dispersion curves for the diffused surface waveguides, in which $n_e=\beta/k_o$ is the mode effective index The differences around the cutoff region are apparently demonstrated.

Applying this method to the solution of the cladded diffused surface waveguide problems (see Fig. II-7), we set up the transverse resonance equation

$$
Z_1(\beta) + Z_2(\beta) = 0 \qquad \text{or} \qquad Z_1'(\beta) + Z_2'(\beta) = 0
\tag{II-57}
$$

According to the impedance transform formula for the uniform transmission lines, Z_1' can be found as follows

$$
\begin{aligned}
Z_1' = Z_c'\frac{Z_a' + Z_c'\tanh(k_c t)}{Z_c' + Z_a'\tanh(k_c t)} &= \frac{1}{k}\,\frac{k\cos(kt)+k_a\sin(kt)}{k_a\cos(kt)-k\sin(kt)} && \text{for } n_c>\beta/k_o \\
&= \frac{1}{k'}\,\frac{(k_a+k')\exp(k't)-(k_a-k')\exp(-k't)}{(k_a+k')\exp(k't)+(k_a-k')\exp(-k't)} && \text{for } n_c<\beta/k_o \\
&= (1 + k_a t)/k_a && \text{for } n_c=\beta/k_o
\end{aligned}
\tag{II-58}
$$

for TE modes, and

$$Z'_1 = \frac{k}{n_c^2}\,\frac{k_a\cos(kt)-k\sin(kt)/n_c^2}{k\cos(kt)/n_c^2+k\sin(kt)} \qquad \text{for } n_c>\beta/k_o$$

$$= \frac{k}{n_c^2}\,\frac{(k_a+k'/n_c^2)\exp(k't)+(k_a-k'/n_c^2)\exp(-k't)}{(k_a+k'/n_c^2)\exp(k't)-(k_a-k'/n_c^2)\exp(-k't)} \qquad \text{for } n_c<\beta/k_o$$

$$= k_a/(1 + k_a t) \qquad \text{for } n_c=\beta/k_o \tag{II-59}$$

for TM modes, where $k=(k_o^2n_c^2-\beta^2)^{1/2}$ and $k'=(\beta^2-k_o^2n_c^2)^{1/2}$. As for Z'_2, it can be provided by the equations (II-49) or (II-50). By root- searching equation (II-56), we can find each β of the guided mode in the waveguide. Table II-1, 2 show the numerical results with comparison to the WKB method for TE and TM modes, respectively.

Since many trigonometric function evaluations are involved in the calculations, this scheme usually consumes more computation time than the WKB method.

II-5. Effective Index Modelling

In the above two sections, we have discussed the approximate and numerical methods to study the one dimensional waveguide problems involving an arbitrary index distribution. They are very useful for the planar diffused optical waveguide characterization analysis. In fact, combined with the effective index method [11], these techniques can be extended to study two dimensional channel waveguide problems [4]. Since the weakly guiding condition is always valid in glass optical waveguides, the propagating modes are almost linearly polarized and can be classified into TE-like and TM-like modes for the strong **E** field components parallel and perpendicular to the waveguide surface, respectively. This property allows for some approximations to provide quite accurate results for predicting the dispersion properties of channel waveguides. Next, we are going to illustrate how the wave equation for the 2-D graded index waveguides can be split into two 1-D wave equations under the effective index modelling.

For the diffused glass surface waveguides, since the graded index variation is very small in distance of the order of the wavelength over the whole cross section, the terms with $\nabla_{\perp} ln[n^2(x,y)]$ are negligible from the vectorial wave equations (II-9) and (II-10). Therefore, the channel waveguide modes can be studied under the scalar approximation and the dominant optical field distribution function can be assumed to have $E(x,y) = P(x)Q(y)$. Hence, equation (II-9) becomes

$$\frac{P''(x)}{P(x)} + \frac{Q''(y)}{Q(y)} + k_o^2[n^2(x,y)-N_e^2(y)] + k_o^2[N_e^2(y)-N^2] = 0 \tag{II-60}$$

where $N=\beta/k_o$ is defined as the effective index of the propagating mode, $N_e(y)$ is the lateral effective index profile function. Equation (II-54) can be separated into two 1-D differential equations by using the effective index method. The effective index essentially slices the 2-D graded index waveguide in the lateral direction. The mode index $N_e(y_o)$ corresponds to a given thin slice at a specific value $y=y_o$. However the guide with an index profile $n(x,y_o)$ at $y=y_o$ is now assumed to be infinitely extended for the purpose of evaluating $N_e(y_o)$ Thus the application of the effective index method results in the following separated equations:

$$\frac{d^2P(x)}{dx^2} + k_o^2[n^2(x,y) - N_e^2(y)]P(x) = 0 \tag{II-61}$$

$$\frac{d^2Q(y)}{dy^2} + k_o^2[N_e^2(y) - N^2]Q(y) = 0 \tag{II-62}$$

In (II-60), since y is regarded as a constant, we can solve $N_e(y)$ at each value of y by applying the boundary condition along x, that is, along the depth direction.

The index profile of single channel waveguide formed by the diffusion process is separable usually which can be assumed as

$$n^2(x,y) = n_b^2 + 2n_b\Delta n\ f(x/a)g(y/b) \qquad x \le 0$$

$$= n_o^2 \qquad\qquad x > 0$$

(II-63)

where $a=d_x$, $b=d_y$ are the effective diffusion depths in the depth and lateral directions respectively. Substituting (II-62) into (II-60), we have

$$\frac{d^2P}{dx^2} + k_o^2[n_b^2 + 2n_b\Delta n\ f(x/a)g(y/b) - N_e^2(y)]P = 0$$

(II-64)

After some algebraic manipulation, equations (II-63) and (II-61) can be normalized as

$$\frac{d^2P}{d\xi^2} + V_x^2 g(\eta)[f(\xi) - B_m(\eta)]P = 0 \qquad \text{(II-65)}$$

$$\frac{d^2Q}{d\eta^2} + V_y^2[g(\eta)B_m(\eta) - B_{mn}]Q = 0 \qquad \text{(II-66)}$$

where $V_x=k_o d_x\sqrt{2\Delta nn_b}$, $V_y=k_o d_y\sqrt{2\Delta nn_b}$ are the normalized frequencies; $g(\eta)B_m(\eta)=[N_e^2(\eta)-n_b^2]/2\Delta nn_b$, $B_{mn}=(N^2-n_b^2)/2\Delta nn_b$, and m, n correspond to the mode number with respect to the variations in the depth and lateral direction, respectively. $g(\eta)B_m(\eta)$ and B_{mn} are called the normalized effective lateral index profile and the normalized effective index, respectively [5].

By way of the WKB method or ray treatment, the eigenvalue equation for the equation (II-64) can be expressed as the phase integral form

$$V_x\sqrt{g(\eta)}\int_0^{\xi_t}[f(\xi)-B_m(\eta)]^{1/2}d\xi = m\pi + \varphi_s + \varphi_t \qquad \text{(II-67)}$$

where $\varphi_s=\tan^{-1}[n_s^p\sqrt{(B_m+A)/(1-B_m)}\ ]$ is the phase shift due to the total reflection between the air-waveguide interface; p=0 for TE-like modes and p=2 for TM-like modes; $A=(n_b^2-1)/(n_s^2-n_b^2)$ is a measure of the waveguide asymmetry. φ_t is the phase shift experienced by the ray at the turning point $\xi=\xi_t$ and equals $\pi/4$ [7]. Similarly, for the lateral direction, the equation (II-65) will give

$$V_y \int_{-\eta_t}^{\eta_t} [g(\eta)B_m(\eta) - B_{mn}]^{1/2} d\eta = (m + \frac{1}{2})\pi \qquad \text{(II-68)}$$

where η_t is the lateral turning point, i.e. $g(\eta_t)B_m(\eta_t)-B_{mn}=0$. Therefore, applying equations (II-66) and (II-67), the diffused optical waveguide dispersion properties can be studied by the effective index approximation.

As the matter of fact, in the slab waveguide case, equation (II-66) becomes

$$V_x \int_{0}^{\xi_t} [f(\xi)-B_m]^{1/2} d\xi = m\pi + \varphi_s + \varphi_t \qquad \text{(II-69)}$$

where $V_x=kd_x\sqrt{2\Delta n n_b}$ and $B_m=\beta_m/k$. For a fixed m, B_m is a single value function of V_x, i.e. $B_m=F(V_x)$. Therefore, as long as we find the dispersion relation for B_m to V_x in the slab case, the function can be applied to set up the lateral effective index profile $g(\eta)B_m(\eta)$ = $g(\eta)F[V_x\sqrt{g(\eta)}]$ for any channel diffused waveguide which possesses the same index distribution function $f(x/a)$ in the depth direction Therefore, using the normalized notations can save much computation for analyzing the diffused channel waveguides by the effective index approximation method [5].

In order to demonstrate the effectiveness of this approach, we apply the index profile characterized from the K^+-Na^+ ion exchange in soda-lime glass substrates in the calculation, i.e. the lateral and depth index profiles in the formula (II-62) are $g(y/b)=\frac{1}{2erf(w/2b)}\left[erf\left(\frac{y+w/2}{b}\right)-erf\left(\frac{y-w/2}{b}\right)\right]$ (erf is the error function) and $f(x/a)=exp(-x^2/a^2)$, respectively. Fig. II-8 (a)-(b) show some samples together with the variational analysis. The results indicate, by effective index modelling, not only the diffused channel waveguides can be studied by the planar techniques with accuracy, but also the discrepancy between the different polarization modes can be distinguished by equation (II-66).

II-6. Scalar Variational Analysis

As we have demonstrated in the previous section, by the effective index modelling, the 2-D channel waveguide problems can be transformed into two coupled 1-D planar waveguide problems. Since the effective index approximation produces larger dispersion values [12] but WKB method gives smaller ones around the cutoff region (see Fig. II-6), the combination of them can still produce quite good results for predicting the channel waveguide dispersion property studies under the weak guidance condition. However, this method is still not suitable for providing the modal field patterns which is useful for further device design application. Comparatively, the scalar variational technique is a more rigorous and flexible method used to study channel waveguides with an arbitrary index distribution. By the stationary and extreme properties, this method can produce very reliable dispersion results. Furthermore, with the modal field information produced by the analysis, the polarization corrections can also be carried out by this perturbation techniques [13].

Under the scalar approximation, the wave equation for the propagating modes can be written as

$$(\nabla_{\perp}^2 + k_o^2 n^2(x,y) - \beta_o^2)\phi = 0 \tag{II-70}$$

where β_o is the propagation constant of the scalar mode and $\mathbf{E}=\phi\mathbf{x}$ or $\mathbf{E}=\phi\mathbf{y}$ are the field patterns characterizing the transverse electric fields which are linearly polarized along x or y directions.

Multiplying equation (II-69) with ϕ^* and integrating by part yields

$$\beta_o^2 = \frac{k_o^2 \iint_s n^2(x,y)|\phi|^2 \, dxdy - \iint_s |\nabla_\perp \phi|^2 \, dxdy}{\iint_s |\phi|^2 \, dxdy} \tag{II-71}$$

where the surface integral is over the entire cross section. The expression (II-70) is variational, i.e. the exact solution of equation (II-69) assumes an extrema of β_o^2 in (II-70). Because of the stationary and extrema properties, the variational method can provide very reliable results in predicting the dispersion characteristics for waveguides with an arbitrary index profile. However, the accuracy of the variational analysis is critically dependent on the proper choice of the field trial functions.

For the diffused channel waveguides, due to weak guidance and a step index change on the substrate surface, we can assume that the E field trial functions are separable, i.e.

$$\phi(x,y) = P(x)Q(y) \tag{II-72}$$

As proposed in the literature [14], we extend the trial function form to approximate two dimensional channel waveguide field distribution, i.e., on the x and y coordinate directions, we propose the trial function as following

$$\begin{aligned} P(x) &= \cos(p\sigma)\exp[p\tan(p\sigma)x/a] && x/a \geq 0 \\ &= \cos[p(x/a-\sigma)] && 0 \geq x/a \geq \xi \\ &= \cos[p(\xi-\sigma)]\exp\{-p\tan[p(\xi-\sigma)](x/a-\xi)\} && x/a \leq \xi \end{aligned} \tag{II-73}$$

for even modes

$$\begin{aligned} Q_e(y) &= \cos(qy/b) && |y/b| \leq \zeta \\ &= \cos(q\zeta)\exp[-q\tan(q\zeta)(|y/b|-\zeta)] && |y/b| \geq \zeta \end{aligned} \tag{II-74}$$

and odd modes

$$Q_o(y) = \sin(qy/b) \qquad |y/b| \leq \zeta$$

$$= \sin(q\zeta)\exp[q\operatorname{ctan}(q\zeta)(|y/b|-\zeta)] \qquad |y/b| \geq \zeta$$

(II-75)

Actually, we choose the trial functions in this form so as to allow the fields and their derivatives to be continuous at each boundary and matching point Of the variables in the trial functions, a, b are the effective diffusion depths in the depth and lateral directions respectively; p, σ, ξ, q, ζ are all variational parameters. Since we choose a single function form here instead of a sum of orthogonal functions (Rayleigh-Ritz Procedure), as in some earlier work [15-16], to determine these parameters, a nonlinear optimization routine should be employed. In fact, the single form trial function not only provides a better approximation for the fundamental (and low order) modal field of the diffused waveguide, but also enable us to obtain an analytical expression of the coupling coefficient which can be more easily interpreted physically for the multi-waveguide coupling problems.

Substituting the field trial functions and index distribution function (II-62) into the variational expression of the scalar wave equation (II-70), we obtain

$$\beta^2 = k_o^2 n_b^2 + 2k_o^2 n_b \Delta n \frac{I_{x1} I_{y1}}{I_x I_y} - \frac{I_{x2}}{I_x} - \frac{I_{y2}}{I_y} - k^2(n_b^2-1)\frac{I_{x3}}{I_x}$$

(II-76)

where $I_x = \int_{-\infty}^{\infty} P^2(x)dx$, $I_y = \int_{-\infty}^{\infty} Q^2(y)dy$, $I_{x1} = \int_{-\infty}^{0} f(x/a)P^2(x)dx$, $I_{y1} = \int_{-\infty}^{\infty} g(y/b)Q^2(y)dy$, $I_{x2} = \int_{-\infty}^{\infty} (\frac{\partial P}{\partial x})^2 dx$, $I_{y2} = \int_{-\infty}^{\infty} (\frac{\partial Q}{\partial x})^2 dy$ and $I_{x3} = \int_{0}^{\infty} P^2(x)dx$.

For the index profile we discussed in the last section, nearly all of these integrals are analytically integrable which reduce the computing time significantly (see Appendix).

By the perturbation approach, i.e. by employing the trial function used in scalar analysis as a "zero" order solution to the vector wave equation (II-9), the discrepancy between different polarization modes can be distinguished by the first-order vector corrections:

$$\beta^2_{TE} \approx \beta^2_o - \frac{\iint_s \phi \frac{\partial \phi}{\partial y} \frac{\partial}{\partial y} \ln n^2(x,y)\, dxdy}{\iint_s |\phi|^2\, dxdy} \tag{II-77}$$

and

$$\beta^2_{TM} \approx \beta^2_o - \frac{\iint_s \phi \frac{\partial \phi}{\partial x} \frac{\partial}{\partial x} \ln n^2(x,y)\, dxdy}{\iint_s |\phi|^2\, dxdy} \tag{II-78}$$

for TE and TM modes respectively. In deriving (II-76) and (II-77), equations (II-9) and (II-69) have been used. As for the effect of the step index change on the waveguide surface, the term $(\partial n^2/\partial x)/n^2$ gives a delta function so that the integral in the numerator of (II-77) becomes

$$\sin(2p\sigma)\ p/2a \int_{-\infty}^{\infty} \frac{n^2(0,y)-1}{n^2(0,y)} Q^2(y)dy \tag{II-79}$$

It is worth noting that, in a direction of the refractive index decrease, the slope of ϕ is negative so that the integrand in the numerators of (II-76) and (II-77) remains nonnegative. Therefore, the polarization correction always reduces the magnitude of the propagation constants obtained from the scalar analysis.

With the same channel waveguide structure as in the last section, we present the analytical results in Fig. 8 (a)-(b) together with the EIM analysis. In order to examine the reliability of our analysis, for the slab case, we compare the variational results with the exact solution by the transverse resonance method. An excellent agreement is observed even in the vicinity of cutoff. For the channel guides, the variational analysis provides an apparent improvement around the cutoff region compared to the effective index method. Also, both methods show very good agreement in the region far from cutoff. Fig. II-9 gives an approximate model field distribution contour for channel waveguide produced by the variational technique.

For the wide, i.e. large aspect ratio R, channel waveguides, the diffusion depth is comparatively small compared with the waveguide width. The side diffusion effects are, hence, insignificant to the waveguide properties. Therefore, the 1-D diffusion approximation (i.e., $g(y)\approx 1$) provides very good approximation [11]. However, for the waveguide aspect ratio $R=0.5$, and 2, we find that two dimensional diffused channel waveguides have quite different dispersion properties from the one dimensional diffused channel waveguides (Figs. II-10, II-11 and II-12). And, because of the side diffusion effects, the waveguide dispersion properties varied by channel width are much more gentle than the step index profile (no diffusion in the y direction) waveguides. As a matter of fact, this property is determined by the lateral index distribution function $g(y)$. Fig. II-13 shows an example, by keeping the diffusion depth $d=6\mu m$, the diffused channel waveguide index distribution is almost unchanged as the channel width varies from $w=6\mu m$ to $w=3\mu m$. Therefore, for the aspect ratio $R=w/d_x<1$ diffused channel waveguides, the side diffusion effects can not be ignored (see Fig. II-10).

II-7. Conclusion

In this Chapter, we have discussed some approximate and numerical methods used for studying the arbitrary index distribution of optical planar and channel waveguide problems. Under the weakly guiding condition, the glass integrated optical device designs and analysis can be well performed with these techniques from the engineering viewpoint.

Appendix:

Substituting the trial functions (II-72) to (II-74) into the variational expression (II-70), for the index profile function as discussed in Section II-5, the integrals used in the equation become

$$I_x=\int_{-\infty}^{\infty} P^2(x)dx = \frac{a}{2p}\{\xi p+ctan(p\sigma)+ctan(p[\xi-\sigma])\}$$

$$I_{x1}=\int_{-\infty}^{0} f(x/a)P^2(x)dx = \frac{a\sqrt{\pi}}{2}\cos^2(p[\xi-\sigma])\exp(t^2+2\xi t)\mathrm{erfc}(\xi+t) + I_{f1}$$

$$I_{x2}=\int_{-\infty}^{\infty} (\frac{\partial P}{\partial x})^2 dx = \frac{\xi p^2}{2a}$$

$$I_{x3}=\int_{0}^{\infty} P^2(x)dx = \frac{a\cos^2(p\sigma)}{2p\tan(p\sigma)}$$

where $t=p\tan(p[\xi-\sigma])$ and $I_{f1}=\int_{\xi a}^{0}\cos^2(p[x/a-\sigma])\exp(-x^2/a^2)dx$ which should be evaluated numerically. For the even mode,

$$I_{y}=\int_{-\infty}^{\infty} Q^2(y)dy = \zeta b+\frac{b}{q}\mathrm{ctan}(q\zeta)$$

$$I_{y1}=\int_{-\infty}^{\infty} g(y/b)Q^2(y)dy = 2\int_{0}^{\infty} g(y/b)Q^2(y)dy = 2b(I_{g1}+I_{g2})$$

$$I_{y2}=\int_{-\infty}^{\infty} (\frac{\partial Q}{\partial y})^2 dy = q^2\zeta/b$$

where $I_{g2}=\int_{\zeta}^{\infty} g(y')\cos^2(q\zeta)\exp[-2q\tan(q\zeta)(y'-\zeta)]dy'$ and $I_{g1}=\int_{0}^{\zeta} g(y')\cos^2(qy')dy'$ could be evaluated numerically because $\mathrm{erf}(y')$ 1 when $y'>6$. Similarly, for odd mode

$$I_{y}=\int_{-\infty}^{\infty} Q^2(y)dy = \zeta b-\frac{b}{q}\tan(q\zeta)$$

$$I_{y1}=\int_{-\infty}^{\infty} g(y/b)Q^2(y)dy = 2\int_{0}^{\infty} g(y/b)Q^2(y)dy = 2b(I_{g1}+I_{g2})$$

$$I_{y2}=\int_{-\infty}^{\infty} (\frac{\partial Q}{\partial y})^2 dy = q^2\zeta/b$$

where $I_{g2}=\int_{\zeta}^{\infty} g(y')\sin^2(q\zeta)\exp[-2q\tan(q\zeta)(y'-\zeta)]dy'$ and $I_{g1}=\int_{0}^{\zeta} g(y')\sin^2(qy')dy'$ can also be evaluated numerically.

References:

[1] R V. Ramaswamy and R. Srivastava, "Ion-exchanged glass waveguides: a review", J. Lightwave Technol., vol. LT-6, pp. 984-1001, 1988.

[2] N Mabava, P. E. Lagasse and P Vandenbulcke, "Finite element analysis of optical waveguides", IEEE Trans. Microwave Theory Tech., vol. MTT-29, pp. 600-605, 1981.

[3] S M. Saad, "Review of numerical methods for the analysis of arbitrarily-shaped microwave and optical dielecrtic waveguides", IEEE Trans. Microwave Theory Tech., vol. MTT-33, pp. 894-899, 1985.

[4] J Ctyroky, M Hofman, J. Janta and J. Schrofel, "3-D analysis of $LiNbO_3$ Ti channel waveguides and directional couplers", IEEE J. Quantum Electron., vol. QE-20, pp. 400- 409, 1984.

[5] C. M. Kim and R. V. Ramaswamy, "WKB analysis of asymmetric directional couplers and its application to optical switches", J. Lightwave Technol., vol. LT-6, pp. 1109-1118, 1988.

[6] M. J. Adams, "An introduction to optical waveguides", John Wiley & Sons, New York, 1981.

[7] G. B. Hocker and W. K. Burns, "Modes in diffused optical waveguides of arbitrary index profile", IEEE J. Quantum Electron., vol. QE-11, pp. 270-276, 1975.

[8] R. E. Collin, "Foundations for microwave engineering", McGraw-Hill, New York, 1966.

[9] E. F. Kuester and D. C. Chang, "Propagation, attenuation and dispersion characteristics of inhomogeneous dielectric slab waveguides", IEEE Trans. Microwave Theory Tech., vol. MTT-23, pp 98-106, 1975.

[10] G. G. Bach, Course notes on "Numerical analysis", Mechanical Engineering Department, McGill University, 1982.

[11] G. B. Hocker and W. K. Burns, "Mode dispersion in diffused channel waveguides by the effective index method", Appl Opt., vol. 16, pp. 113-118, 1977.

[12] C. M Kim, B. G. June and C. W. Lee, "Analysis of dielectric rectangular waveguide by modified effective-index method", Electro. Lett., vol. 22, No. 6, pp. 296-298, 1986.

[13] H. A. Haus, W. P. Huang and N. M. Whitaker, "Optical waveguide dispersion characteristics from the scalar wave equation", J Lightwave Technol., vol. LT-5, pp. 1748-1754, 1987.

[14] P. K. Mishra and A. Sharma, "Analysis of single mode inhomogeneous planar waveguides", J. Lightwave Technol., vol. LT-4, pp. 204-212, 1986.

[15] H. F. Taylor, "Dispersion characteristics of diffused channel waveguides", IEEE J. Quantum Electron., vol. QE-12, pp. 748-752, 1976.

[16] R. A. Sammut and A. W. Snyder, "Graded monomode fibers and planar waveguides", Electron. Lett., vol.16, pp. 32-33, 1980.

Table II-2. The Effective Indices of Cladded Diffused Waveguides (TM Mode)

1.55μm			1.31μm			t
Exact(TRM)	WKB	Error	Exact(TRM)	WKB	Error	
1.499559	1.499272	.000287	1.503213	1.502947	.000267	0.0
1.499705	1.499409	.000295	1.503376	1.503107	.000268	0.1
1.499836	1.499531	.000305	1.503517	1.503237	.000280	0.2
1.499949	1.499641	.000308	1.503631	1.503346	.000285	0.3
1.500042	1.499730	.000312	1.503719	1.503437	.000281	0.4
1.500116	1.499798	.000318	1.503783	1.503496	.000286	0.5
1.500173	1.499857	.000316	1.503829	1.503544	.000285	0.6
1.500215	1.499893	.000322	1.503861	1.503569	.000293	0.7
1.500248	1.499927	.000320	1.503884	1.503592	.000292	0.8
1.500271	1.499952	.000320	1.503899	1.503609	.000290	0.9
1.500289	1.499969	.000320	1.503910	1.503620	.000290	1.0
1.500301	1.499978	.000323	1.503917	1.503627	.000290	1.1
1.500311	1.499984	.000327	1.503922	1.503633	.000289	1.2
1.500317	1.499991	.000326	1.503925	1.503636	.000289	1.3
1.500322	1.499996	.000326	1.503927	1.503638	.000289	1.4
1.500325	1.500000	.000325	1.503929	1.503640	.000289	1.5
1.500328	1.500003	.000325	1.503930	1.503641	.000289	1.6
1.500329	1.500005	.000325	1.503930	1.503642	.000289	1.7
1.500331	1.500006	.000325	1.503931	1.503642	.000289	1.8
1.500332	1.500007	.000325	1.503931	1.503643	.000289	1.9
1.500332	1.500008	.000325	1.503931	1.503643	.000288	2.0

Remark:

Fabrication Technique: K^+-N_a^+ ion exchange

Diffusion Time: 170 min

t: cladding thickness (μm)

Cladding Material: SiO_2

Substrate: Soda-Lime

	1.55μm	1.31μm
Cladding Index:	1.44403	1.44679
Substrate Index:	1.49806	1.50104
Surface Index:	1.50664	1.50961

Table II-1. The Effective Indices of Cladded Diffused Waveguides (TE Mode)

1.55μm			1.31μm			t
Exact(TRM)	WKB	Error	Exact(TRM)	WKB	Error	
1.499130	1.498862	.000268	1.502684	1.502463	.000222	0 0
1.499235	1.498959	.000276	1.502805	1.502577	.000228	0.1
1.499325	1.499041	.000284	1.502904	1.502672	.000231	0.2
1.499398	1.499110	.000287	1.502979	1.502744	.000236	0 3
1.499456	1.499164	.000292	1.503035	1.502793	.000242	0.4
1.499501	1.499207	.000294	1.503075	1.502836	.000239	0.5
1.499535	1.499239	.000296	1.503104	1.502865	.000239	0.6
1.499560	1.499265	.000296	1.503124	1.502882	.000242	0.7
1.499579	1.499278	.000301	1.503137	1.502892	.000245	0.8
1.499593	1.499293	.000300	1.503146	1.502902	.000244	0 9
1.499603	1.499303	.000300	1.503153	1.502909	.000244	1.0
1.499610	1.499311	.000299	1.503157	1.502914	.000243	1.1
1.499616	1.499316	.000299	1.503160	1.502917	.000243	1.2
1.499620	1.499320	.000299	1.503162	1.502919	.000243	1.3
1.499622	1.499323	.000299	1.503163	1.502920	.000243	1.4
1.499624	1.499325	.000299	1.503164	1.502921	.000243	1.5
1.499626	1.499327	.000299	1.503165	1.502922	.000243	1.6
1.499627	1.499328	.000299	1.503165	1.502922	.000243	1.7
1.499628	1.499328	.000299	1.503166	1.502923	.000243	1.8
1.499628	1.499329	.000299	1.503166	1.502923	.000243	1.9
1.499629	1.499329	.000299	1.503166	1.502923	.000243	2.0

Remark:

Fabrication Technique: K^+-N_a^+ ion exchange

Diffusion Time: 170 min

t: cladding thickness (μm)

Cladding Material: SiO_2

Substrate: Soda-Lime

	1.55μm	1.31μm
Cladding Index:	1.44403	1.44679
Substrate Index:	1.49806	1.50104
Surface Index:	1.50664	1.50961

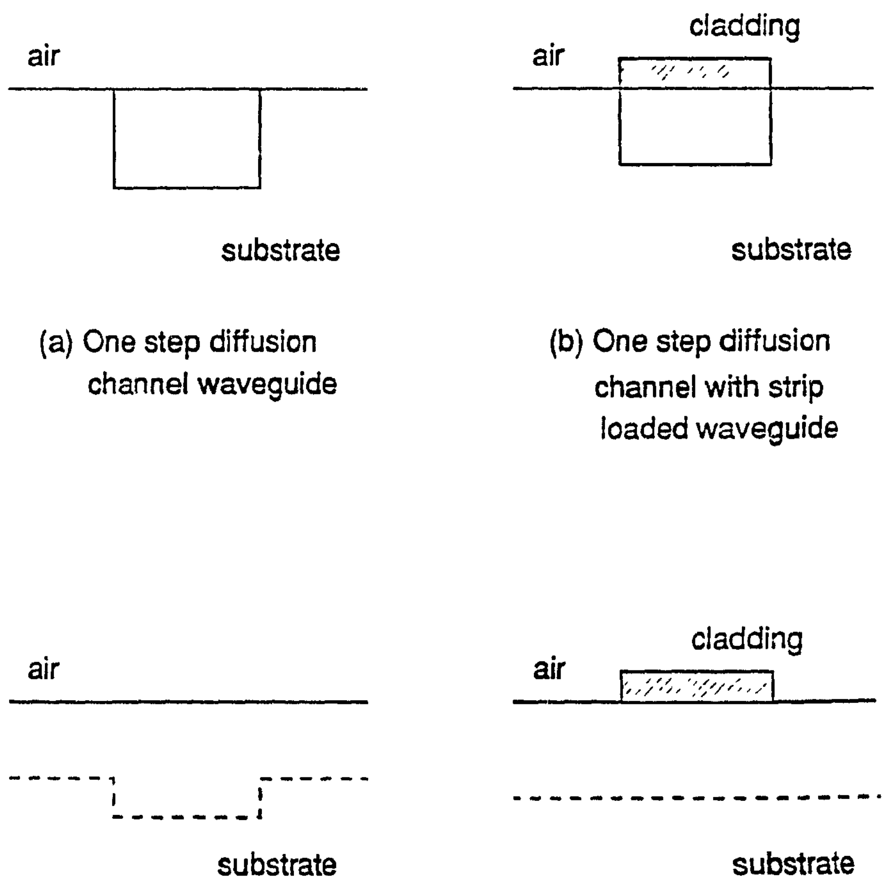

(a) One step diffusion channel waveguide

(b) One step diffusion channel with strip loaded waveguide

(c) Two step diffusion waveguide

(d) Strip cladded diffusion waveguide

Fig. II-1 Cross sections of typical diffused optical channel waveguides

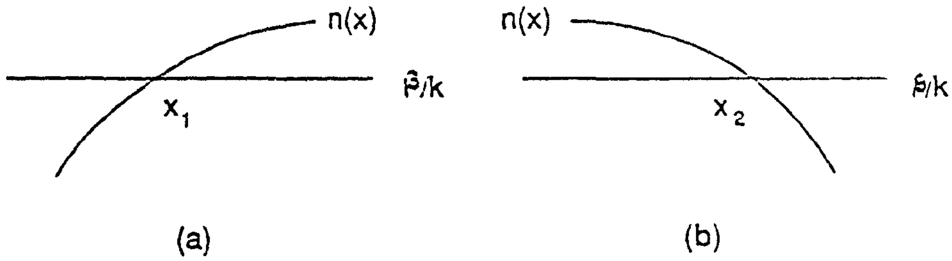

Fig. II-2. Turning point for a mode in smoothly varying index:
(a) increasing index profile,
(b) decreasing index profile.

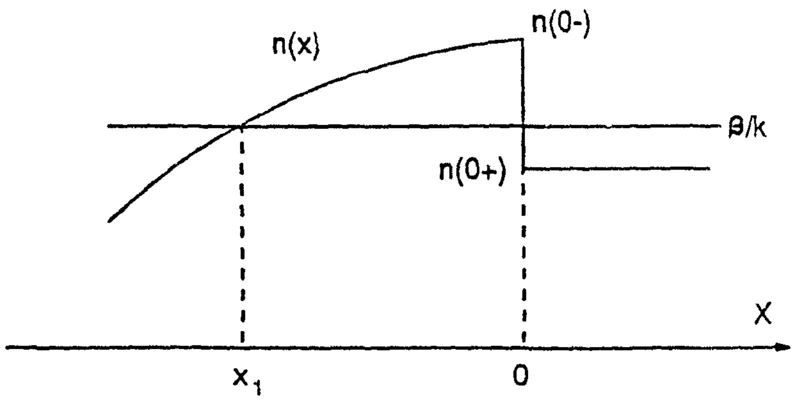

Fig. II-3. The case of an index discontinuity occurring at the caustic x=0.

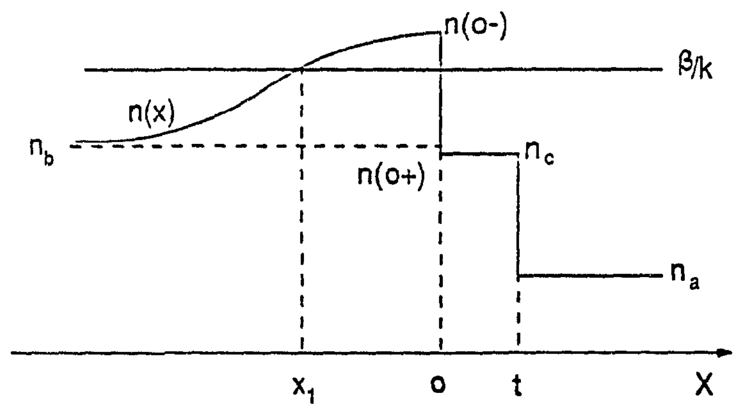

Fig. II-4. The index profile for the cladded diffused surface waveguide, where t is the cladding thickness.

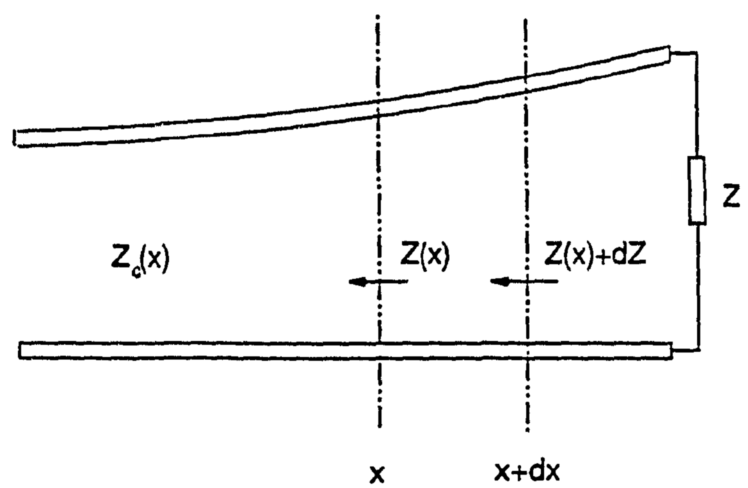

Fig. II-5. The graded characteristic impedance transmission line.

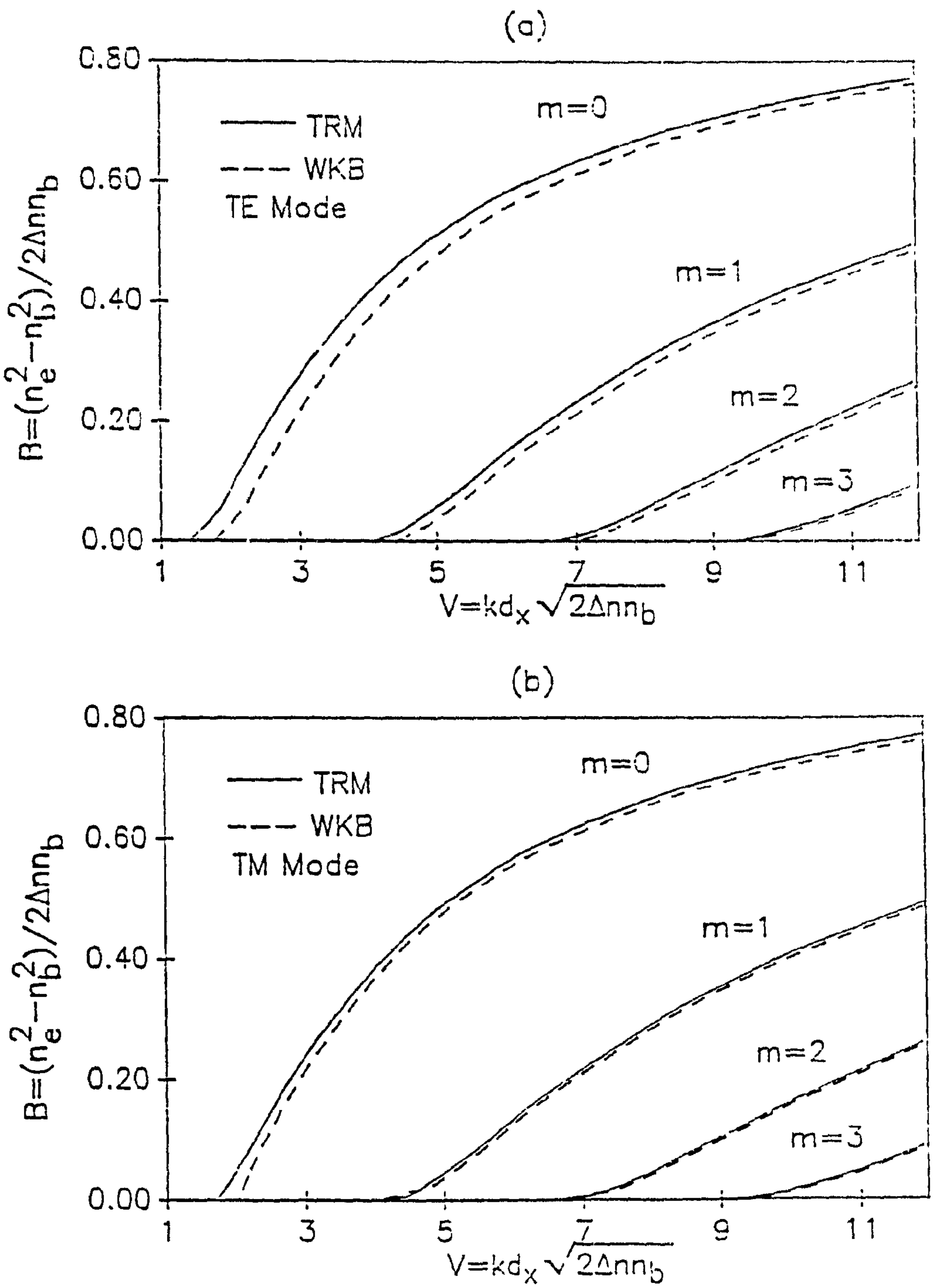

Fig. II-6. Comparison between TRM (exact) and WKB solutions for the diffused surface waveguide dispersion properties. (a) TE modes; (b) TM modes, where $n_e=\beta/k$. The index profile is assumed as in Eq. II-41.

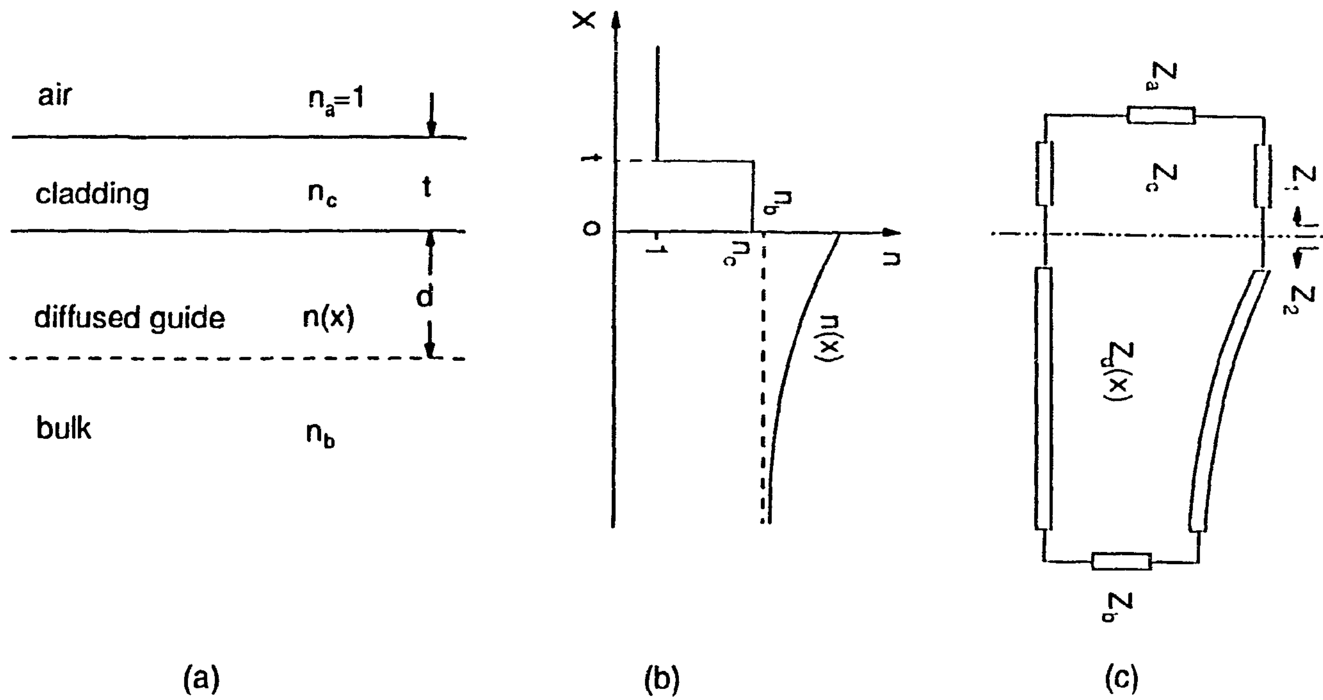

Fig. II-7. Cladded diffused surface waveguides. (a) Waveguide structure; (b) Index distribution; (c) Equivalent transmission line circuit.

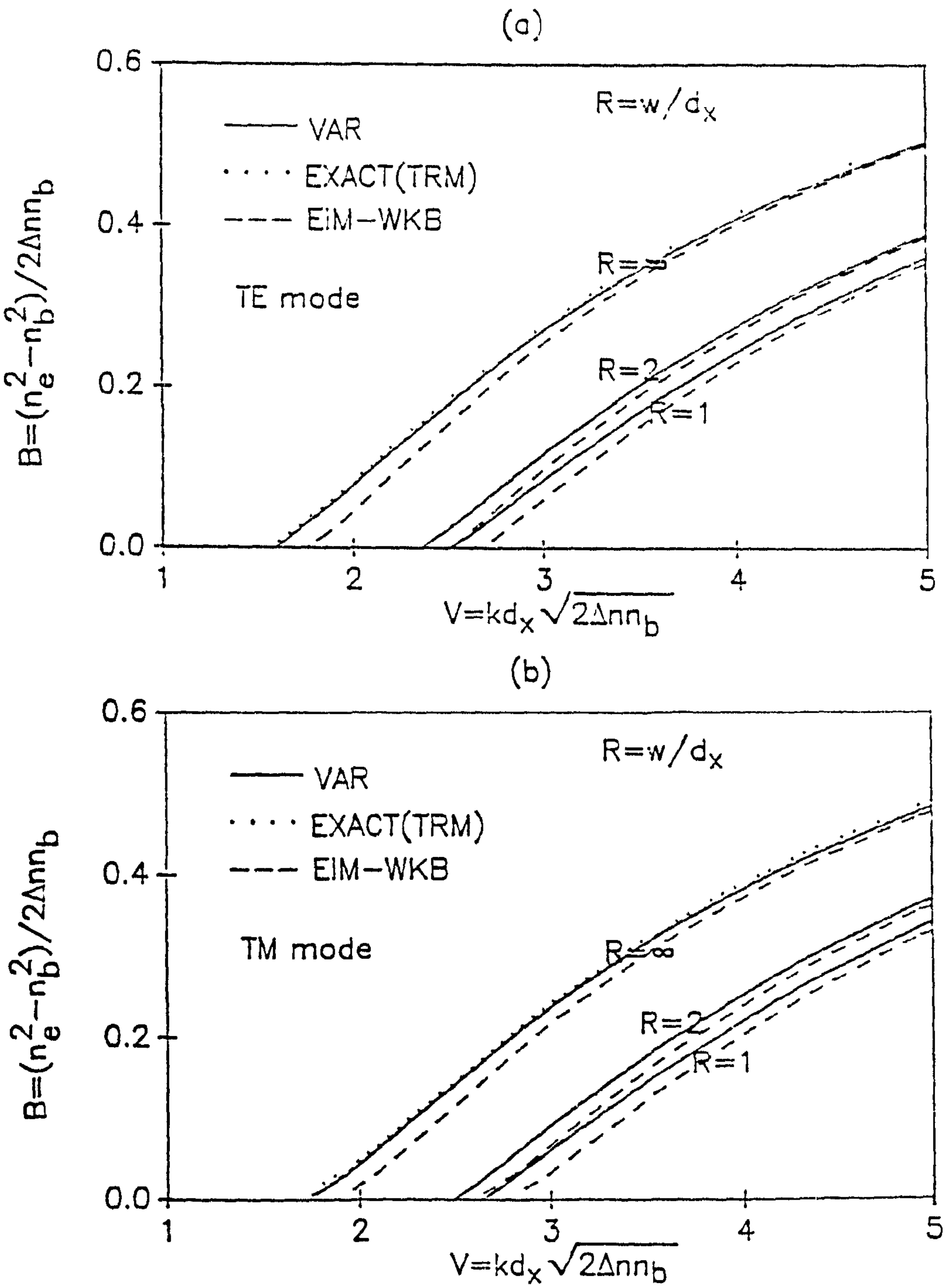

Fig. II-8. The dispersion properties of the 2-D diffused channel surface waveguides. (a) TE modes; (b) TM modes, where $n_e=\beta/k$. The index profile is assumed as in Eq. II-62.

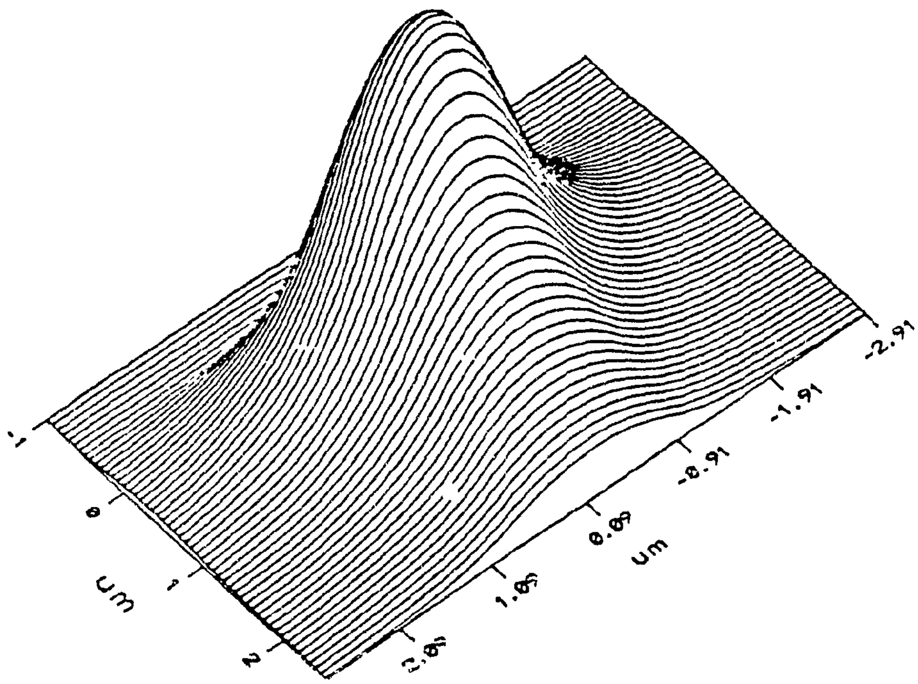

Fig. II-9. The approximate modal field pattern for a channel waveguide produced by the scalar variational technique.

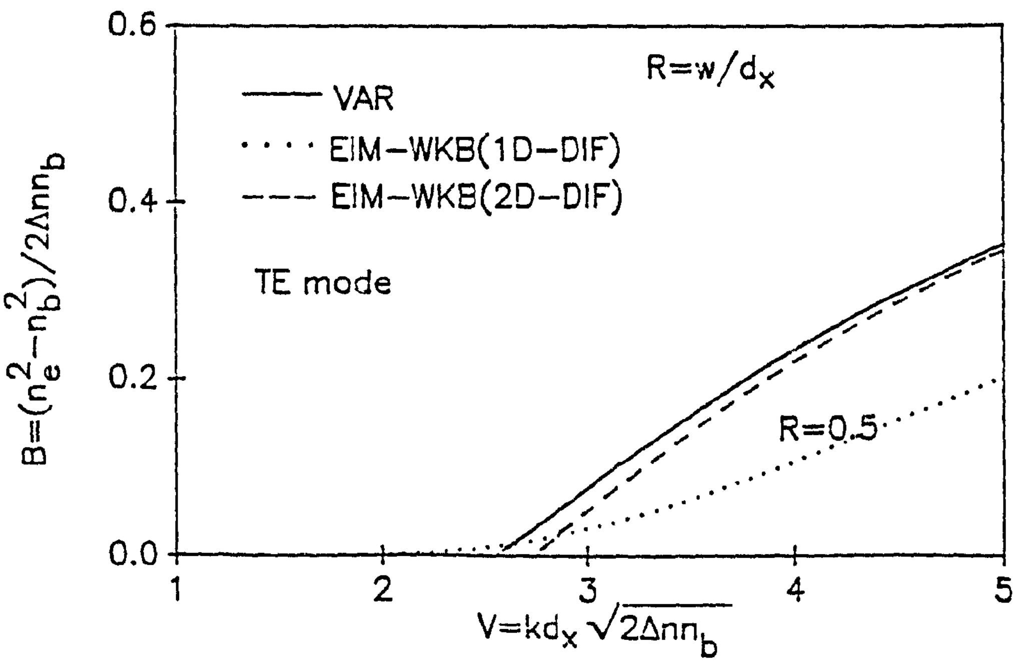

Fig. II-10. The dispersion property comparisons between the 1-D and 2-D diffused channel waveguides with aspect ratio *R=0.5*, where $n_e=\beta/k$.

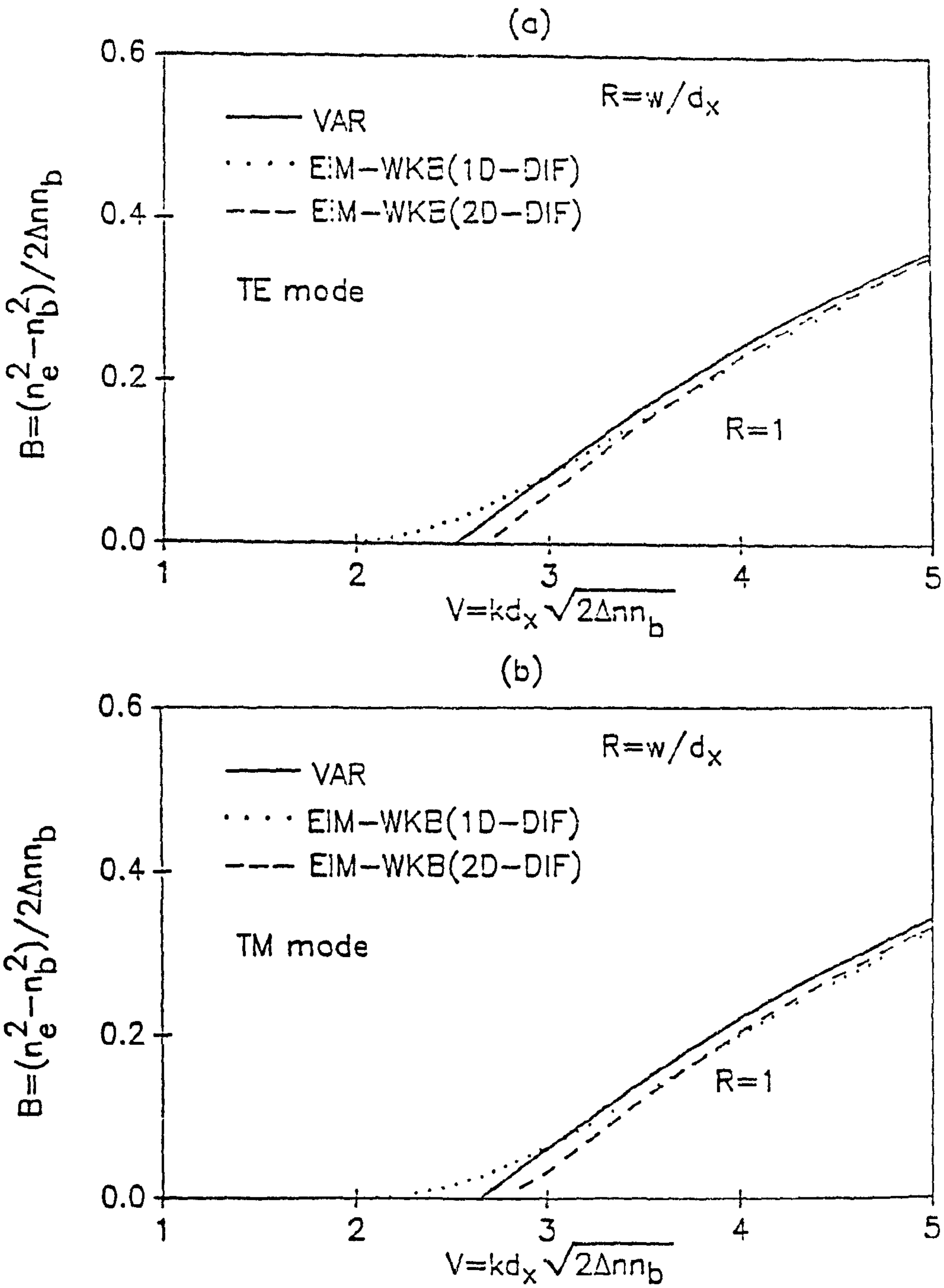

Fig. II-11. The dispersion property comparisons between the 1-D and 2-D diffused channel waveguides with aspect ratio *R=1.* (a) TE modes; (b) TM modes, where $n_e = \beta/k$.

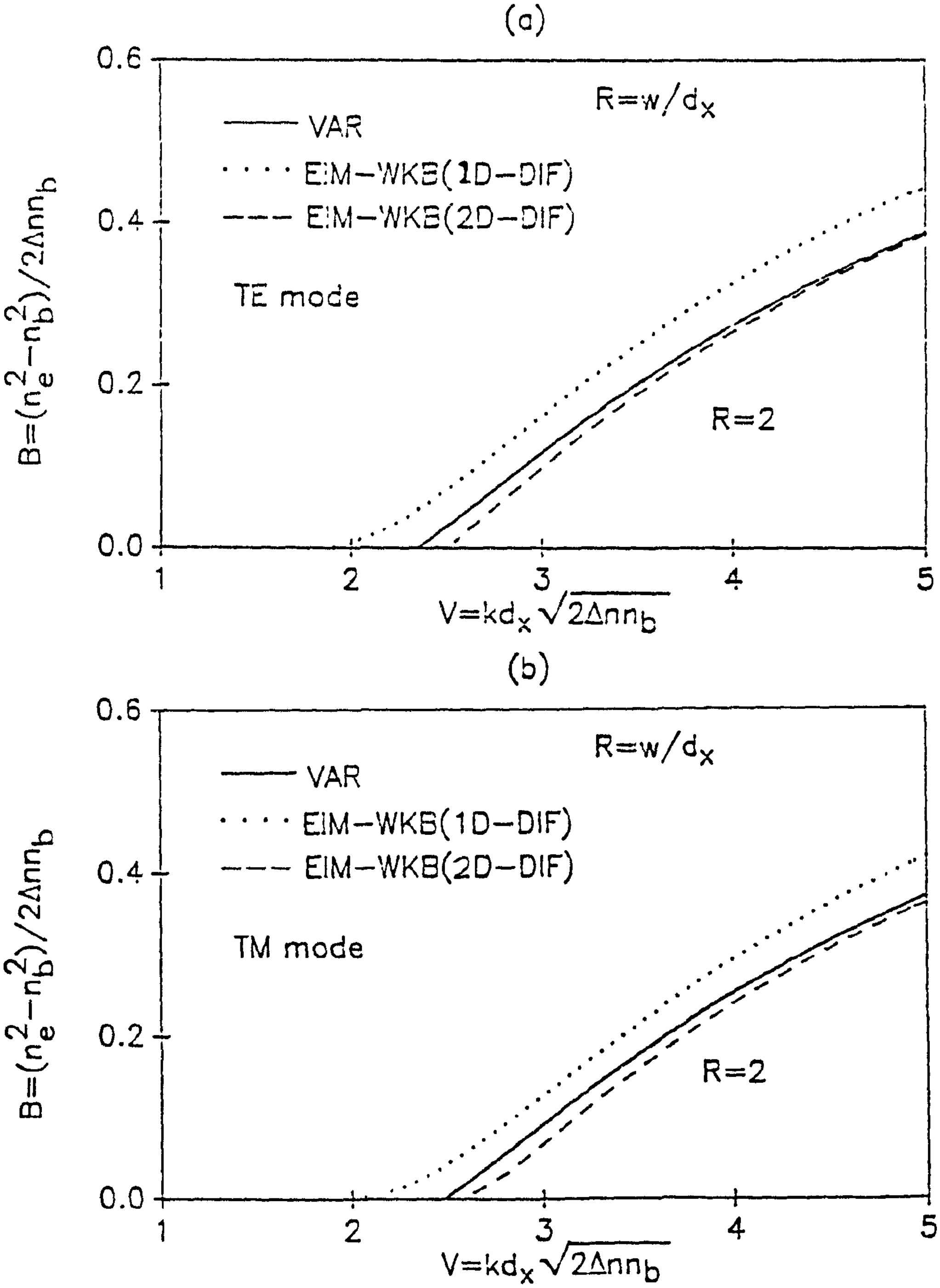

Fig. II-12. The dispersion properties comparison between the 1-D and 2-D diffused channel waveguides with aspect ratio R=2. (a) TE modes; (b) TM modes, where $n_e=\beta/k$.

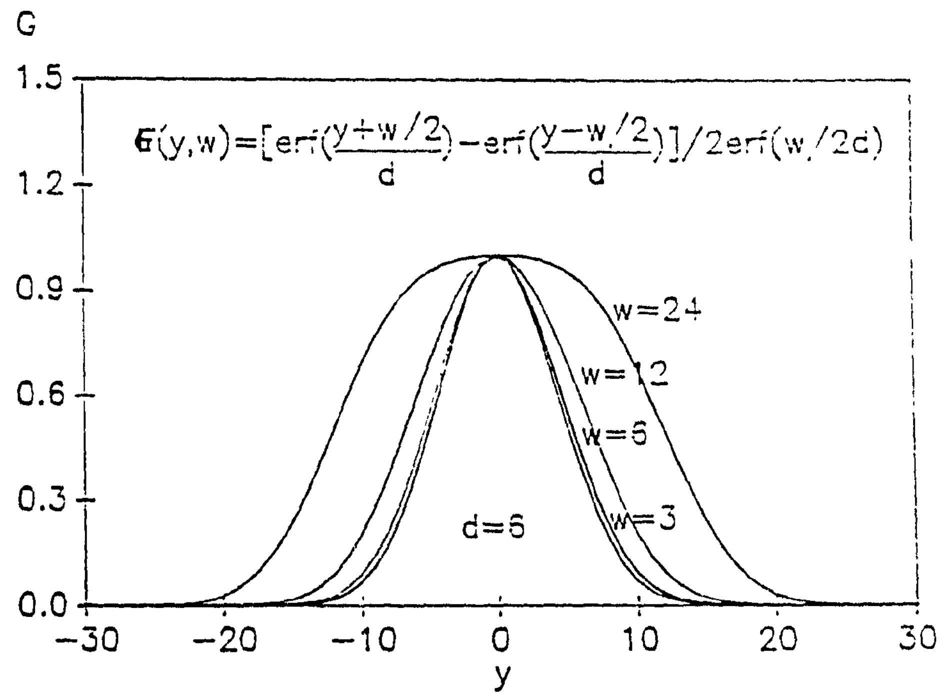

Fig. II-13. The lateral index distribution function of the 2-D diffused surface channel waveguides.

CHAPTER III

DESIGNS OF A SINGLE-MODE X-BRANCH TYPE DEMULTIPLEXER

III-1. Introduction

Since first proposed as a TIR device in 1978 [1], the X- branch waveguides, either symmetric or asymmetric, have been extensively studied in a number of publications [2-3]. Especially, in single mode integrated optics, the X-branch has become a competitive structure with the directional coupler in many device designs. Most of these devices offer important performance advantages such as a low insertion loss, high extinction ratio, small device dimension, moderate drive voltage, simple electrode configuration and etc.. Therefore, it has led to the possibility of more truly integrated optical circuits [4-5].

Optical multi/demultiplexers are essential components for the Wavelength-Division-Multiplexing (WDM) optical fiber communication systems, which can transmit different channels of modulated signals simultaneously. The device functions are to combine and separate the wavelengths carrying different information channels. Because of their compact structures, ruggedness with simplified assembly and planar fabrication technology, integrated optical WDM devices are particularly attractive for single-mode fiber system [6-9].

In this chapter, we will use the X-branch waveguide structure to design a single-mode dual-channel integrated optical multi/ demultiplexer which can be fabricated on soda-lime glass by using single-step ion-exchange techniques [10]. The theoretical background of the device is introduced in Section III-2. Under the effective index method approximation, the dispersion equation for studying the X-branch waveguide properties is derived in Section III-3. Then, detailed device property studies and design considerations will be carried out in Section III-4. Lastly, some further improvements are discussed in Section III-5.

III-2. Device Operation Principle

As shown in Fig. III-1, the principle of the X-branch type single-mode WDM device is based on the wavelength-dependent two- mode interference in a two-mode waveguide, which is adiabatically coupled to the single-mode input and output waveguides by tapered directional couplers. The two-mode region of WDM waveguide can be designed to consist of a higher refractive index central region with an approximately doubled index increase, or a wider central region with an approximately doubled waveguide width. In any case, for optimum operation, the central region must contain two guided modes of each polarization. In such a waveguide system, due to the adiabatic coupling, an input signal from one of the arms can be converted into two normal modes (one symmetric and another antisymmetric). Propagating through the symmetric entrance taper, two-mode center region, and then the symmetric exit taper again, these two normal modes do not exchange energy along the device, i.e.

$$\int_S \psi_s(x,y,z)\psi_a(x,y,z)dxdy = 0 \tag{III-1}$$

because the symmetric mode ψ_s is orthogonal to the antisymmetric mode ψ_a at any cross section z.

However, since the two normal modes have different propagation constants, a phase difference is accumulated. The output state of the coupled guide structure is determined by the interference of these two modes [11]

$$P_{=}/P_{in} = 2(\alpha_s \alpha_a)\cos^2(\phi/2) + (\alpha_s - \alpha_a)^2/2 \tag{III-2}$$

$$P_{\times}/P_{in} = 2(\alpha_s \alpha_a)\sin^2(\phi/2) + (\alpha_s - \alpha_a)^2/2 \tag{III-3}$$

where P_{in} is the input power, α_s is the relative excitation amplitude of the symmetric mode ψ_s, and α_a is that of antisymmetric mode ψ_a.

The accumulated propagation phase difference ϕ is the sum of that in the converging and diverging region ϕ_t and in the two-mode center region ϕ_c

$$\phi(\lambda) = \phi_c(\lambda) + \phi_t(\lambda) = \Delta\beta_c(\lambda)L + \int_{\substack{\text{taper}\\ \text{region}}} \Delta\beta_t(\lambda,z)dz \tag{III-4}$$

with $\Delta\beta_t = \beta_{st}(\lambda,z) - \beta_{at}(\lambda,z)$, in the tapering region and $\Delta\beta_c = \beta_{sc}(\lambda) - \beta_{ac}(\lambda)$ in the center region, where β_s, β_a are the propagation constants of the symmetric and antisymmetric modes, respectively, and the subscript t denotes the taper region and c denotes the two-mode center region. The accumulated phase difference ϕ depends on the wavelength as a result of the different waveguide dispersions of the two modes. Near an operating wavelength λ_o, the modal dispersion may be approximated by

$$\Delta\beta_i(\lambda_o + \Delta\lambda) = \Delta\beta_i(\lambda_o) + \gamma_i \Delta\lambda \qquad i = t,\ c \tag{III-5}$$

where γ represents the differential waveguide dispersion at λ_o

$$\gamma_i = \left.\frac{\partial(\beta_s - \beta_a)_i}{\partial\lambda}\right|_{\lambda_o} \qquad i = t,\ c \tag{III-6}$$

From (III-5), the wavelength dependence of the phase difference in the two-mode center region can be approximated by

$$\phi_c(\lambda_o + \Delta\lambda) = \Delta\beta_c(\lambda_o + \Delta\lambda)L = \phi_{co} + \gamma_c \Delta\lambda L \tag{III-7}$$

where $\phi_{co} = \Delta\beta_c(\lambda_o)L$ is the relative phase difference at λ_o.

On the other hand, as will be shown in Section III-4, wavelength dependence of modal dispersion in the taper region is much smaller than that in the two-mode center region, i.e., ϕ_t is much less wavelength dependant than ϕ_c. Hence, the relative phase difference in the taper region can be approximated as being nearly wavelength independent compared with that in the center region:

$$\phi_t(\lambda_o+\Delta\lambda) \approx \phi_t(\lambda_o) \equiv \phi_{to} \tag{III-8}$$

(i.e., $\partial\phi_t/\partial\lambda \ll \gamma_c L$ near $\lambda=\lambda_o$).

Combining (III-2), (III-4), (III-5) and (III-8) and assuming the branch waveguides are sufficiently separated in the input and output flare, i.e., two α's will be nearly identical $\alpha_s \approx \alpha_a \approx 1/\sqrt{2}$ when one arm is excited, we can have

$$P_j/P_{in} = \cos^2\left(\frac{\pi}{2}\frac{\Delta\lambda}{\Delta\lambda_\pi} + \frac{\phi_{co}}{2} + \frac{\phi_{to}}{2} \right) \tag{III-9a}$$

where

$$\Delta\lambda_\pi=\pi/\gamma_c L \tag{III-9b}$$

From (III-9a) it can be seen that the channel separation, i.e., wavelength difference between ON and OFF wavelength, is mainly dependent on the waveguide length in the two-mode region and seems to have a nearly constant value of (III-9b) regardless of the branching angle.

In order to demultiplex the signal λ_1 and λ_2 which are input together from port *1*, i.e., export them to port *2* and *3* respectively, the total propagation phase differences should be:

$$\phi(\lambda_1) = \Delta\beta_c(\lambda_1)L + \phi_t(\lambda_1) = 2n\pi \tag{III-10}$$
$$\phi(\lambda_2) = \Delta\beta_c(\lambda_2)L + \phi_t(\lambda_2) = (2n+1)\pi \tag{III-11}$$

where n is a integral number. Therefore, the output states become:

$$P_=(\lambda_1)/P_{in}(\lambda_1) = cos^2[\phi(\lambda_1)/2] = cos^2[n\pi] = 1 \qquad \text{(III-12)}$$

$$P_x(\lambda_1)/P_{in}(\lambda_1) = sin^2[\phi(\lambda_1)/2] = sin^2[n\pi] = 0 \qquad \text{(III-13)}$$

and

$$P_=(\lambda_2)/P_{in}(\lambda_2) = cos^2[\phi(\lambda_2)/2] = cos^2[(n+1/2)\pi] = 0 \qquad \text{(III-14)}$$

$$P_x(\lambda_2)/P_{in}(\lambda_2) = sin^2[\phi(\lambda_2)/2] = sin^2[(n+1/2)\pi] = 1 \qquad \text{(III-15)}$$

These mean that the WDM devices operate like a bandpass filter to separate the signals λ_1 and λ_2 input from the same port *1* to different output ports *2* and *3*, respectively.

However, since the extinction ratios for the two signals λ_1 and λ_2 are described by the following formulas:

$$D(\lambda_1) = 10log_{10}(P_=/P_x) = 10log_{10}\{ctg^2[\phi(\lambda_1)/2]\} \qquad \text{(III-15)}$$

$$D(\lambda_2) = 10log_{10}(P_x/P_=) = 10log_{10}\{tg^2[\phi(\lambda_2)/2]\} \qquad \text{(III-16)}$$

any device parameter errors caused by fabrication deviations might degrade the extinction ratio seriously as:

$$\frac{dD(\lambda_1)}{d\phi} = \frac{20}{ln10} \times \frac{1}{sin[\phi(\lambda_1)]}$$

$$\text{(III-17)}$$

$$\frac{dD(\lambda_2)}{d\phi} = \frac{20}{ln10} \times \frac{1}{sin[\phi(\lambda_2)]}$$

$$\text{(III-18)}$$

since $sin\phi=0$ when $\phi=2n\pi$ and $\phi=(2n+1)\pi$. Therefore, in order to minimize the fabrication tolerance, the device properties via the structure parameters should be studied elaborately.

III-3. Dispersion Equation

For the symmetric X-branch waveguides, the analysis based upon the normal mode interference needs not refer to the modal field information because the condition (III-1) is satisfied. Therefore, as we have discussed in the last chapter, the effective index method provides a very good approximation to be applied. As shown in Fig. III-2, in the taper region, the branched waveguide is equivalent to a five-layer planar waveguide system with their respective effective indices Next, we apply the transverse resonance method to derive the normal modes' dispersion equations for this five layer planar waveguide system

In the five-layer waveguide system, because $\partial/\partial x=0$, for the TE modes, as we have discussed in Chapter II, these are

$$H_y = \frac{j}{\omega\mu_o}\frac{\partial E_x}{\partial z} \qquad \text{and} \qquad H_z = \frac{-j}{\omega\mu_o}\frac{\partial E_x}{\partial y} \tag{III-19}$$

and the local transverse wave impedances are defined as

$$Z^+ = -\frac{E_x^+}{H_z^+} \qquad \text{or} \qquad Z^- = \frac{E_x^-}{H_z^-} \tag{III-20}$$

where + means that the propagation is along the y direction and follows the right-hand screw rule with the tangential field components E_x and H_z.

The field solution for the five layer planar waveguide system (See Fig. III-3) can be expressed as

$$
\begin{aligned}
E_x &= E_1^- \exp(k_b y) && y \le 0 \\
&= E_2^+ \exp(-jk_e y) + E_2^- \exp(jk_e y) && 0 \le y \le w_2 \\
&= E_3^+ \exp(-k_b y) + E_3^- \exp(k_b y) && w_2 \le y \le w_2+p \\
&= E_4^+ \exp(-jk_e y) + E_4^- \exp(jk_e y) && w_2+p \le y \le w_2+p+w_4 \\
&= E_5^+ \exp(-k_b y) && w_2+p+w_4 \le y
\end{aligned}
$$

(III-21)

where

$$k_b=(\beta^2-n_b^2k^2)^{1/2} \qquad \text{and} \qquad k_e=(n_{ef}^2-\beta^2)^{1/2}$$

(III-22)

Therefore, the local transverse wave impedances in each region are

$$Z_1^+ = \frac{j\omega\mu_o}{k_b} = Z_1^-, \qquad Z_2^+ = \frac{\omega\mu_o}{k_e} = Z_2^-$$

(III-23)

and

$$Z_1^\pm = Z_3^\pm = Z_5^\pm, \qquad Z_2^\pm = Z_4^\pm$$

(III-24)

where the physical meaning of $Z_1^+=Z_1^-$ is that the media in which the light wave propagates are reciprocal. Therefore, according to the transmission line theory, at $y=0$, we have

$$Z_{in1}^L = Z_1^- = \frac{j\omega\mu_o}{k_b}$$

(III-25)

Since

$$Z_{in} = Z_c \frac{Z_l + Z_c tanh(jk_y y)}{Z_c + Z_l tanh(jk_y y)}$$

(III-26)

at $y=w_1$, we obtain

$$Z_{in2}^L = Z_2^- \frac{Z_{in1}^L + Z_2^- tanh(jk_e y)}{Z_2^- + Z_{in1}^L tanh(jk_e y)} = \frac{j\omega\mu_o}{k_e} \frac{k_e + k_b tan(k_e w_1)}{k_b - k_e tan(k_e w_1)}$$

(III-27)

and, at $y=w_1+p$,

$$Z_{in3}^L = Z_3^- \frac{Z_{in2}^L + Z_3^- tanh(k_b y)}{Z_3^- + Z_{in2}^L tanh(k_b y)}$$

$$= \frac{j\omega\mu_o}{k_b} \frac{[k_e+k_b tan(k_e w_1)]k_b + k_e[k_b-k_e tan(k_e w_1)]tanh(k_b p)}{k_e[k_b-k_e tan(k_e w_1)] + k_b[k_e+k_b tan(k_e w_1)]tanh(k_b p)}$$

$$= \frac{j\omega\mu_o}{k_b} \frac{2k_b k_e+(k_b^2+k_e^2)tan(k_e w_1)exp(-2k_b p)+(k_b^2-k_e^2)tan(k_e w_1)}{2k_b k_e-(k_b^2+k_e^2)tan(k_e w_1)exp(-2k_b p)+(k_b^2-k_e^2)tan(k_e w_1)}$$

(III-28)

On the other hand, at $y=w_1+p+w_2$,

$$Z^R_{in4} = Z_5^+ = \frac{j\omega\mu_o}{k_b}$$

(III-29)

and, at $y=p+w_1$

$$Z^R_{in3} = Z_4^+ \frac{Z^R_{in4} + Z_4^+ tanh(jk_e y)}{Z_4^+ + Z^R_{in4} tanh(jk_e y)} = \frac{j\omega\mu_o}{k_e} \frac{k_e + k_b tan(k_e w_2)}{k_b - k_e tan(k_e w_2)}$$

(III-30)

To satisfy the transverse resonance condition $Z^L_{in3}+Z^R_{in3}=0$, we have

$$\frac{j\omega\mu_o}{k_b} \frac{2k_b k_e+(k_b^2+k_e^2)tan(k_e w_1)exp(-2k_b p)+(k_b^2-k_e^2)tan(k_e w_1)}{2k_b k_e-(k_b^2+k_e^2)tan(k_e w_1)exp(-2k_b p)+(k_b^2-k_e^2)tan(k_e w_1)} + \frac{j\omega\mu_o}{k_e} \frac{k_e + k_b tan(k_e w_2)}{k_b - k_e tan(k_e w_2)} = 0$$

(III-31)

at $y=w_1+p$, that is,

$$\{2k_b k_e+(k_b^2-k_e^2)tan(k_e w_2)\}\{2k_b k_e+(k_b^2-k_e^2)tan(k_e w_1)\} - exp(-2k_b p)(k_b^2+k_e^2)^2 tan(k_e w_1)tan(k_e w_2) = 0$$

(III-32)

This is the dispersion equation for TE modes in the five layer planar waveguides. When $w_2=w_1=w$, i.e., the waveguide is symmetric, the above equation can be split into

$$2k_b k_e+(k_b^2-k_e^2)\tan(k_e w)-\exp(-k_b p)(k_b^2+k_e^2)\tan(k_e w) = 0 \tag{III-33}$$

for the even modes

$$2k_b k_e+(k_b^2-k_e^2)\tan(k_e w)+\exp(-k_b p)(k_b^2+k_e^2)\tan(k_e w) = 0 \tag{III-34}$$

for odd modes, respectively. Actually, because H_z and E_x equal to 0 at $y=w_1+p/2$ for TE even and odd modes, respectively, we can build up the equivalent boundary conditions as open and short circuits there for them respectively. By applying the transverse resonance condition again, the dispersion equations (III-33,34) can be verified directly by repeating the similar derivations as above.

Similarly, with the definitions of the local transverse wave impedance for TM modes as

$$Z_1^+= k_b/j\omega\varepsilon_o n_b^2 =Z_1^- \qquad Z_2^+= k_e/\omega\varepsilon_o n_{ef}^2 =Z_2^- \tag{III-35}$$

and

$$Z_1^\pm = Z_3^\pm =Z_5^\pm, \qquad Z_2^\pm = Z_4^\pm \tag{III-36}$$

we can obtain the dispersion equation for TM modes as

$$\{2g_b g_e+(g_b^2-g_e^2)\tan(k_e w_2)\}\{2g_b g_e+(g_b^2-g_e^2)\tan(k_e w_1)\}$$
$$-\exp(-2k_b p)(g_b^2+g_e^2)^2\tan(k_e w_1)\tan(k_e w_2) = 0 \tag{III-37}$$

where $g_b=k_b/n_b^2$ and $g_e=k_b/n_e^2$. If the waveguide is symmetric, i.e., $w_2=w_1=w$, for the even and odd modes, respectively, the dispersion equations are

$$2g_b g_e+(g_b^2-g_e^2)\tan(k_e w)-\exp(-k_b p)(g_b^2+g_e^2)\tan(k_e w) = 0 \tag{III-38}$$

and

$$2g_b g_e+(g_b^2-g_e^2)\tan(k_e w)+\exp(-k_b p)(g_b^2+g_e^2)\tan(k_e w) = 0$$

(III-39)

Same as the TE modes, the equivalent boundary conditions as short and open circuits can be built up respectively for TM even and odd modes at $y=w_1+p/2$ since E_y of even modes and H_x of odd modes are zero there. By satisfying the transverse resonance condition, the equations (III-38,39) can also be obtained independently.

It is worth mentioning that the same results can also be found in the literature [12] by the field-matching approach. However, for the multilayer dielectric waveguide problems, that approach requires the solution of a set of high order linear equations which is difficult to obtain as the layer number increases On the other hand, the transverse resonance method provides an easier manner to derive the dispersion equations as shown above in spite of the layer number increasing

III-4. Design Considerations

As we mentioned in the Section III-2, when we design the X-branch waveguides, there are two ways to obtain the two-mode region [11].

1) by doubling the index increase.
2) by doubling the guide width.

For the double index choice, since it makes a larger difference of the propagation constants between the symmetric and antisymmetric modes, the overall device length can be reduced. However, it also makes the output of the devices very sensitive to the induced refractive index perturbation. It may make the fabrication conditions more stringent. In fact, the required two-step processes might cause an index asymmetry during fabrication. Further, there may exist many modes in the intersection region as the index is doubled. Therefore, any unintentional fabrication error may cause the device performances to degrade [13]. Alternatively, using a wider width to replace the double refractive index in the intersection region might be simpler on fabrication since only one lithography and one ion-exchange step are involved. To be relatively free from asymmetry (since the device properties are mainly dependent on the two-mode center region), this approach could also be easier to get a better extinction ratio than that using the double index structures. For the soda-lime glass substrate, since the refractive index can not be adjusted by applying an electric field as in $LiNbO_3$ material, it would be better to choose the second method in the design and the eventual realization of this device.

According to the device configuration in Fig. III-1, the double width symmetric X-branch waveguide possesses four structure parameters: the waveguide width W, the waveguide diffusion depth d (or diffusion time t), two-mode interaction region length L, and the entrance and exit taper flare angle θ. Essentially for the dual channel WDM devices, three conditions have to be met. Namely, equations (III-10), (III-11) and n must be an integral number under the single-mode operation condition. Next, we are going to discuss the device property dependence on these parameters. All of the numerical analyses are based upon the ion exchange characterization data in reference [16] under the working temperature $T=385^{\circ}C$ (See Table III-1, in which $d=\sqrt{D_e t}$ and D_e is the effective diffsuion coefficient).

A. Effect of the taper flare angle

Fig. III-4 shows that the propagation constant differences between the symmetric and antisymmetric local normal modes decrease very rapidly as the separation between the two branch waveguides increases. It means that the contribution of the accumulated propagation phase differences are very small beyond the two-mode center region ($a/w=1$). Moreover, Fig. III-5 shows that the wavelength dependence of the accumulated phase difference ϕ_t (obtained from equation (III-4) where the taper region length for the integral is set as $l=p/2tg(\theta/2)$, $p=50\mu m$ is the separation between the two branches) is very small ($\Delta\phi_t/\Delta\lambda\approx 0.5\ rad/\mu m$) as we stated before. Comparatively, Fig. III-4 at $a/w=1$ also reveals that, in the two-mode center region, the wavelength dependence of the phase difference between the symmetric and antisymmetric modes is much more significant since L is long usually (around $3500\mu m$) and $\Delta\phi_c(\lambda)/\Delta\lambda=\Delta\beta_c(\lambda)L/\Delta\lambda\approx 14.6\ rad/\mu m$). Therefore, in order to minimize the device length, it would be better to choose the taper flare angle as large as possible. However, since K^+-ion exchanged surface waveguides are weakly guiding structures, too large a branching angle will generate the apparent radiation field. Therefore, a fuller investigation of this problem should employ some other numerical methods such as the Beam Propagation Method (Refer to Chapter IV).

Since the wavelength dependence of the accumulated phase difference in the taper region ϕ_t is small (See Fig. III-5), and as the branching angle varies, it changes almost the same amount for all wavelengths, especially for the larger flare angles. Therefore, the variation of the branching angle will result in nearly parallel shift of all the channel wavelengths while maintaining nearly constant channel separation $\Delta\lambda$ value (See Fig. III-6) [9]. This property is very interesting in considering the realization of cascaded multichannel WDM devices [14] especially in soda-lime glass substrates where no electrooptic tuning can be applied to effect the same shift.

Fig. III-7(a) shows a multichannel WDM structure constructed by cascading dual-channel demultiplexer with proper parameters, where the angle tuning is adopted. For the structure, it is convenient to let all individual X-branch waveguides have the same waveguide width and depth (for one step ion-exchange) in the design. As an example of multichannel WDM design, a four-channel Wavelength Division Multiplexer is shown in Fig. 7(b). The proper operation of this structure requires that the channel wavelengths of waveguide 1 and 2 should lie on the successive channel wavelengths of waveguide 3 as shown in Fig III-7(c). For example, waveguide 3 selects signales λ_2 and λ_4 to pass by waveguide 2 If the peak and node of the waveguide 2 transmission curve coincide with the peaks of the waveguide 3 transmission curve, then the signals λ_2 and λ_4 can be further separated to port P_2 and P_3, respectively. From the two-mode interference model expressed by equation (III-9b), we know that $\Delta\lambda_{\pi}$ is inversely proportional to the length of the center two-mode region. Hence, the channel separation of waveguide 3 can be half that of waveguides 1 and 2 if the center two-mode region of waveguide 3 is two times longer than that of waveguides 1 and 2. Again, by adjusting the flare angles of X-branch waveguide 1 and 2 to shift their channel wavelengths horizontally to the desired positions, the four channel wavelength division multiplexer can be constructed.

B. Effect of the waveguide width

The waveguide width is also an important parameter to determine the channel separation $\Delta\lambda$ of the WDM devices. Since the total accumulated phase difference arises mainly from the two-mode center waveguide region, we can approximately discuss the effect of width on the device dispersion properties by considering this region first.

Figs. III-8,9 show two typical channel waveguide dispersion curves by the width variations for the TE and TM modes respectively, where the heavy dark lines indicate the range in which waveguide supports two modes only for both wavelengths. From them, firstly, we can find that the propagation constant difference $\Delta\beta(\lambda)$ between the first two (even and odd) modes are increased as the waveguide width decreases. This means that narrower waveguide width for the two-mode center region produces larger propagation constant differences, hence resulting in shorter overall WDM device dimension. Secondly, the propagation constant difference at the longer wavelength is smaller than that at the shorter wavelength despite being nearer to cutoff. This is because the refractive index of glass at the longer wavelength is smaller than that at the shorter wavelength (material dispersion properties [15]). Therefore, for the K^{+}-ion exchanged glass surface waveguide, material dispersion has the stronger effects than the waveguide dispersion. Thirdly, the dispersion curves for the longer wavelength are much flatter than those for the shorter wavelength. According to the two-mode interference principle, we can expect that, as a WDM device, the output of the shorter wavelength will be more sensitive to the waveguide width deviations. To see this more clearly, some further results are presented in Figs. III-10-14 where all of the width variation ranges correspond to the case that two modes only are supported in the waveguide for either wavelength. It can be seen clearly that the $\Delta\beta$ courves for the shorter wavelength are almost all linear with large slopes Moreover, the longer the diffusion time is, the larger slopes they have.

By solving the equations (III-10) and (III-11), for a pair of given channel wavelengths after setting the diffused time t (i.e. the diffused depths d), the waveguide width of X-branch type demultiplexer can be uniquely determined. Since L is the same in both equations, we can substitute equation (III-10) into (III-11) then solve the resulting equation by a root-search technique. Hence, we can not choose the waveguide width arbitraryly to design a demultiplxer, given the diffused depths or vice versa. In the Figs. III-10-14, we use the vertical dash lines to show the solutions of waveguide width $2W$ for demultiplexers. It is worth noting that numerical calculations indicate, if we choose a too shallow waveguide deptn d (or a too short diffusion time t), there may not exist a proper width $2W$ to let n take an integer number for the given channel wavelength pair. Although the device parameter number is one more than the working condition number, these is still no vertical dash line in Fig. III-11 which means we can not find a proper solution for equations (III-10) and (III-11) within the two-mode working range

C. Effects of the Waveguide Parameter Errors

Since the propagation constant difference between symmetric and antisymmetric modes is small for both wavelengths in the X-branch waveguide (about $5\times10^{-3} rad/\mu m$), a few micron length error in the center two-mode waveguide would hardly cause any extinction ratio to degrad significantly in device output. The calculations show the length usually is about $3500\mu m$ long.

On the another hand, because the waveguide depth is determined by the ion diffusion time. According to our own characterization work of the K^+-ion exchanged in soda-lime glass substrates [16], we know that, in infrared region, the index profile in the depth direction can be expressed approximately as

$$n(x) = n_b + \Delta n_s \, exp(-x^2/d^2) \qquad \text{(III-40)}$$

where Δn_s=*0.010* or *0.009* for TM and TE modes respectively and are almost independent of the light wavelength, $d=(D_e t)^{1/2}$ is the effective diffusion depth, D_e is the effective diffusion coefficient which depends on the light wavelength and polarization. For example, under a working temperature $T=385C^\circ$, they are [16]

$D_e=0.06198(\mu m)^2/min$	for TE modes	
$D_e=0.06024(\mu m)^2/min$	for TM modes	at $\lambda=1.152\mu m$
$D_e=0.06918(\mu m)^2/min$	for TE modes	
$D_e=0.06762(\mu m)^2/min$	for TM modes	at $\lambda=1.523\mu m$

As to the data for the other wavelengths, they can be obtained by interpolation or extrapolation from them (See Table III-1). Therefore, a diffusion time error will cause the diffused waveguide index to differ from the design value, namely, cause the effective index errors of the equivalent waveguides in the effective index modeling (See Fig. III-2). Figs. III-15 show two computation sample results for $t=170min$ and $t=350min$ (For both times, the waveguides all support single depth mode at both wavelength $1.31\mu m$ and $1.55\mu m$). Because the derivative of $exp(-x^2/d^2)$ versus d is a monotonic decreasing function as $d=(D_e t)^{1/2}$ or t increase. The longer the diffusion time is, the smaller the index error is caused by the same amount of diffusion time deviation Δt, i.e., $\delta n_{ef}(t_1)>\delta n_{ef}(t_2)$ if $t_1<t_2$, where $\delta n_{ef}=n_{ef}(t+\delta t)-n_{ef}(t)$ and n_{ef} is the effective index of the equivalent channel waveguide (See Fig. III-2). It seems we can choose a longer diffusion time in design to gain the

fabrication tolerance on the diffusion time. However, as the refractive index of channel waveguide increases, in order to maintain the single mode operation in the branch waveguides, the channel width has to be narrower which will cause the width deviation to affect the extinction ratio more significantly. Therefore, a trade-off is necessary. In our design, we choose the diffusion time such that the device extinction ratio due to *±2min* diffusion time deviation will not decrease to less than *20dB* (See Fig. III-19). Since the effective diffusion coefficients are not the same for the different wavelengths, the device output extinction ratio degradations due to the same diffusion time deviations are also different. With the same amount of the diffusion time deviation, the longer channel wavelength always have more adverse effects. This is because the ratio $\delta n_{ef}/\Delta n_{ef}$ for the longer wavelength is larger than the shorter wavelength (See Table III-2), where $\Delta n_{ef}=n_{ef}-n_{b}$ is the refractive index difference between the channel and substrate (See Fig. III-2).

Employing the photolithography technique, due to the exposure and etching qualities, a *±0.3μm* width deviation of the channel waveguide is unavoidable in fabrication. Figs. III-16. present two design samples whose output extinction ratio degradations versus the width errors at both wavelengths. They show the degradations at $\lambda_1=1.31\mu m$ are always worse than those at $\lambda_2=1.55\mu m$. Actually, this is because, for $\lambda_1<\lambda_2$, $\frac{2\pi}{\lambda_1}>\frac{2\pi}{\lambda_2}$ and $\Delta n_{ef}(\lambda_1)>\Delta n_{ef}(\lambda_2)$, where $\Delta n_{ef}=n_{ef}-n_{b}$ (See Table III-2), therefore,

$$\frac{2\pi}{\lambda_1}\,\Delta n_{ef}(\lambda_1) > \frac{2\pi}{\lambda_2}\,\Delta n_{ef}(\lambda_2) \qquad \text{(III-41)}$$

Because $2\pi n_b/\lambda<\beta<2\pi n_{ef}/\lambda$, the dispersion curves for the longer wavelength are always flatter than those of the shorter wavelength (see Fig. III-8,9). Therefore, we can conclude that applying the two-mode interference principle to design the optical multi-/demultiplexer for any structure in glass substrates, the extinction ratio degradations caused by the width deivations at the shorter wavelength is always larger than that at the longer wavelength. It is very important to choose the correct design parameters so that the highest extinction ratios can be obtained in the absence of fabrication errors as designed. Otherwise, results as shown in Fig. III-17 would be obtained, implying that some deliberate fabrication error would yield higher extinction ratios

As for the asymmetry of the waveguide width in the branch region, since the device dispersion properties are determined mainly by the center two-mode region, it will not cause more adverse effect on the extinction ratio at the output [13]. Actually, this is also a main advantage of this structure over the directional coupler.

D. Effective Index Calculation.

In most of the integrated optics design, people usually apply the well-known WKB method to calculate the effective index. The WKB approximation is based upon the assumption that the variation of dielectric index is very small over a distance of optical wavelength order. From the discussions in the last chapter, we know that WKB method shows deviation from the TRM (exact) results around the fundamental mode cutoff region In calculating properties of waveguides by ion-exchange in the soda-lime glass in the infrared region, the WKB approximation yields an error within 1×10^{-4} in multimode region and around 2.5×10^{-4} in the single mode region (Refer to Fig. II-6). Although these can satisfy the design requirements for most of the single-mode integrated optics devices, they will cause larger design deviations for our X-branch type WDM device. Table III-3 gives an example to show the differences of the device design parameter values provided by WKB and transverse resonance methods, respectively. The reason for the surprising differences is mainly because the two-mode interference principle is used and our device length is quite long compared with the wavelengths, a small error in the effective index calculation (or $\Delta\beta$) will be amplified in ϕ, which is the accumulated phase difference over the device length. For example, by the channel width $2W=17.74\mu m$, the effective indices by WKB (see Table

III-3) give the propagation constant differences between the even and odd modes as $2.17\times10^{-3} rad/\mu m$ and $3.199\times10^{-3} rad/\mu m$ for the wavelengths $1.55\mu m$ and $1.31\mu m$, respectively. However, by the transverse resonance method, the propagation constant differences are obtained as $2.729\times10^{-3} rad/\mu m$ and $3.38\times10^{-3} rad/\mu m$ for the wavelengths $1.55\mu m$ and $1.31\mu m$, respectively. Multiplying the length $3464\mu m$, we will have accumulated phase differences as $\Delta\phi_{WKB}(1.55)= 7.5169rad$, $\Delta\phi_{WKB}(1.31)= 11.0813rad$ and $\Delta\phi_{TRM}(1.55)= 9.4532rad$, $\Delta\phi_{TRM}(1.31)= 11.7083rad$. The differences $\Delta\phi_{TRM}(1.55)-\Delta\phi_{WKB}(1.55)=1.9363rad$ is very large (over $\pi/2$). Hence, to have the same accumulated phase differences, a few hundred micron of length difference is expected. Besides, the longer the wavelength, the larger error the WKB approximation yields. This wavelength dependent effective index calculation errors also make the device parameter determinations differ more from the exact values since for WDM device equations (III-10) and (III-11) should be satisfied at the same time with n being 4 or 5 usually (for power divider $n=1$). Therefore, we decide to use the transverse resonance method in all of our design calculation and believe that all passive single-mode integrated optical device designs, based on the phase interference principle, should be carried out with caution.

III-5. Improvements

From the above design calculations and discussions, we know that fabricating a double width X-branch type WDM devices requires only one-step ion-exchange, hence, involving only one photolithographic process, which not only simplfies the fabrication process, but also reduce any asymmetry possibilities induced by a multi-step fabrication process. However, the above analyses show that the device dispersion properties are still very sensitive to the waveguide width deviations. From a practical viewpoint, less than $20dB$ channel isolations due to $\pm0.3\mu m$ width deviation is still too rigorous to realize under the present state of art. Hence, seeking a compensation method for the device fabrication is very necessary for obtaining good device performances. Similar problems also occurred in the directional coupler-type WDM device design [17], where the authors used the cladding deposition method to adjust the channel wavelength shift (or output extinction ratio degradations) due to the width deviations in fabrication As discussed above (see Fig. III-16(a)), under $\pm 0.3\mu m$ width deviation, the extinction ratio degradation of the longer channel wavelength is still acceptable and only that of the shorter channel wavelength needs to be improved. However, when the shorter channel wavelength shifting is improved by a cladding, the center wavelength at the longer channel wavelength needs to be adjusted also for the more significant effective index increment. Therefore, it is difficult to use a compensation method to improve the device properties for both wavelengths at the same time. Consequently, a cascaded structure (see Fig. III-18(a)) was proposed [17] to separate two signals first by coupler A, then compensate their wavelength shifts in couplers B and C separately. According to the discussion in reference [18], to function as multi/demultiplexers, this configuration can also have the advantage of having higher stop-band rejections since the outputs are described by

$$P_2/P_{in} = \frac{P^C_=}{P^A_=} \times \frac{P^A_=}{P_{in}} = \cos^4(\phi/2) \qquad \text{(III-42)}$$

$$P_4/P_{in} = \frac{P^B_x}{P^A_x} \times \frac{P^A_x}{P_{in}} = \sin^4(\phi/2) \qquad \text{(III-42)}$$

and the extinction ratios are

$$D(\lambda_1) = 10\log_{10}(P_2/P_4) = 20\log_{10}\{ctg^2[\phi(\lambda_1)/2]\} \qquad \text{(III-44)}$$

$$D(\lambda_2) = 10\log_{10}(P_4/P_2) = 20\log_{10}\{tg^2[\phi(\lambda_2)/2]\} \qquad \text{(III-45)}$$

which mean the stopband rejections are doubled (Refer to equations (III-15,16)).

To solve the similar problems, we also apply the configuration shown in Fig III-18(b) to get the adjustable and high stopband rejection X-branch type multi/demultiplexers Since our waveguides are embedding, the cladding compensation effects on the center wavelength shift are monotonic (See Tables II-1,2) However, employing the photolithographic technique, the waveguide width deviation is uncontrollable in being + or − in fabrication. In order to be able to compensate for any width fabrication deviation within $\pm 0.3\mu m$, we let the width of coupler B be $0.3\mu m$ larger than the design value In this case, the outputs for port #2 and #4 are described by

$$P_2/P_{in} = cos^4[\phi(W_1)/2] \tag{III-46}$$

$$P_4/P_{in} = sin^2[\phi(W_1)/2]\times sin^2[\phi(W_1+0.3)/2] \tag{III-47}$$

So, the extinction ratios can be written as

$$D(\lambda_1) = 10log_{10}\{ctg^2[\phi(W_1,\lambda_1)/2]\}+10log_{10}\{cos^2[\phi(W_1,\lambda_1)/2]\}$$
$$-10log_{10}\{sin^2[\phi(W_1+0.3,\lambda_1)/2]\} \tag{III-48}$$

$$D(\lambda_2) = 10log_{10}\{tg^2[\phi(W_1,\lambda_2)/2]\}-10log_{10}\{cos^2[\phi(W_1,\lambda_2)/2]\}$$
$$+10log_{10}\{sin^2[\phi(W_1+0.3,\lambda_2)/2]\} \tag{III-49}$$

where ϕ is the total accumulated phase difference for passing a single X-branch waveguide. Figs. III-19,20 present the calculated results of a design example. They indicate that, when the waveguide width deviations are positive (within $0.3\mu m$), we can ignore the wavelength shift at $\lambda_1=1.55\mu m$, since the extinction ratios are still very high, and compensate that at $\lambda_2=1.31\mu m$ by depositing a cladding over the two-mode center region of coupler B to get better extinction ratios Principally, a cladding can increase the effective index of a waveguide, hence, increase the propagation constant difference between the even and odd modes in the waveguide. Because positive width deviations reduce that difference (See Figs. III-8,9), we can apply the cladding compensation method to offset the effects. The larger the positive width deviation is, the thicker cladding is required for that purpose In Fig III-20(b), the material SiO_2 is used ($n=1.44679$ at $1.31\mu m$ [15]) where the signs o indicate the improved output extinction ratio results by the corresponding cladding thicknesses. On the other hand, for the negative width deviations within *0.3μm*, the extinction ratios for both wavelengths are almost all over *30dB*. Such extent of the extinction ratio degradations needs not be compensated. Therefore, applying this new configuration and with the cladding compensation method for the positive width deviations, we, under the condition of the same fabrication deviations, are able to make a demultiplexer with an extinction ratio above *30dB*.

III-6. Conclusion

In this chapter, we have carried out the preliminary design of a single-mode X-branch type optical WDM device and the fabrication tolerance studies Based upon these analyses, we know, under the present laboratory conditions, any passive integrated single-mode device, based on the phase interference principle in the design for glass materials, would still be very challenging if we could not find the compensation method to improve the device properties. Hence, we have applied the three cascaded zero gap coupler to design an adjustable single-mode demultiplexer in the soda-lime glass with high stopband rejections. The theoretical analyses indicate that it is possible to achieve an extinction ratio greater than *30dB* for both wavelengths with the cladding deposition improvement.

References:

[1] Chen S. Tsai, Bumman Kim and Fathi R. El-Akkari, "Optical channel waveguide switch and coupler using total internal reflection", IEEE J. Quantum Electron., vol QE-14, pp. 513- 517, July, 1978.

[2] A. Neyer, "Electro-optic X-switch using single-mode Ti:$LiNbO_3$ channel waveguides", Electron. Lett., pp. 553-514, 1983.

[3] Gary E. Betts and William S. C. Chang, "Crossing-channel waveguide electrooptic modulators", IEEE J. Quantum Electron., vol. QE-22,

pp 1027-1038, July, 1986.

[4] A. Neyer, "Optimization of X-switch for integrated optical switching networks", Proceedings of IOOC-ECOC, Venise, Italy, pp. 369-372, 1985.

[5] L. Thylen, "Integrated optics in $LiNbO_3$: recent developments in devices for telecommunications", IEEE J. Lightwave Technol. vol LT-6, pp. 847-861, June, 1988

[6] A. Neyer, "Integrated optical multichannel wavelemgth multiplexer for monomode systems", Electron. Lett., vol. 20, pp 744-746, 1984.

[7] F. Rottmann and E. Voges, "Low-insertion-loss, turnable wavelength multiplexer on Lithium Niobate", Electron. Lett , vol. 23, pp. 1007-1008, 1987.

[8] F. Rottmann, A. Neyer, W Mevenkamp and E Voges, "Integrated optical Wavelength Multiplexers on lithium niobate based on two-mode interference", J. Lightwave Technol , vol LT-6, pp 946-951, 1988.

[9] Y. Chung, J. C. Yi, S. H. Kim and S. S. Choi, "Analysis of a tunable multichannel two-mode-interference wavelength division multi/demultiplexer", J. Lightwave Technol., vol. LT-7, pp. 766-776, 1989.

[10] G. L. Yip and J. Albert, "Characterization of planar optical waveguides by K^+-ion exchange in glass", Opitcs Lett., Vol 10, pp 151-153, 1985.

[11] R. A. Forber and E. Marom, "Symmetric directional coupler switches", IEEE J. Quantum Electron., vol. QE-22, pp. 911- 919, 1986.

[12] H. Yajima, "Theory and applications of dielectric branching waveguides", in Proc. Symp. Optical and Acoustical Micro-Electronics, pp. 339-359, (New York, Apr. 1974).

[13] Kamal Geol & William S. C. Chang, "Extinction ratio degradation due to asymmetry in zero-gap directional coupling and crossing channel switches", IEEE J. Quantum Electron., vol. QE-23, pp. 2216-2223, 1987.

[14] J. P. Lin, R. Hsiao and S. Thaniyavanrn, "Four-channel wavelength division multiplexer on Ti:$LiNbO_3$", Electron. Lett., vol. 25,

pp 1608-1609, 1989.

[15] Edward D. Palik, "Handbook of Optical Constants of Solids", Academic Press Inc., 1985.

[16] G. L. Yip, K. Kishioka, F. Xiang and J. Y. Chen, "Characterization of planar optical waveguides by K^+-ion exchange in glass at 1.152 and 1.523 μm", Submitted to OE/FIBERS '91, SPIE, Boston, 1991.

[17] K Imoto, H Sano, M Miyazaki, H. Uethuka and M. Maeda, "Compensation for fabrication-induced center wavelength shift in a coupled waveguide type Multi/Demultiplexer", Appl. Opt., vol. 28, pp. 1904-1909, 1989

[18] K Imoto, H. Sano and M. Miyazaki, "Guided-wave multi/demultiplexers with high stopband rejection", Appl. Opt., vol. 26, pp. 4214-4219, 1987.

Table III-1. Surface Index Change and Effective Diffusion Coefficient

$\lambda(\mu m)$	Δn_{sTE}	Δn_{sTM}	$D_{eTE}(\mu m^2/min)$	$D_{eTM}(\mu m^2/min)$	n_b
1.152	8.56×10^{-3}	10.09×10^{-3}	0.06198	0.06024	1.5030
1.31	8.564×10^{-3}	10.06×10^{-3}	0.06505	0.06338	1.50104
1.523	8.57×10^{-3}	10.03×10^{-3}	0.06918	0.06762	1.4984
1.55	8.571×10^{-3}	10.02×10^{-3}	0.06970	0.06816	1.49806

Remark: The working temperature of ion exchange is $T=385^{\circ}C$

Table III-2. Channel Guide Effective Index Deviations by Diffusion Time

Time	$1.55\mu m$			$1.31\mu m$		
min	n_{ef}	δn_{ef}	$\delta n_{ef}/\Delta n_{ef}$	n_{ef}	δn_{ef}	$\delta n_{ef}/\Delta n_{ef}$
167	1.4988299	-3.83×10^{-5}	-4.74%	1.5024282	-4.15×10^{-5}	-2.90%
168	1.4988426	-2.56×10^{-5}	-3.17%	1.5024420	-2.77×10^{-5}	-1.94%
169	1.4988555	-1.27×10^{-5}	-1.57%	1.5024558	-1.39×10^{-5}	-0.97%
170	1.4988682	0.00×10^{-5}	0.00%	1.5024697	0.00×10^{-5}	0.00%
171	1.4988808	1.26×10^{-5}	1.56%	1.5024833	1.36×10^{-5}	0.95%
172	1.4988936	2.56×10^{-5}	3.17%	1.5024969	2.72×10^{-5}	1.90%
173	1.4989061	3.79×10^{-5}	4.69%	1.5025103	4.06×10^{-5}	2.84%
	$n_b=1.49806$	$\Delta n_{ef}=8.08\times10^{-4}$		$n_b=1.50104$	$\Delta n_{ef}=1.43\times10^{-3}$	

Table III-3. Design Example Comparision

Time	Method	$n_{ef}(1.55\mu m)$	$n_{ef}(1.31\mu m)$	Width(μm)	Length(μm)
170 min	WKB	1.4988682	1.5024697	8.87	3464
	TRM	1.4991346	1.5026902	7.19	2476
$\theta=1^{\circ}$	Δ	2.66×10^{-4}	2.20×10^{-4}	1.68	988

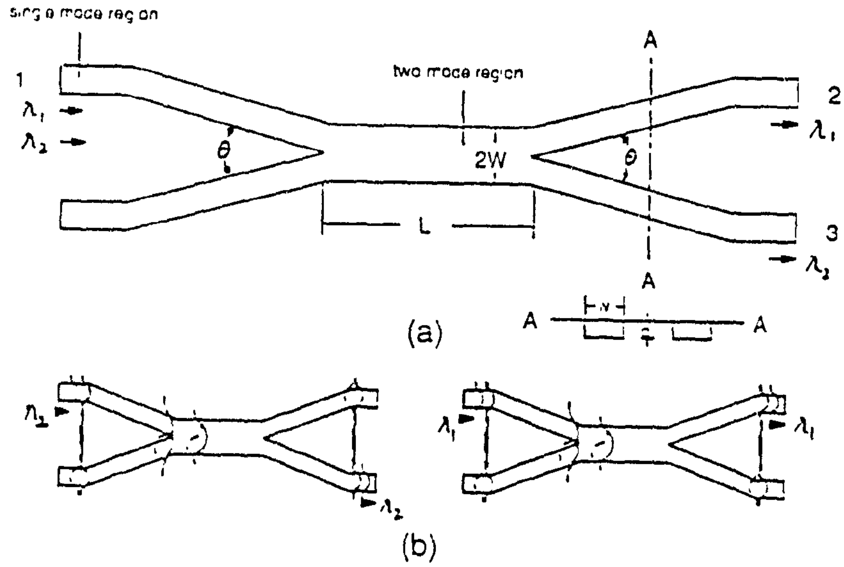

Fig. III-1 (a) Device waveguide structure.
(b) Modal field evolutions in the device.

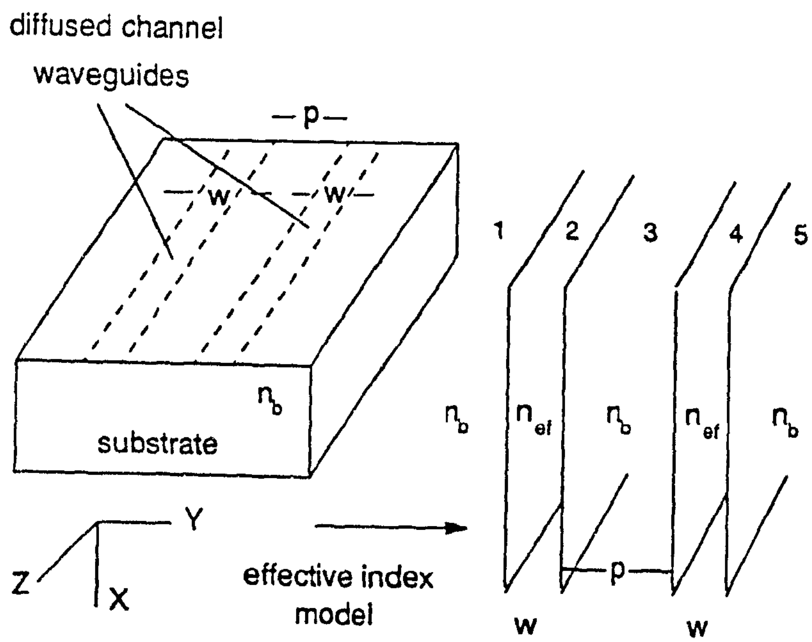

Fig. III-2. Illustration of the effective index
model of channel waveguides.

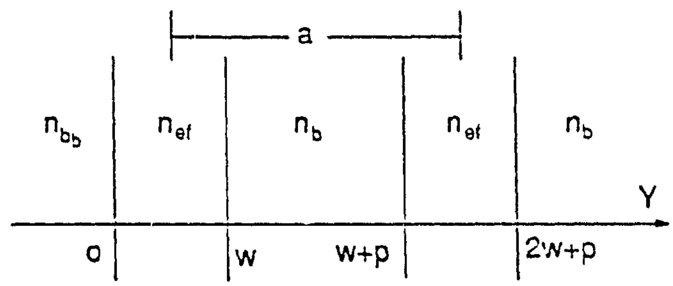

Fig. III-3 The coordinate of the equivalent of the five layer slab waveguide.

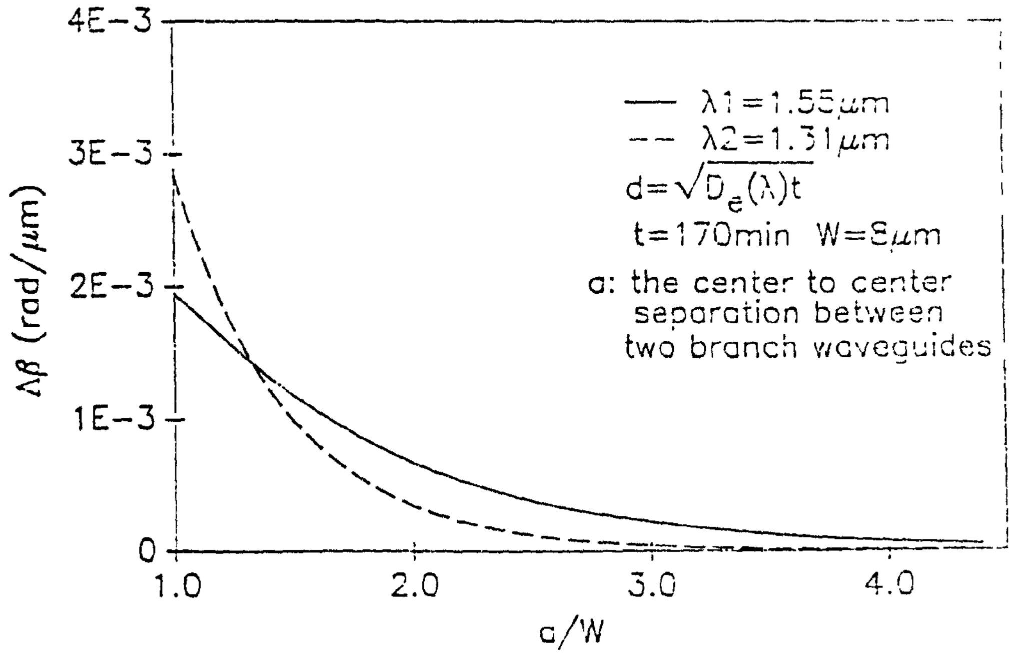

Fig. III-4 The propagation constant differences between the symmetric and antisymmetric modes against the normallized waveguide separation a/w in the taper region, where $a=w+p$

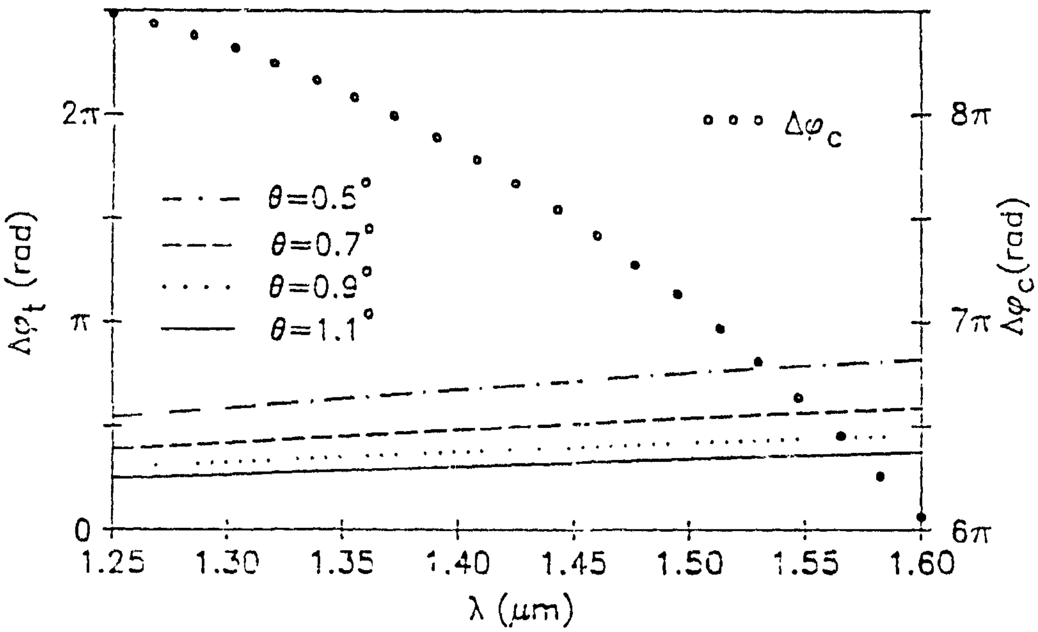

Fig. III-5 The accumulated phase differences $\Delta\phi_t$ and $\Delta\phi_c$ as the functions of wavelength (w=8μm, t=170mn and L_c=3500μm).

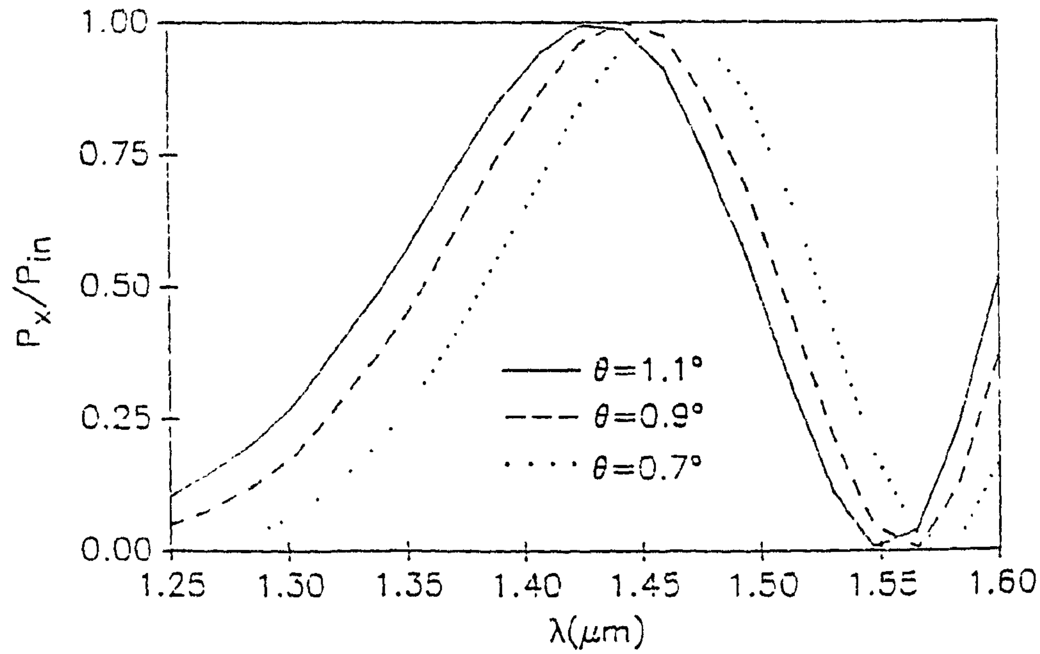

Fig III-6 Influence of branching angle on transmission characteristic (P_x/P_{in}) of dual-channel MUX/DEMUX as a function of wavelength.

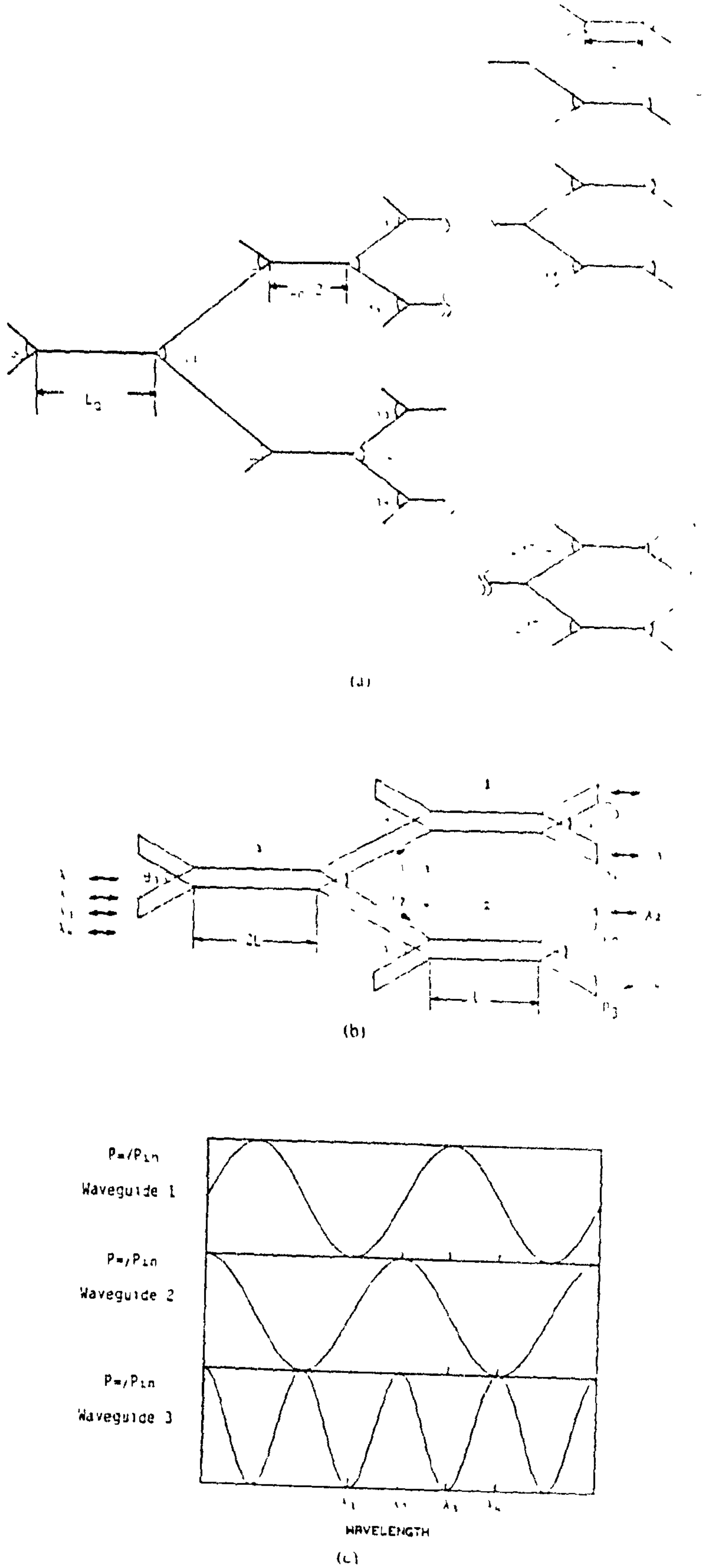

Fig. III-7 (a) Configuration of 2^N-channel MUX/DEMUX. (b) Configuration of four-channel MUX/DEMUX. (c)Requirement of transmission characteristic ($P_=/P_{in}$) of each X-branch waveguide.

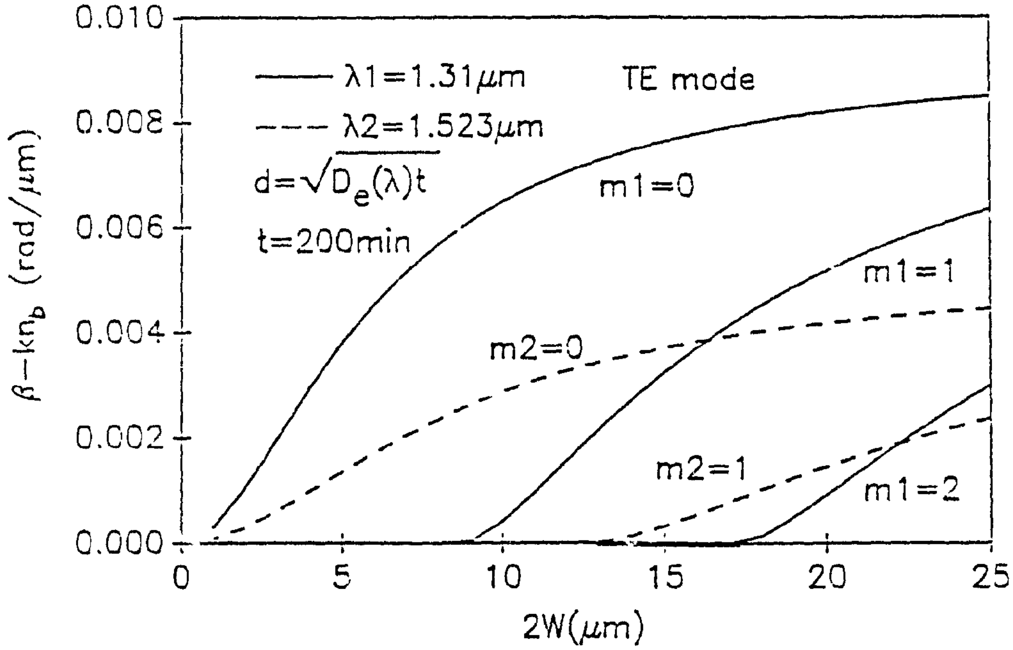

Fig III-8 The propagating mode dispersion relation with the waveguide width for wavelengths λ_1=*1.523μm* and λ_2=*1.31μm*.

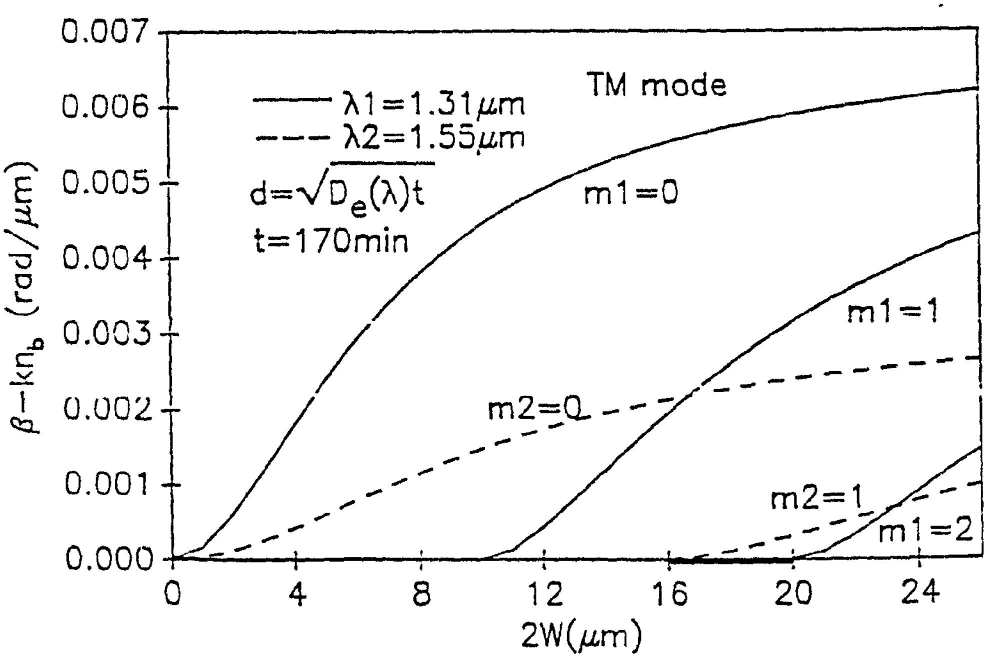

Fig III-9 The propagating mode dispersion relation with the waveguide width for wavelengths λ_1=*1.55μm* and λ_2=*1.31μm*.

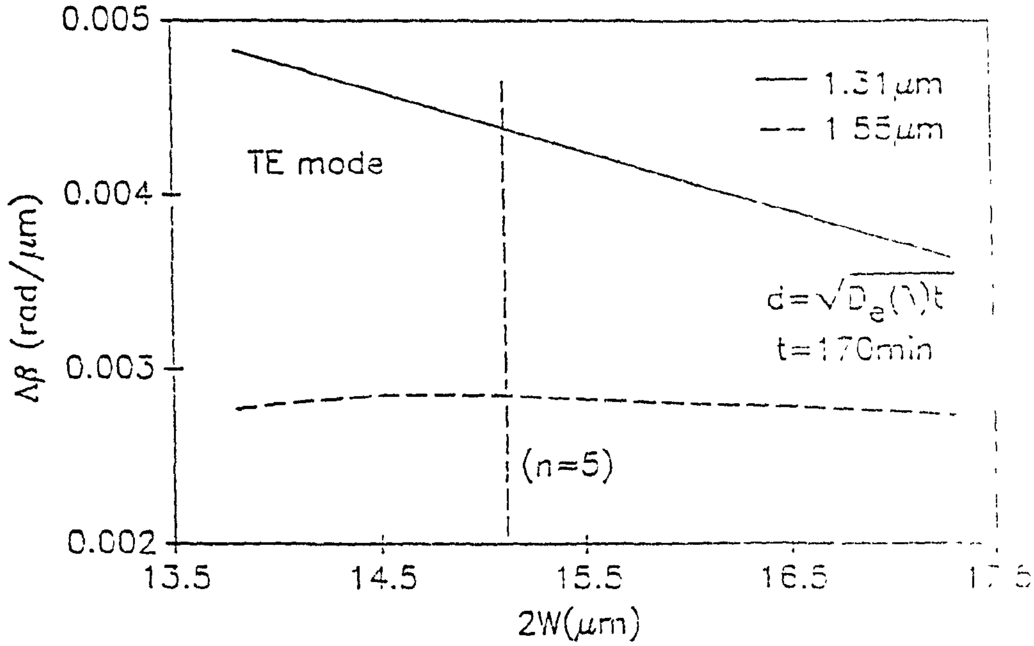

Fig. III-10 The propagation constant differences between symmetric and antisymmetric modes as a function of waveguide width in the double width center region.

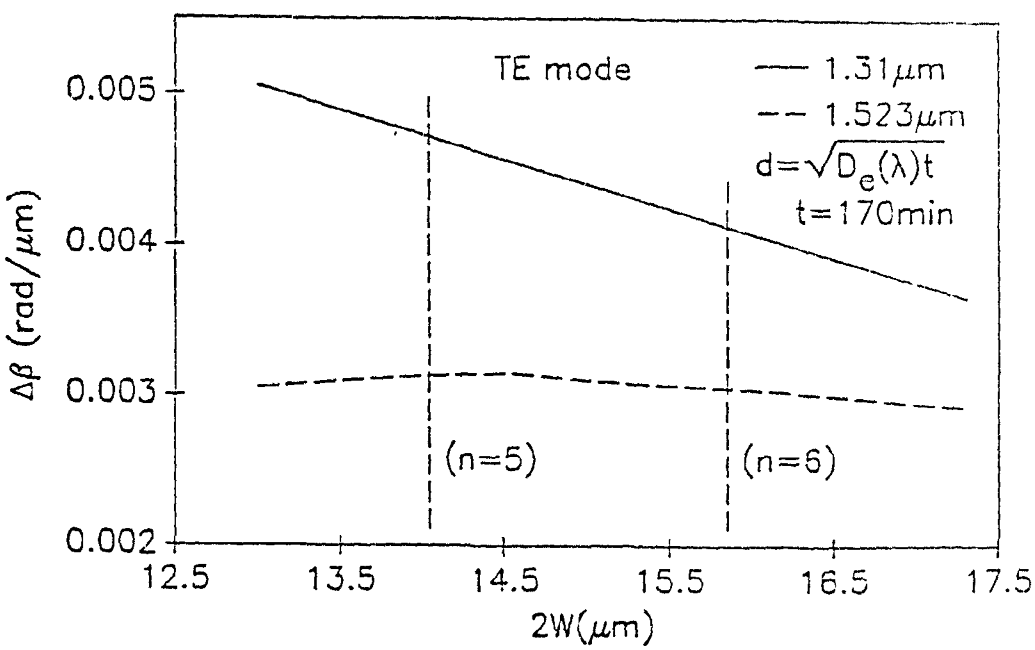

Fig. III-11 The propagation constant differences between symmetric and antisymmetric modes as a function of waveguide width in the double width center region.

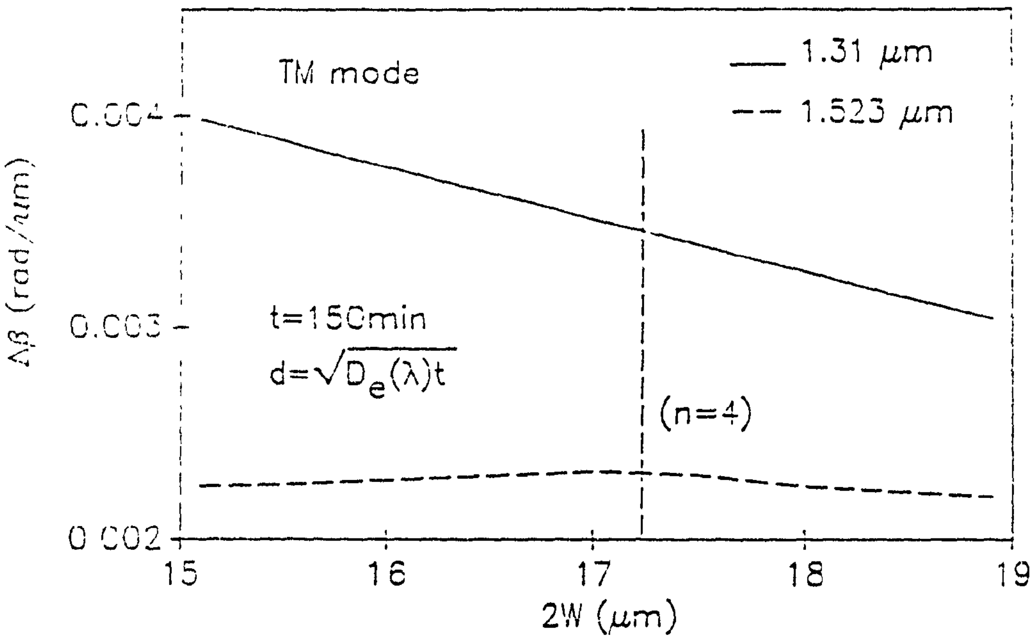

Fig III-12 The propagation constant differences between symmetric and antisymmetric modes as a function of waveguide width in the double width center region.

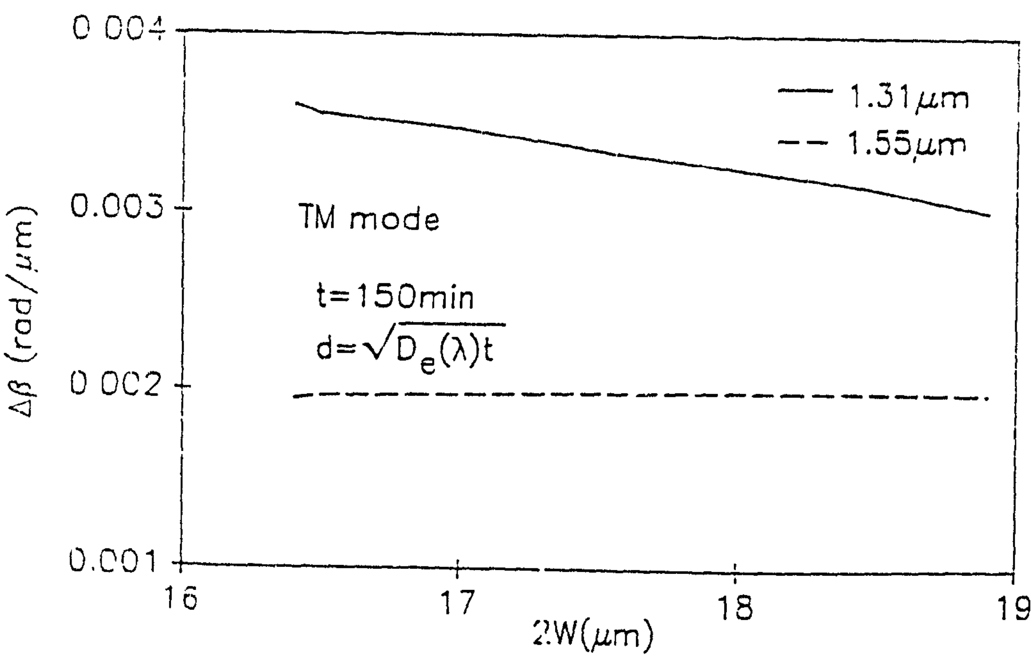

Fig. III-13 The propagation constant differences between symmetric and antisymmetric modes as a function of waveguide width in the double width center region.

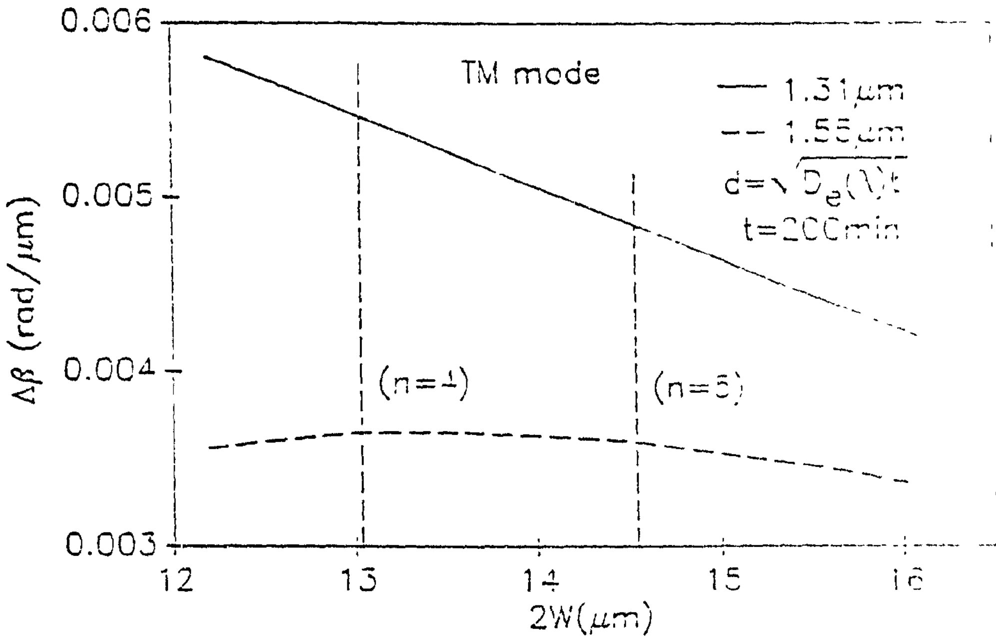

Fig. III-14 The propagation constant differences between symmetric and antisymmetric modes as a function of waveguide width in the double width center region.

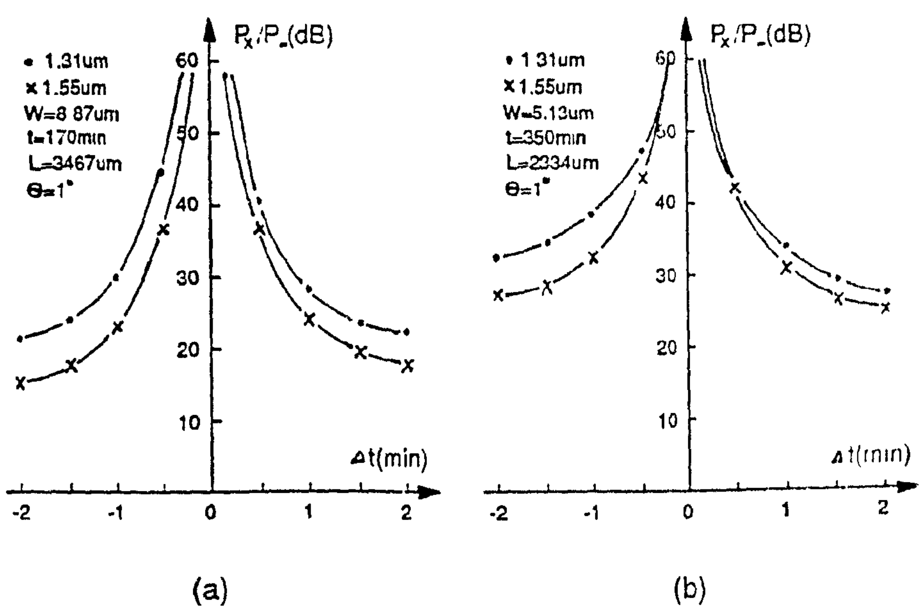

Fig. III-15 Extinction ratio degradations as diffusion time deviations.

(a) t=170min, W=8.87um; (b) t=350min, W=5.13um

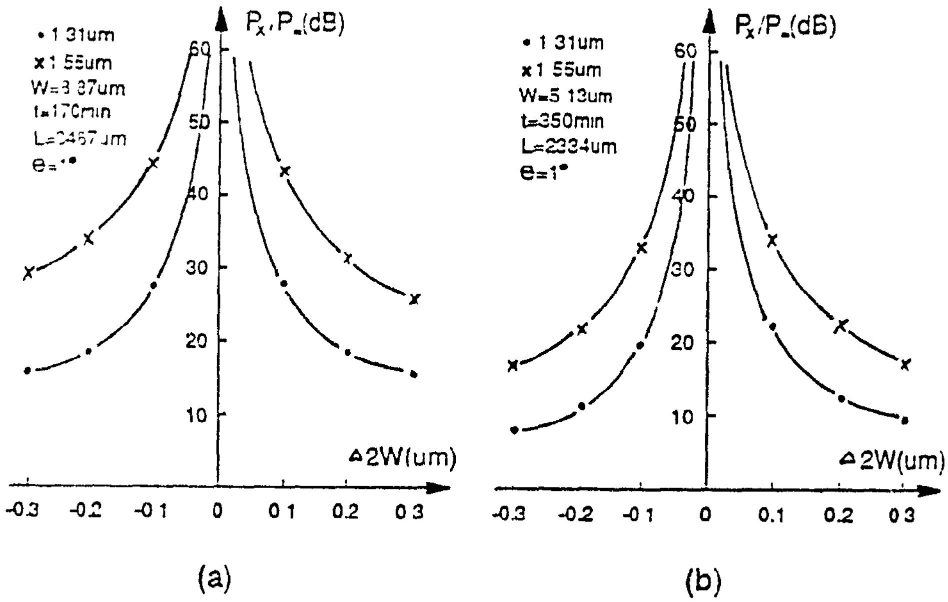

Fig. III-16 Extinction ratio degradations as waveguide width deviations. (a) t=170min, W=8.87um; (b) t=350min, W=5.13um.

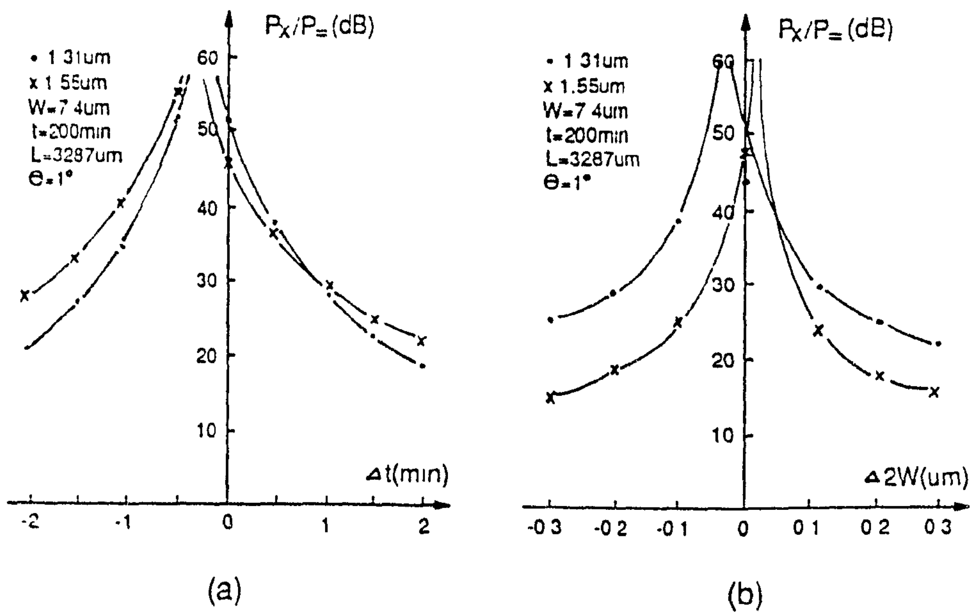

Fig. III-17 An example of bad design with uncarefully chosen waveguide width and two mode center region length. (a) Extinction ratio degradations by diffusion time deviations. (b) Extinction ratio degradations by waveguide width deviations.

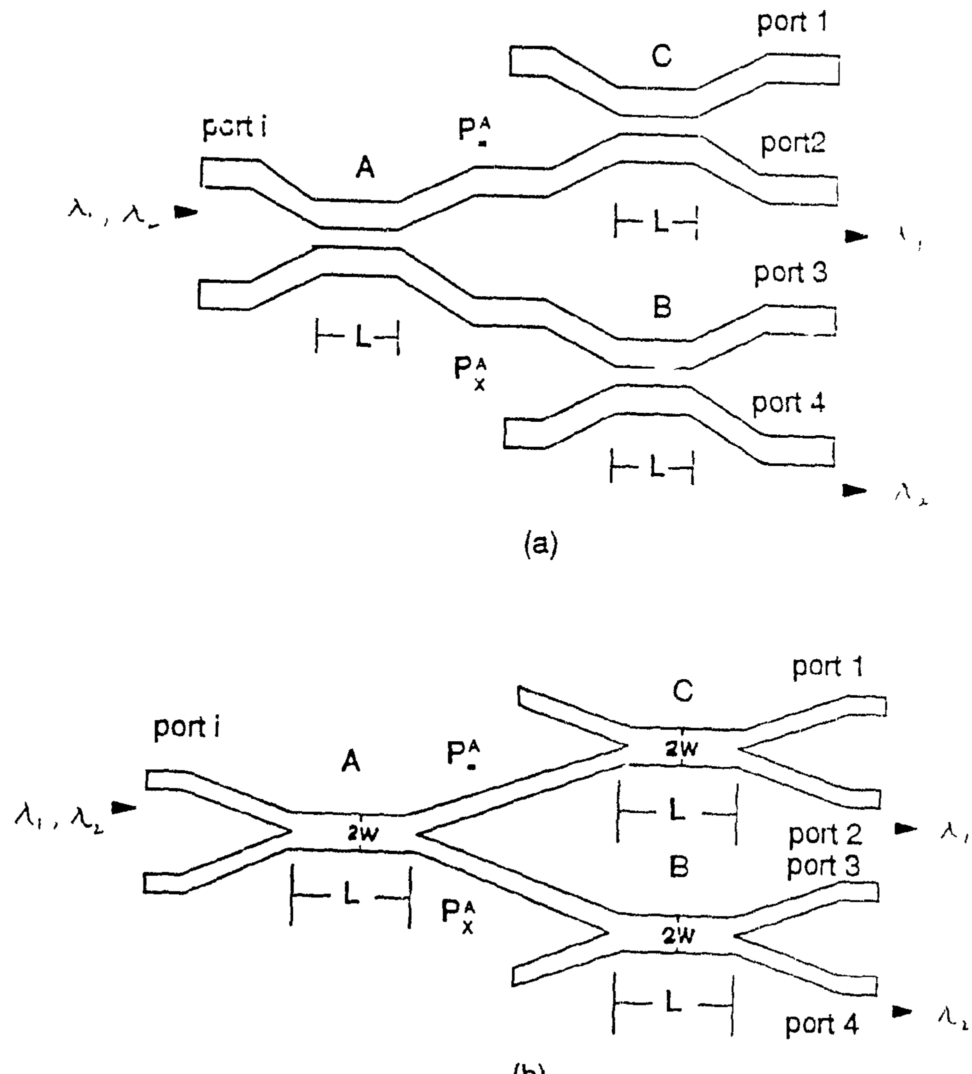

Fig. III-18 (a) cascaded coupler type WDM [17].

(b) Cascaded X-branch type WDM.

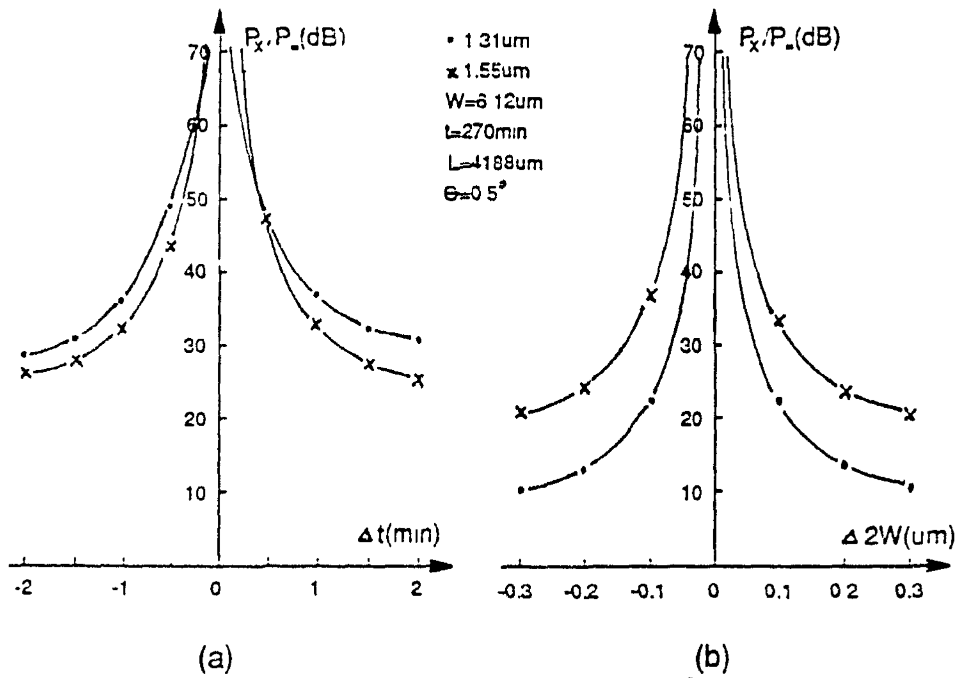

(a) (b)

Fig. III-19. Extinction ratio degradations of a single X-branch waveguide. (a) by diffusion time deviation; (b) by waveguide width deviation.

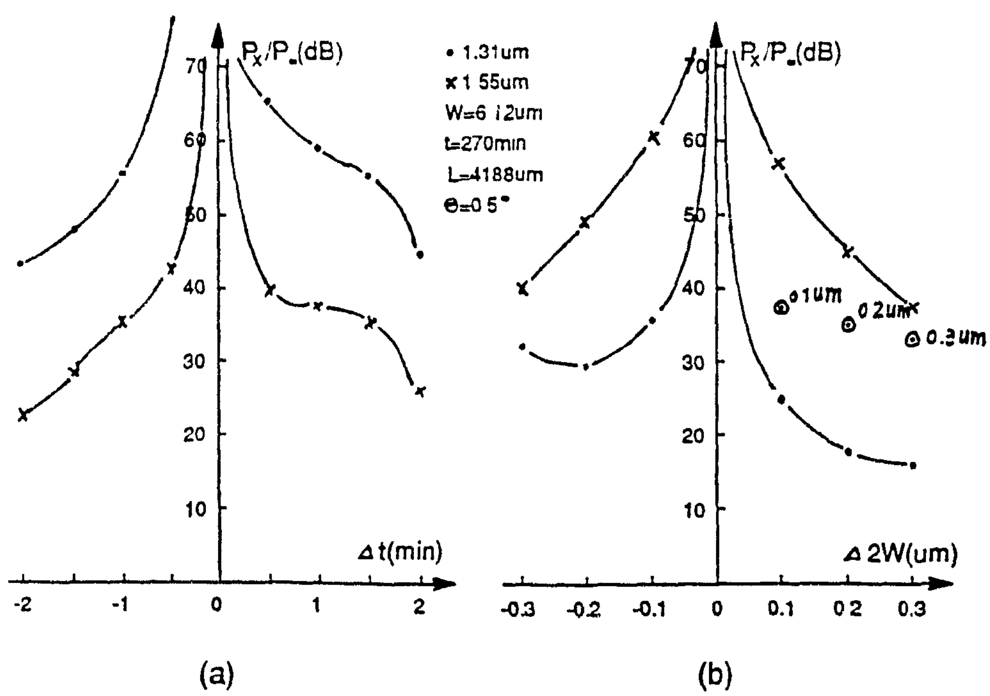

(a) (b)

Fig. III-20 Extinction ratio degradations of a cascaded structure. (a) by diffusion time deviation; (b) by waveguide width deviation, where ⊙ indicates improvements due to a dielectric cladding at 1.31um for a thickness of 0.1um, 0 2um and 0.3um, respectively.

CHAPTER IV

BPM SIMULATION OF A SINGLE MODE X-BRANCH TYPE DEMULTIPLEXER

IV-1. Introduction

In fiber and integrated optics, a typical waveguide problem involves the solution of Maxwell's equations in an infinite domain, subject to the radiation condition at infinity and for a given incident field or source. For many guiding structures of practical interest there is no cylindrical symmetry and radiation losses need to be calculated. In this situation, it turns out that the classical eigenmode theory, which is so successful for (closed) metal clad waveguides, is difficult to apply. The complete set of eigenmodes for such open waveguides must contain the continuum of radiation modes and this makes the use of eigenmode very unwieldy. In 1978, Feit and Fleck introduced a new numerical modeling method, the so-called Beam Propagation Method (BPM) [1]. Under appropriate circumstances, the BPM allows a unified treatment of guided and radiation modes in optical structures and can provide a detailed and accurate description of the propagating field for a variety of realistic sources of illumination. Since then, this method has gained considerable popularity in the past decade in the area of guided-wave optoelectronics and fiber optics. Many optical structures such as tapers [2], bends [3-4], gratings [5], coupler [6], Y-junctions [7], waveguide crossing [8], electrooptic waveguide modulators [9], and nonlinear directional couplers [10] have been modeled and analyzed by the Beam Propagation Method.

In order to verify our design considerations in the last chapter and further study the X-branch waveguide properties, the Beam

Propagation Method is employed in this chapter to simulate and analyze the single X-branch type demultiplexer We first give a general description about the BPM and its development in Section IV-2. Then, a detailed theoretical derivation from the scalar wave equation is presented in Section IV-3 Further, the applications of the discrete Fourier transform techniques and the absorber function chosen in the BPM are also discussed in Section IV-4 and IV-5, respectively Lastly, the applications of the BPM in analyzing integrated optics devices are discussed in Section IV-6 and the numerical results for the X-branch type demultiplexer is presented in Section IV-7. The BPM method has also been used as a design tool in two previous M. Eng. thesis [9,11].

IV-2. Description of BPM

For a given field or source, the Beam Propagation Method allows one to observe the optical field evolution as it propagates through a medium of arbitrary refractive index profile within the following limitations.

First, the BPM is based upon the scalar wave equation. For this to accurately approximate the true vectorial equation, the polarization effects must be negligible, which requires that the index profile be a slowly varying function over one wavelength in transverse directions However, by taking a reference index n_b, typically the value in the substrate of the circuit or the cladding of fiber, as a periodic extension of refractive index step between the guide and air [6] or choosing an extremely small longitudinal integration steps — $2\Delta z \ll \lambda n_b / [n_s^2 - 1]$ (n_s is the maximum index value in the guiding region) [12], it is still possible to model the transverse index profile discontinuities such as those occurring in integrated optical structures.

Second, the BPM converts the boundary value problem into an initial-value problem for which the solution can be found in a propagative manner. This requires that the field propagates in a more or less paraxial fashion, and all reflections in this direction are neglected, which implies that all variations of refractive index along z must be slow or small and not add up coherently. In cases where incident and reflected waves can be described by means of a coupled mode formalism [12,13], an extension to the normal BPM algorithm can be found, but the solution becomes much more complicated because iterations of forward and backward propagation are necessary [14].

Most practical fiber and integrated optics applications satisfy the conditions above. In such cases, it can be shown [1] that the propagation of a beam over a small distance can be computed by propagating the field through a homogeneous medium and later phase correcting for index inhomogeneities The homogeneous propagation is most efficiently performed in the angular spectrum, obtained through the use of the Fast Fourier Transform (FFT) Repeated applications of the procedure then allows the beam to be followed over any distance The advantage here is that no distinction between the guided and radiated field is required, nor are modal decompositions necessary This makes the method particularly useful when coupling between the radiated field and the guided modes is significant and other methods, which neglect the effect of the radiated field, cannot be used Although not provided directly, radiation and modal information can be extracted from the BPM generated data [15].

IV-3. General Theory of BPM

In an optical waveguide whose index profile varies very slowly over one wavelength in the transverse direction, the propagation of a single frequency light field can be described by the scalar Helmholtz equation as

$$\frac{\partial^2 \phi}{\partial x^2} + \frac{\partial^2 \phi}{\partial y^2} + \frac{\partial^2 \phi}{\partial z^2} + \frac{\omega^2}{c^2} n^2(\omega,x,y,z)\ \phi = 0 \qquad \text{(IV-1)}$$

where $\phi(\omega,x,y,z)$ is the transverse field distribution function, ω is the angular frequency of the light, $n(\omega,x,y,z)$ is the refractive index. Under the weakly guiding condition, the index profile can be written as

$$n(x,y,z) = n_b + \Delta n(x,y,z), \qquad |\Delta n/n_b| \ll 1 \tag{IV-2}$$

where n_b is a constant, typically the value in the substrate of the circuit or the cladding of fiber.

In term of the field at z , the solution of equation (IV-1) at $z+\Delta z$ may be written formally as

$$\phi(x,y,z+\Delta z) = exp\left[\pm j\Delta z(\nabla_\perp^2+k_o^2n^2)^{1/2}\right] \phi(x,y,z) \tag{IV-3}$$

where $\nabla_\perp^2=\partial^2/\partial x^2+\partial^2/\partial y^2$ and $k_o=\omega/c$ is the wavenumber of free space. With some algebraic manipulation, the square root in the right hand side of equation (IV-3) can be rewritten as

$$(\nabla_\perp^2+k_o^2n^2)^{1/2} = \frac{\nabla_\perp^2}{(\nabla_\perp^2+k_o^2n^2)^{1/2}+k_on} + k_on \tag{IV-4}$$

The essential point in the BPM lies in the following approximation, in which $n(x,y,z)$ in the denominator of the first term of (IV-4) is approximated by the constant n_b, so that

$$(\nabla_\perp^2+k_o^2n^2)^{1/2} \approx \frac{\nabla_\perp^2}{(\nabla_\perp^2+k_o^2n_b^2)^{1/2}+k_on_b} + k_on_b + k_on_b(n/n_b-1) \tag{IV-5}$$

The approximation gives satisfactory accuracy when the weakly guiding condition holds.

If the index variation along z is also small and slow, we can restrict the solution for a single wave propagation in the positive z direction, therefore the transverse field can be expressed in the form

$$\phi(x,y,z) = \psi(x,y,z)exp(-jk_o n_b z)$$

(IV-6)

Substitute the above expression into equation (IV-3) by using the approximation of equation (IV-5), we have

$$\psi(x,y,z+\Delta z) = exp\left[-j\Delta z\left(\frac{\nabla_\perp^2}{(\nabla_\perp^2+k_o^2 n_b^2)^{1/2}+k_o n_b} + X(x,y,z)\right)\right] \psi(x,y,z) + O^3(\Delta z)$$

(IV-7)

where

$$X(x,y,z) = k_o n_b\left(\frac{n(x,y,z)}{n_b} - 1\right) = k_o \Delta n(x,y,z)$$

(IV-8)

and the final term $O^3(\Delta z)$ gives the remaining computational error [1]. To second order in Δz, equation (IV-7) can be rewritten in the symmetrized split operator form

$$\psi(x,y,z+\Delta z) = exp\left[\frac{-j\Delta z}{2}\left(\frac{\nabla_\perp^2}{(\nabla_\perp^2+k_o^2 n_b^2)^{1/2}+k_o n_b}\right)\right] exp(-j\Delta z\ X\ ) \\ exp\left[\frac{-j\Delta z}{2}\left(\frac{\nabla_\perp^2}{(\nabla_\perp^2+k_o^2 n_b^2)^{1/2}+k_o n_b}\right)\right]\psi(x,y,z) + O^3(\Delta z)$$

(IV-9)

where the error also includes those arising from the noncommutation of $\nabla_\perp^2$ and $X(x,y,z)$ (see Appendix). The above expression is suitable for generating a numerical solution. Due to the unitarity of the operators in equation (IV-9), the solution will be unconditionally stable.

To improve the accuracy of the phase operator, we can introduce the mean index change

$$X = \frac{k_o}{\Delta z}\int_z^{z+\Delta z} \Delta n(x,y,z)\ dz$$

(IV-10)

over the distance Δz instead of $n=n(z)$ [16].

Actually, the operation

$$exp\left[\frac{-j\Delta z}{2}\left(\frac{\nabla_\perp^2}{(\nabla_\perp^2+k_o^2n_b^2)^{1/2}+k_on_b}\right)\right]\psi(x,y,z)$$

$$= exp\left[-j\Delta z/2\left((\nabla_\perp^2+k_o^2n_b^2)^{1/2}-k_o^2n_b^2\right)\right]\psi(x,y,z)$$

(IV-11)

is equivalent to solving the Helmholtz equation in a homogeneous medium

$$\frac{\partial^2\phi}{\partial x^2}+\frac{\partial^2\phi}{\partial y^2}+\frac{\partial^2\phi}{\partial z^2}+\frac{\omega^2}{c^2}n_b^2\,\phi=0$$

(IV-12)

for a distance $\Delta z/2$ with $\phi(x,y,z)$ as the initial condition. Therefore, the physical interpretation of equation (IV-10) is that we have replaced the actual continuous refractive-index distribution of the optical element with a series of infinitely small thin lenses separated by a distance Δz in a homogeneous medium with the reference refractive index n_b as shown in Fig IV-1. Each lens gives an coordinate-dependent phase shift given by $X(x,y,z)\Delta z$ to the beam, wheras the beam propagating between lenses is governed by equation (IV-12). These enables the propagation of the beam to be treated in a step-by-step manner.

In many practical applications, the optical fields vary slowly along the propagation direction over distances of the order of a wavelength For these problems, the scalar Helmholtz equation can be approximated sufficiently by the Fresnel equation

$$-j2k_on_b\frac{\partial\phi}{\partial z}+\nabla_\perp^2\phi+k_o^2(n^2-n_b^2)\phi=0$$

(IV-13)

and the BPM algorithm takes the form

$$\psi(x,y,z+\Delta z)=exp\left[\frac{-j}{4k_on_b}\Delta z\,\nabla_\perp^2\right]exp\left[\frac{-j}{2k_on_b}\Delta z\int_z^{z+\Delta z}k_o^2(n^2-n_b^2)dz\right]$$
$$exp\left[\frac{-j}{4k_on_b}\Delta z\,\nabla_\perp^2\right]\psi(x,y,z)$$

(IV-14)

Actually, one can recover it from the equations (IV-7) and (IV-9) by assuming that $\nabla_{\perp}^{2}$ is negligible in comparison with $k_o^2 n_b^2$ in the denominator of the equations This approximation is valid for small beam divergences (paraxial beam propagation) or steady-state propagation of light in dielectric waveguides. In the early stages of propagation, however, plane waves with large angular deviations from the z axis may be present in the beam, and the parabolic approximation can break down Under these conditions, the solution form in equation (IV-9) should still give an accurate description of light propagation Since a numerical solution is no more difficult to generate with equation (IV-9) than with the Fresnel or the so call parabolic approximation equation (IV-14), equation (IV-9) is to be preferred in the applications to the fiber and integrated optics problems.

With some efforts, the derivation of the BPM can also be adapted for anisotropic media [17]. Since these cases generally involve a nondiagonal dielectric tensor, the Helmholtz equation is used in its matrix form. The resulting propagation and phase operators, which are applied to a two-component electric field vector, contain matrices in their exponents and are defined by their perturbation series expansions

IV-4. Numerical Calculations

Under the assumption of limited spectral bandwidth, the Sampling Theory [18] allows the field alternatively to be represented in terms of its sampled values $\psi(p,q)=\psi(p\Delta x,q\Delta y,z)$ at the equally spaced points $x=p\Delta x$ and $y=q\Delta y$ on the computational grids, where $\pi/\Delta x$ and $\pi/\Delta y$ are the highest spectral frequency components of the field in transverse and lateral directions, respectively. The sampled field values then are given as a 2-D Fourier series with a finite number of terms, which is more suitable for numerical calculations:

$$\psi(x,y,z) = \sum_{n=-N/2}^{N/2-1} \sum_{m=-M/2}^{M/2-1} \psi_{nm}(z)\ exp\left[j2\pi(\frac{nx}{L_x} + \frac{my}{L_y}) \right]$$

(IV-15)

where L_x and L_y are the lengths of the computational grid area and the Fourier coefficients $\psi_{nm}(z)$ have a one-to-one correspondence to the elements of the discrete Fourier transform [18]

$$\psi_{nm} = \sum_{p=0}^{N-1} \sum_{q=0}^{M-1} \psi(p,q)\ exp\left[-j2\pi(np/N+mq/M) \right]$$

(IV-16)

Consider one section in Fig. IV-1 which consists of a homogeneous medium having a refractive index of n_b and length $\Delta z/2$, a thin lens, and again a homogeneous medium of length $\Delta z/2$. The Fourier component ψ_{nm} at $z+\Delta z/2$ can be obtained, by substituting equation (IV-15) and $X(x,y,z)=0$ into equation (IV-7), as

$$\psi_{nm}(z+\Delta z/2) = \psi_{nm}(z)\ exp\left[\frac{j\Delta z}{2} \left(\frac{k_{xn}^2 + k_{ym}^2}{(-k_{xn}^2 - k_{ym}^2 + k_o^2 n_b^2)^{1/2} + k_o n_b} \right) \right]$$

(IV-17)

where k_{xn}'s and k_{ym}'s denote discrete transverse wavenumbers defined as

$$k_{xn} = 2\pi n/L_x \qquad \text{and} \qquad k_{ym} = 2\pi m/L_y$$

(IV-18)

and, for $k_{xn}^2 + k_{ym}^2 > k_o^2 n_b^2$, the components express the evanescent waves in the equation (IV-17) [11].

Then, we reconstruct the real-space function ψ in the real space just behind the thin lens, that is, $\psi(z+\Delta z/2-0)$, by using the Fourier component $\psi_{nm}(z+\Delta z/2)$. The actual computation can be performed by using the widely available Fast Fourier Transform (FFT) algorithm [20]. Again, multiplying it by the "lens" term $exp[-j\Delta z X(x,y,z)]$ in equation (IV-9), we obtain the function just in front of the thin lens: $\psi(x,y,z+\Delta z/2)$. the beam propagation in the following homogeneous space of length $\Delta z/2$ can be calculated again by equation (IV-17) and two FFT processes.

Thus, the beam propagation over a single section is calculated. Of course, the final FFT can be omitted if the beam shape (power distribution) at this point is not needed, and the calculation is to be continued to the following section.

In practice, the spectral bandwidth of $\psi(x,y,z)$ is never perfectly finite. For most optical waveguide studies, however, it is possible to set up a configuration space computational grid with sufficient resolution to keep the spectral power on the boundaries of the corresponding wavenumber space grid extremely small. Spectral power on mesh boundaries is normally monitored, making it possible to confirm the accuracy of a given calculation.

The angle between the direction of a representative plane wave with a transverse wavevector (k_x, k_y) and the z axis is given by

$$\theta = sin^{-1}(k_x^2+k_y^2)/k_o n_b \tag{IV-19}$$

The value of N and M in equation (IV-16) will be determined by L_x, L_y and $\theta_{max} \approx (n_{max}^2 - n_b^2)^{1/2}$, the maximum value of θ for a ray propagating in optical waveguide. Thus, the minimum spatial bandwidth for ψ required to accommodate the steady-state field is defined by the relations [1]

$$\frac{N\pi}{L_x} = |k_x^{max}| > k\ sin\theta_{max} \tag{IV-20}$$

$$\frac{M\pi}{L_y} = |k_y^{max}| > k\ sin\theta_{max} \tag{IV-21}$$

IV-5. Absorbers

The use of discrete Fourier transforms in the BPM algorithm implies a periodic continuation of the computational window $L_x = N\Delta x$ and $L_y = M\Delta y$. Therefore, there is a problem encountered with the BPM which is of primary importance in optical loss calculations. When the radiated field expands out to the boundary of the computational window, in succeeding steps, it will be folded back to the opposite edge of the window. In order to avoid this problem, we must absorb the field at the edge of the window to simulate the radiation condition. This can be done, for example, by setting the field to zero over the last few grid points at the edges of the window or by introducing a large negative complex component into the refractive index, that acts as a lossy cladding [1]. If significant power lies at the window boundaries, however, it has been found that cutting the field off too abruptly generates strong high frequency components associated with diffraction [4]. Thus, an absorber function must be constructed to bring the field smoothly to zero at window edges without affecting the guided field distribution in the central area of the window. In reference [4], a suitable absorber in two-dimensional calculation has been obtained by multiplying the field with the following function (see Fig. IV-2).

$$absorber(x) = \begin{cases} 1 & |x|<|x_0| \\ 1/2\{1+\cos^{\gamma}[\pi(x-x_0)/(x_1-x_0)]\} & |x_0|<|x|<|x_1| \\ 0 & |x_1|<|x|<|w/2| \end{cases} \qquad \text{(IV-22)}$$

where $w/2$ is the coordinate of the grid boundary, x_0 denotes the inner edge of the absorber, and x_1 is the outer edge. The parameters γ, x_0 and x_1 are chosen empirically for each problem configuration and step length to ensure that the field is absorbed gradually over a sufficiently wide region $|x_0|<|x|<|x_1|$. The distance between x_1 and x_0 is adjusted similarly according to the step size and the shape of the Fourier spectrum of the electric field at large wave numbers to ensure that no interference effects will occur as a result of folding back of the electric field at the edges of the computational window. x_0 must be chosen far enough from the axis so that in a lossless waveguide the absorber does not perceptably affect the guided field distributions. In problems where the radiated field is expected to be significant, the accuracy of a calculation should be confirmed by comparing the results of a pair of propagation runs with different choices of the absorber parameters. For our purposes, the role of the parameter γ is not critical, and we have found setting it equal to unity in the computations to give good results [11]. The transverse y direction must be treated likewise.

IV-6. Applications of the BPM in integrated optics

The Beam Propagation Method described in the previous sections is only valid for small changes in refractive index from a reference value n_b. It is obvious that the large index change between the integrated optical device and air cannot be treated in this fashion.

For most typical integrated optical waveguides, however, the refractive index difference in the lateral or y direction is still plausibly small. This allows one to use the effective index method to overcome the guide/air interface problem on applying BPM to analyzing channel waveguide properties. The approach has the advantage of differentiating between the quasi-TE and quasi-TM modes and at the same time reducing the three dimensional guide to a corresponding two dimensional structure which no longer contains large refractive index steps. As long as this equivalent structure satisfies the usual restriction of the BPM algorithm, i.e., the guidance in the y direction is sufficiently weak, this formulation can yield excellent results for both x and y direction polarized modes [14]. It should be pointed out that this dimension reduction reduces the necessary amount of computer memory and processor time greatly, since the BPM now only requires a one-dimensional FFT.

Applying the BPM to the analysis and design of X-branch type demultiplexer involves the power evaluations in the particular waveguide branches. Actually, this can be achieved by overlapping the output field ψ_{out} with the normalized guided mode ϕ_g of the waveguide as

$$P_{out} = \left| \int \psi_{out} \phi_g^* dy \right| \tag{IV-23}$$

where ϕ_g is obtained analytically by the effective index approximation and ϕ_g^* is the complex conjugate of ϕ_g [9]. Since the demultiplexer we design here is a single-mode device, the radiation mode power can be evaluated as

$$P_{rad} = P_{in} - P_x - P_= = 1 - P_x - P_= \tag{IV-24}$$

which also include the power absorbed by the boundary absorber ($P_{in}(\lambda)=1$ since incident power is normalized). Similarly as we discussed in the last chapter, the extinction ratio and radiation loss can be calculated as

$$D_e(\lambda) = 10log_{10}[P_x(\lambda)/P_=(\lambda)] \tag{IV-25}$$
$$L_r(\lambda) = 10log_{10}[P_{rad}(\lambda)/P_{in}(\lambda)] = 10log_{10}[P_{rad}(\lambda)] \tag{IV-26}$$

respectively.

IV-7. Discussions of Results

Fig. IV-3 shows a BPM calculation sample for a single-mode straight channel waveguide, where the waveguide width is $5.5\mu m$ and the substrate and channel indices are $n_b=1.50012$ and $n_1=1.50370$, respectively. By compromising the computing time consummation and the numerical calculation accuracy, we choose grid point number to be 1024 with a $100\mu m$ window width and step length $\Delta z=1\mu m$ (also for Fig IV-4). The numerical results show that the input pulse (generated analytically) propagates in an unperturbed manner along the waveguide for a length of $1mm$ ($\lambda=1.55\mu m$). Therefore, we believe that our BPM program can accurately simulate the optical field propagating through the waveguide (for more complicated structures like Fig. III-1, the grid point was increased to 2048 and $200\mu m$ window width chosen as explain later).

Since glass is a kind of low refractive index optical material, it confines the guided modal fields much more weakly than many other optical materials. Therefore, more attentions should be paid on designing waveguide branching, bending or z dependent variations on the glass substrate. Actually, the radiations due to a waveguide tilt are caused by a very similar mechanism as a waveguide bending physically. And, the smaller the tilt angle is, the smaller the radiated optical field is induced (see Fig IV-4). Since the BPM can treat the guided and radiation modes in a unified manner, we can use this method to study the effect of a branching angle on scattered fields and extinction ratio degradations for the integrated optics device designs.

Fig. IV-5 and Fig. IV-6 show two design examples of an X-branch type demultiplexer The device functions are well simulated and the local normal even-odd mode interference due to the propagation phase differences can be seen clearly by the peak variations of the guided fields in the two mode center region. Actually, when the propagation phase differences between the local even and odd modes are $2n\pi$ (n is an integral), the two modal fields will subtract to each other on one side in the waveguide and add up on another side which lets the superposed field amplitude peak be away from the waveguide center. Similarly, when the propagation phase differences between the local even and odd modes are $(2n+1)\pi$, the superposition of the modal fields will result the amplitude peak to be on another side of the waveguide. This verifies the previous chapter analysis. From Fig. IV-5 and Fig. IV-6, we also know that longer wavelength signals are scattered more significantly since the guided modes are weaker guided and nearer to cutoff due to the lower index value. In spite of their different waveguide widths, both stuctures produce similar extent of radiated fields due to a large branching angle (1°) This means that the radiation loss can not be improved significantly by choosing a wider waveguide for the single-mode X-branch type demultiplexer. By contrast, Fig. IV-7 shows a much better design by choosing a smaller branching angle (0.5°). Actually, better extinction ratios are also obtained from the power evaluation. Therefore, we believe that the appearance of the radiation modes does not just simply increase the scattering loss, but also reduces the branch channel isolation due to some radiated power coupled back into the guided modes in both branches. However, a smaller branching angle also requires the device dimension to be increased significantly which may raise the adverse effects on the fabrication tolerances for the waveguide width or diffusion depth. Hence, a trade-off in the design process between the various parameters affecting the device performances is necessary.

The fabrication tolerance studies can also be performed by the BPM Figs IV-8, 9 show the extinction ratio degradations due to the waveguide width and depth deviations, respectively. Apparently, the output extinction ratio degradation of the longer wavelength are more sensitive to the depth deviation and shorter wavelength ones are more sensitive to width deviation. These agree with our previous analysis. Table IV-1 and Table IV-2 give the comparisons by the BPM and two-mode interference EIM analysis on $\Delta 2w$ and Δt, respectively. Although similar results are produced by both methods, we believe the BPM results provide some more comprehensive information on the radiation and guided modes Because of the computing time limitation (the computing time is proportional to $N \log_2 N$ [18], where N is the grid point number. The current computations take around *2* days to produce one BPM plot in the SPARC station), we only fix the grid point number to be *2048* and window width as *200μm* for these calculations in Fig. IV-5 to IV-9. Due to the device properties discussed in the last chapter, the BPM analysis may be further improved by increasing the grid point number (double or *4* times).

Since our main interest here is to investigate the scattered fields by the waveguide branching and the BPM calculation also is very time consuming, we have not applied the method to simulate the cascaded structure in view of the fact that the single X-branch WDM device simulations and analyses have been demonstarted.

IV-8. Conclusions

In this chapter, we have presented the powerful and accurate numerical method BPM for solving the scalar wave equation and its applications in integrated optics. The method is particularly suitable for analyzing the devices with slowly changing and complicated index profiles involving high-order and radiation modes. The simulation and analysis of the X-branch type demultiplexer show that, for the K^+-ion exchange glass optical surface waveguides, a smaller branching angle (about 0.5°) is needed to reduce the scattering loss and improve the channel isolation. Since the light beam propagation can be seen clearly step by step, the BPM is very helpful for simulating device functions and verifying our designs in the last chapter. However, accuracy in using the BPM method as a design tool has not yet been reached in this thesis

Appendix

The exponent in equation (IV-7) can be expanded in terms of a Taylor series as

$$exp\left(-j\int_0^z A(z')dz'\right) = 1 - j\int_0^z A(z')dz' - \frac{1}{2}\left[\int_0^z A(z')dz'\right]^2 - \frac{j}{3!}\left[\int_0^z A(z')dz'\right]^3 + ...$$

where

$$A(z) = \frac{\nabla_\perp^2}{(\nabla_\perp^2+k_o^2n_b^2)^{1/2}+k_on_b} + X(x,y,z)$$

Since

$$\int_0^z A(z')dz'\left(\int_0^{z'} A(z'')dz''\right)^m = \int d\left(\int_0^{z'} A(z'')dz''\right)\left(\int_0^{z'} A(z'')dz''\right)^m =$$

$$\frac{1}{m+1}\left(\int_0^{z'} A(z'')dz''\right)^{m+1}$$

the terms in the above Taylor series can be replaced as

$$exp\left(-j\int_0^{z} A(z')dz'\right) = 1 - j\int_0^{z} A(z')dz - \int_0^{z} A(z')dz'\left(\int_0^{z'} A(z'')dz''\right)$$

$$-j\int_0^{z} A(z')dz'\int_0^{z'} A(z'')dz''\int_0^{z''} A(z''')dz''' + O(z^4)$$

Substituting for $A(z)$ gives

$$exp\left(-j\int_0^{z} A(z')dz'\right) = 1 - j\frac{\nabla_\perp^2}{(\nabla_\perp^2+k_o^2n_b^2)^{1/2}+k_on_b}z - j\int_0^{z} X(z')dz' -$$

$$\left[\frac{\nabla_\perp^2}{(\nabla_\perp^2+k_o^2n_b^2)^{1/2}+k_on_b}\right]^2\frac{z^2}{2} - \frac{\nabla_\perp^2}{(\nabla_\perp^2+k_o^2n_b^2)^{1/2}+k_on_b}z\int_0^{z'} X(z)dz -$$

$$\int_0^{z} X(z')dz'\int_0^{z'} X(z'')dz'' + O(z^3)$$

Similarly, the split operator form equivalent to (IV-9) can be expanded in terms of a perturbation series. To second order, the individual factors are

$$exp\left[\frac{-jz}{2}\left(\frac{\nabla_\perp^2}{(\nabla_\perp^2+k_o^2n_b^2)^{1/2}+k_on_b}\right)\right] = 1 - \frac{j}{2}\frac{\nabla_\perp^2}{(\nabla_\perp^2+k_o^2n_b^2)^{1/2}+k_on_b}z$$

$$\frac{1}{8}\left[\frac{\nabla_\perp^2}{(\nabla_\perp^2+k_o^2n_b^2)^{1/2}+k_on_b}\right]^2 z^2$$

and

$$\exp\left[-j\int_0^z X(z')dz'\right] = 1 - j\int_0^z X(z')dz' - \int_0^z X(z')dz'\int_0^{z'} X(z'')dz''$$

so that the split operator expression of (IV-7) expands to

$$\exp\left[\frac{-jz}{2}\left(\frac{\nabla_\perp^2}{(\nabla_\perp^2+k_o^2n_b^2)^{1/2}+k_on_b}\right)\right]\exp\left[-j\int_0^z X(z')dz'\right]$$

$$\exp\left[\frac{-jz}{2}\left(\frac{\nabla_\perp^2}{(\nabla_\perp^2+k_o^2n_b^2)^{1/2}+k_on_b}\right)\right] = \left[1 - \frac{j}{2}\frac{\nabla_\perp^2}{(\nabla_\perp^2+k_o^2n_b^2)^{1/2}+k_on_b}z - \right.$$

$$\left.\frac{1}{8}\left(\frac{\nabla_\perp^2}{(\nabla_\perp^2+k_o^2n_b^2)^{1/2}+k_on_b}\right)^2 z^2\right]\left[1 - j\int_0^z X(z')dz' - \int_0^z X(z')dz'\right.$$

$$\left.\int_0^{z'} X(z'')dz''\right]\left[1 - \frac{j}{2}\frac{\nabla_\perp^2}{(\nabla_\perp^2+k_o^2n_b^2)^{1/2}+k_on_b}z - \frac{1}{8}\left(\frac{\nabla_\perp^2}{(\nabla_\perp^2+k_o^2n_b^2)^{1/2}+k_on_b}\right)^2 z^2\right]$$

$$= 1 - j\frac{\nabla_\perp^2}{(\nabla_\perp^2+k_o^2n_b^2)^{1/2}+k_on_b}z - \int_0^z X(z')dz' - \left[\frac{\nabla_\perp^2}{(\nabla_\perp^2+k_o^2n_b^2)^{1/2}+k_on_b}\right]^2\frac{z^2}{2}$$

$$- \frac{\nabla_\perp^2}{(\nabla_\perp^2+k_o^2n_b^2)^{1/2}+k_on_b}z\int_0^z X(z')dz' - \int_0^z X(z')dz'\int_0^{z'} X(z'')dz'' + O(z^3)$$

Thus, the symmetrically splitted operator form can represent the solution of the propagation wave equation (IV-7) to second order of z.

Reference:

[1] M. d. Feit and J. A. Fleck, Jr., "Light propagation in graded-index optical fiber", Appl. Opt., vol. 17, No. 24, pp. 3990-3998, 1978.

[2] B. Hermansson, D Yeivck and Daniesen, "Propagation beam analysis of multimode waveguide tapers", IEEE J. Quantum Electron., QE-19, No. 8, pp. 1146-1251, 1983.

[3] R. Baets and P. E. Lagasse, "Loss calculation and design of

arbitrarily curved integrated-optic waveguides", J Opt Soc, Am , vol. 73, No. 2, pp 177-162, 1983

[4] J. Saijonmaa and D. Yevick, "Beam-propagation analysis of loss in bent optical waveguides and fibers", J. Opt. Soc. Am , vol 73, No 12, pp. 1785-1791, 1983.

[5] D. Yevick and L. Thylen, "Analysis of gratings by the beam-propagation method", J. Opt Soc. Am., vol 72, No 8, pp 1084-1089, 1982.

[6] M. D. Feit and J. A. Fleck, Jr , "Analysis of rib waveguides and couplers by the propagating beam method", J. Opt. Soc Am , A, vol. 7, No. 1, pp. 73-79, 1990.

[7] R. Baets and P E Lagasse, "Calculation of radiation loss in integrated-optic tapers and Y-junctions", Appl Opt , vol 21, No 11, pp 1972-1978, 1981.

[8] A. Neyer, W. Mevenamp, L. Thylen and B. Lagerstrom, " A beam propagation method analysis of active and passive waveguide crossings", J. Lightwave Tech., vol LT-3, pp 635-542, 1985

[9] M. A. Sekerka-Bajbus, "The BPM design optimization and implementation of 3-branch waveguide devices", M. Eng. Thesis, Dept. of Elec. Eng., McGill University, 1989.

[10] L. Thylen, E. m. Wright, G. I. Stegeman, C. T Seaton and J. V Moloney, "Beam-propagation method analysis of a nonlinear directional coupler", Opt. Lett., vol. 11, No 11, pp. 739-741, 1986.

[11] R. Osborne, "A theoretical study of the propagation characteristics of some optical waveguides by the beam propagation method", M. Eng. Thesis, Dept. of Elec. Eng , McGill University, 1986.

[12] J. V. Roey, J. V. D. Donk and P. E. Lagasse, "Beam-propagation method: analysis and assessment", J. Opt. Soc. Am., vol. 71, No. 7, pp.803-810, 1981.

[13] J. V. Roey and P. E. Lagasse, "Coupled wave analysis of obliquely incident waves in thin film gratings", Appl. Opt., vol 20, pp. 423-429, 1981.

[14] P. E. Lagasse and R. Baets, "Application of propagating beam

methods to electromagnetic and acoustic wave propagation problem: a review", Radio Sci , vol. 22, No. 7, pp. 1225-1233, 1987.

[15] M D. Feit and J A. Fleck, Jr., "Computation of mode properties in optical fiber waveguides by a propagating beam method", Appl. Opt., vol. 19, pp. 1154, 1980.

[16] P Danielsen and D. Yevick, "Improved analysis of the propagating beam method in longitudinally perturbed optical waveguides", Appl. Opt., vol. 21, No 23, pp 4188-4192, 1982.

[17] L. Thylen and D Yevick, "Beam propagation method in anistropic media", Appl. Opt., vol. 21, No 15, pp. 2751-2754, 1982.

[18] E. O. Brigham, "The fast Fourier transform", Prentice-Hall, Englewood Cliffs, N J., 1974.

[19] William H. Press and others, *Numerical Recipes,* New York, Cambridge University Press., 1986.

Table IV-1. Extiction ratio degradations due to width deviations (dB)

$\Delta 2W(\mu m)$	1.31μm			1.55μm		
	By EIM	By BPM	L_R	By EIM	By BPM	L_R
-0.3	10.04	11.31	13.95	20.85	21.71	11.87
-0.2	12.41	12.80	12.72	23.91	22.84	10.74
-0.1	22.06	22.46	13.90	37.02	27.83	11.58
0.0	∞	29.52	14.13	∞	33.38	12.32
0.1	21.78	18.06	14.08	23.68	21.65	11.87
0.2	12.87	12.06	12.78	23.41	23.66	12.10
0.3	10.11	10.70	12.98	20.62	18.40	10.75

where L_R is the radiation loss calculated by BPM.

Table IV-2. Extinction ratio degradation due to time deviations (dB)

$\Delta t(min)$	1.31μm			1.55μm		
	By EIM	By BPM	L_R	By EIM	By BPM	L_R
-2.0	28.27	24.47	13.94	26.75	21.72	11.70
-1.0	36.74	27.68	14.21	32.34	25.73	12.79
0.0	∞	29.52	14.13	∞	33.38	12.32
1.0	37.51	27.84	14.49	32.51	27.39	11.55
2.0	32.19	26.71	12.87	25.67	25.40	10.82

where L_R is the radiation loss calculated by BPM.

Remark: (device structure parameters)

Channel width:	*6.1μm*	Diffusion time:	*270min*
Two-mode region length:	*4188μm*	Branching angle:	*0.5°*
Grid point number:	*2048*	Window width:	*200μm*

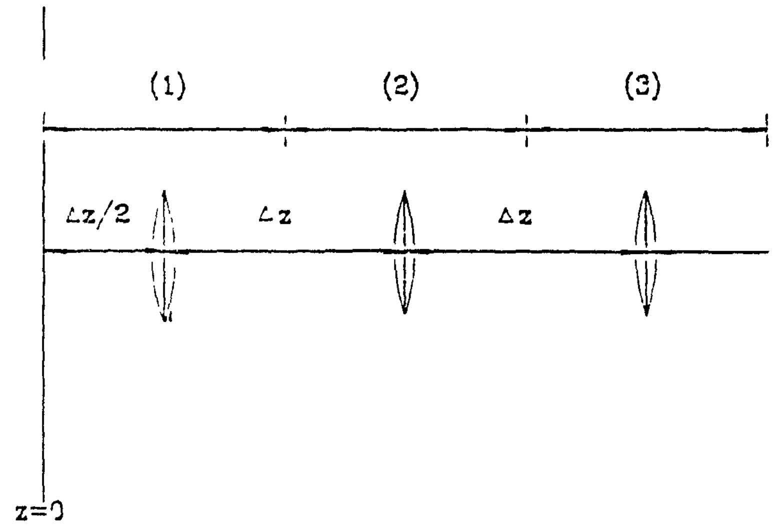

Fig IV-1 An array of lenses equivalent to the beam-shape transfomation expressed by (IV-9). One section consists of a uniform medium with a length ($\Delta z/2$), a thin lens, and a uniform medium with a length ($\Delta z/2$).

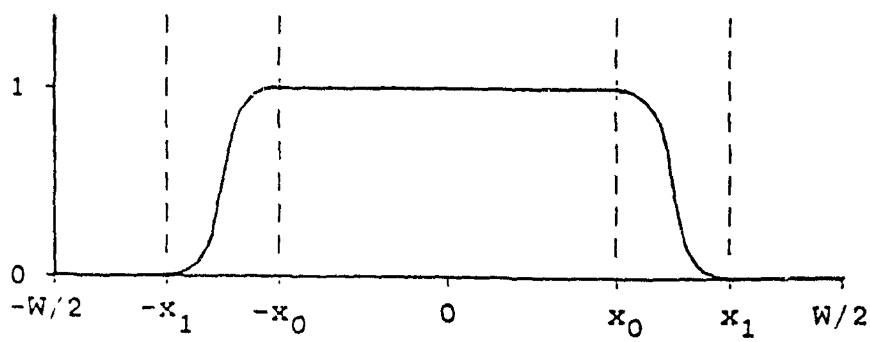

Fig IV-2 Absorber function (see equation IV-22) where $-w/2$ and $w/2$ define the edges of the computation window.

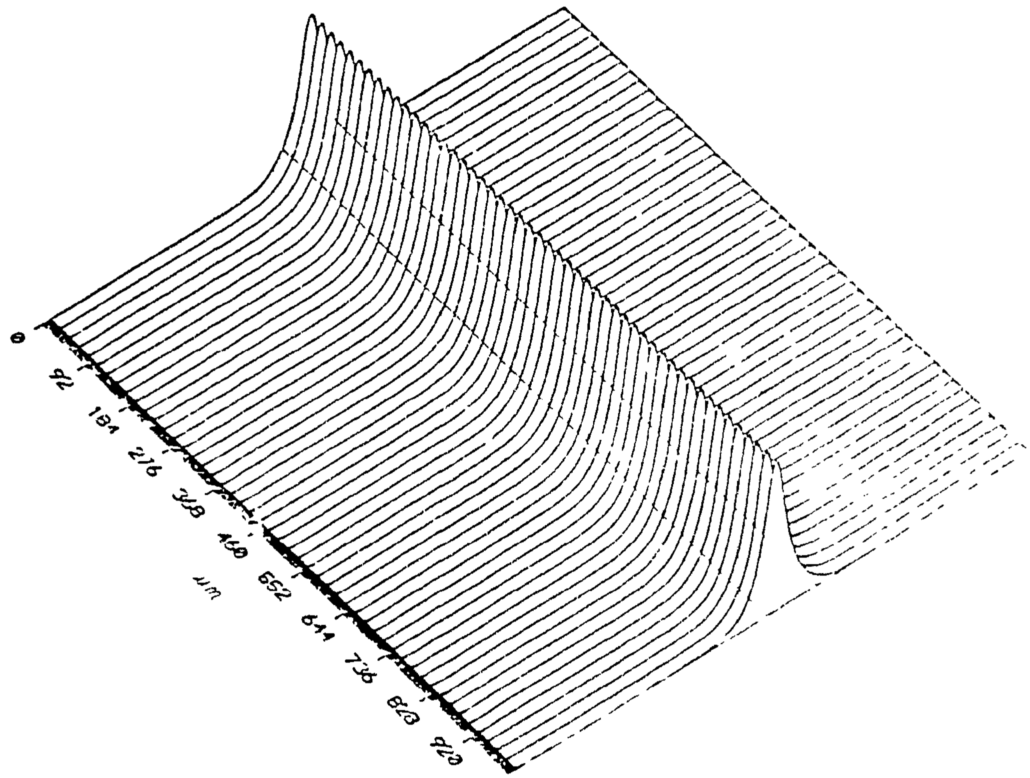

Fig. IV-3 Guided field (TM mode) propagating along a uniform single mode waveguide (Δz=*1mm*) where *1024* grid points and *100μm* window width are used.

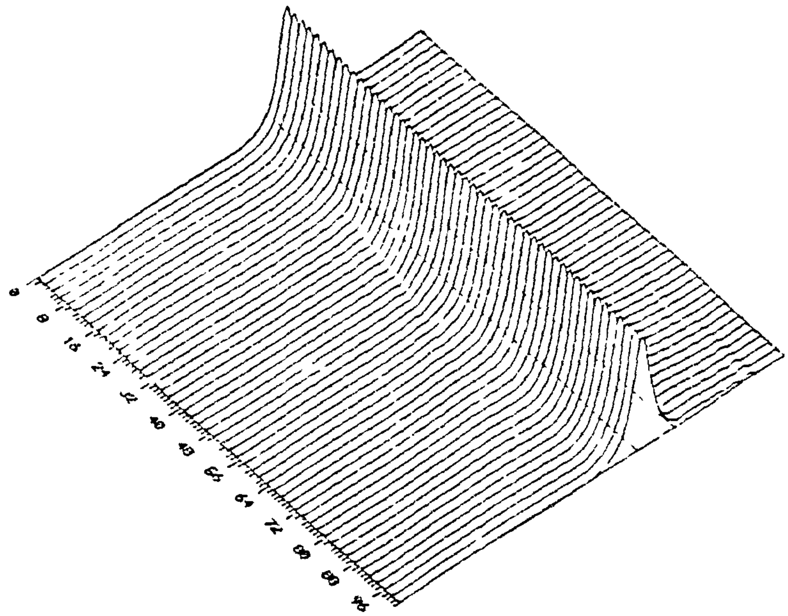

(a)

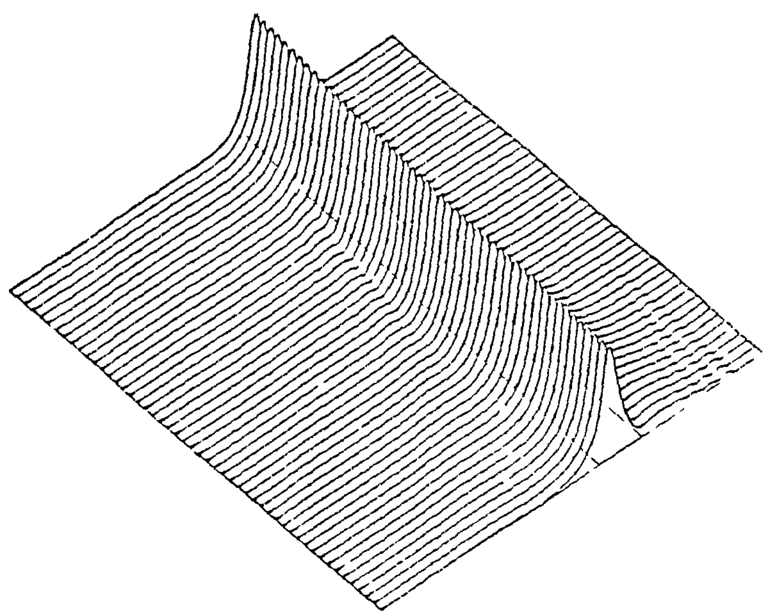

(b)

Fig. IV-4 Optical field (TM modes) scatttered by waveguide tilt ($\Delta z=1mm$) (a) $\alpha=0.5^\circ$; (b) $\alpha=1^\circ$. In both calculations, *1024* grid points and $100\mu m$ window width are used.

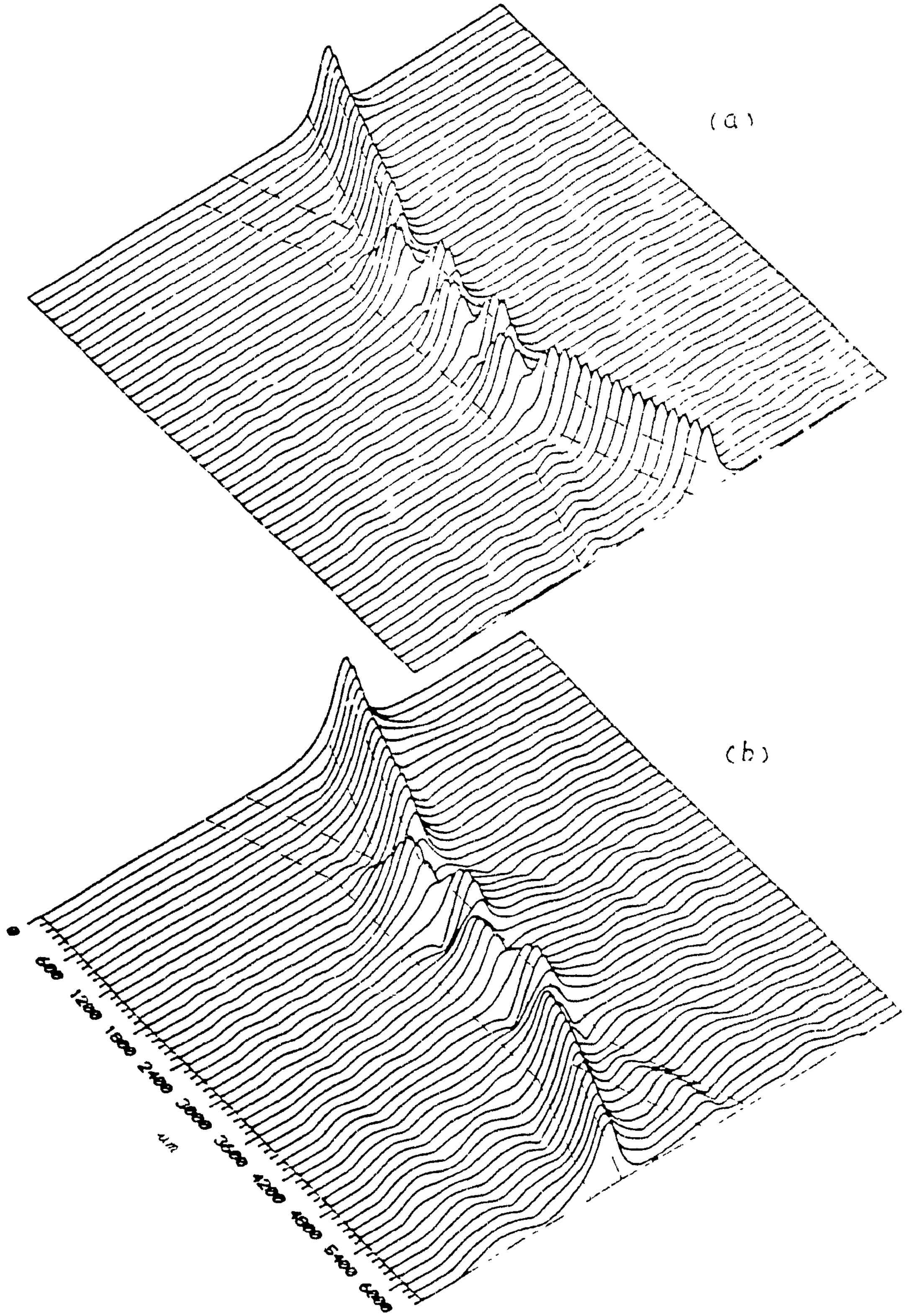

Fig. IV-5 Evolution of the optical field (TM modes) in a X-branch type WDM device, where the structure parameters are $\alpha=1^{\circ}$, $w=5.45\mu m$, $L=2272\mu m$. (a) $\lambda=1.31\mu m$, $D_e=19.66dB$, $L_r=11.85dB$, (b) $\lambda=1.55\mu m$, $D_e=14.95dB$, $L_r=8.24dB$. In both calculations, *2048* grid points and *200μm* window width are used.

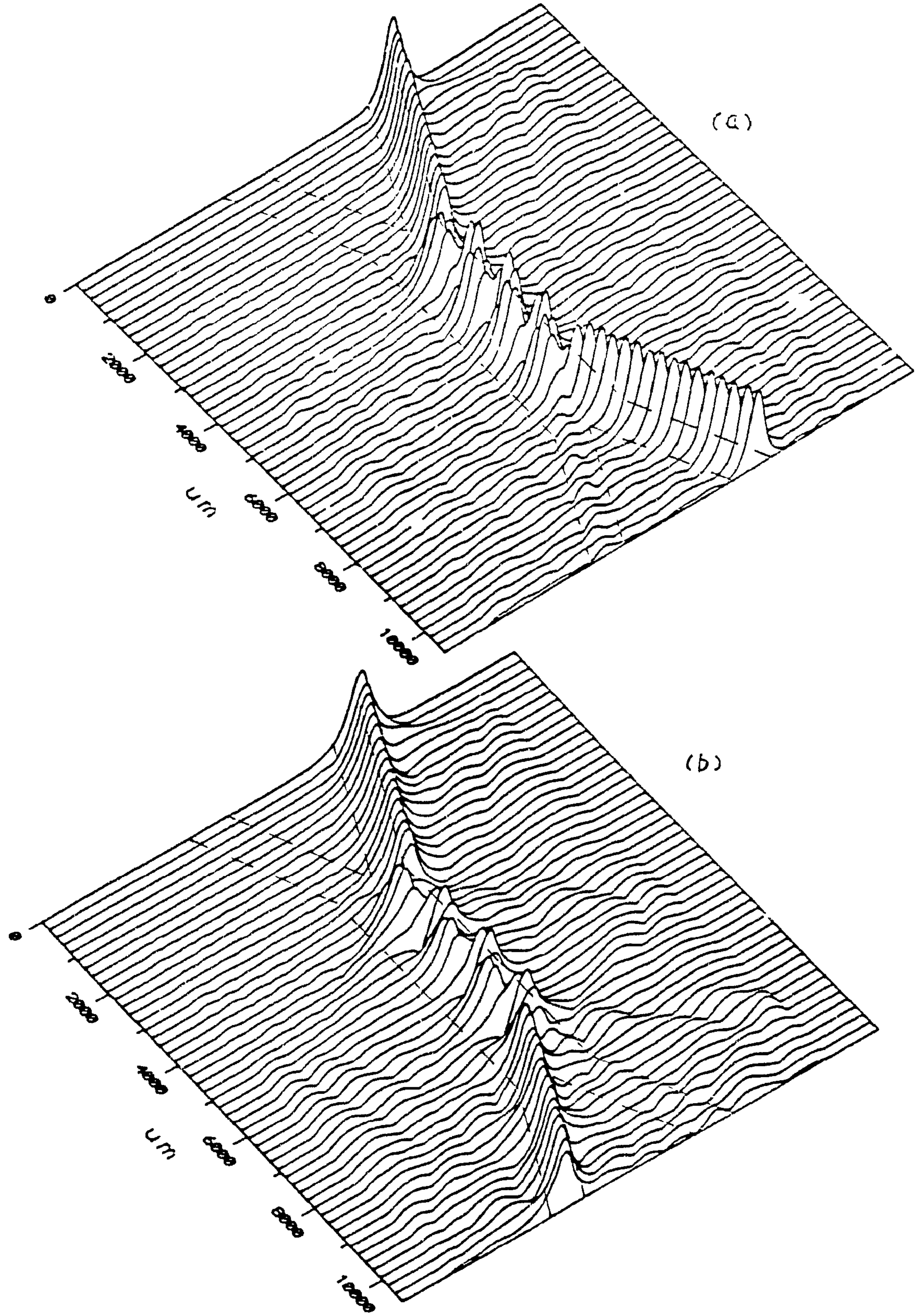

Fig. IV-6 Evolution of the optical field (TM modes) in a X-branch type WDM device, where the structure parameters are $\alpha=1^{\circ}$, $w=6\mu m$, $L=3527\mu m$. (a) $\lambda=1.31\mu m$, $D_e=18.40dB$, $L_r=10.85dB$, (b) $\lambda=1.55\mu m$, $D_e=16.70dB$, $L_r=9.91dB$. In both calculations, *2048* grid points and *200μm* window width are used.

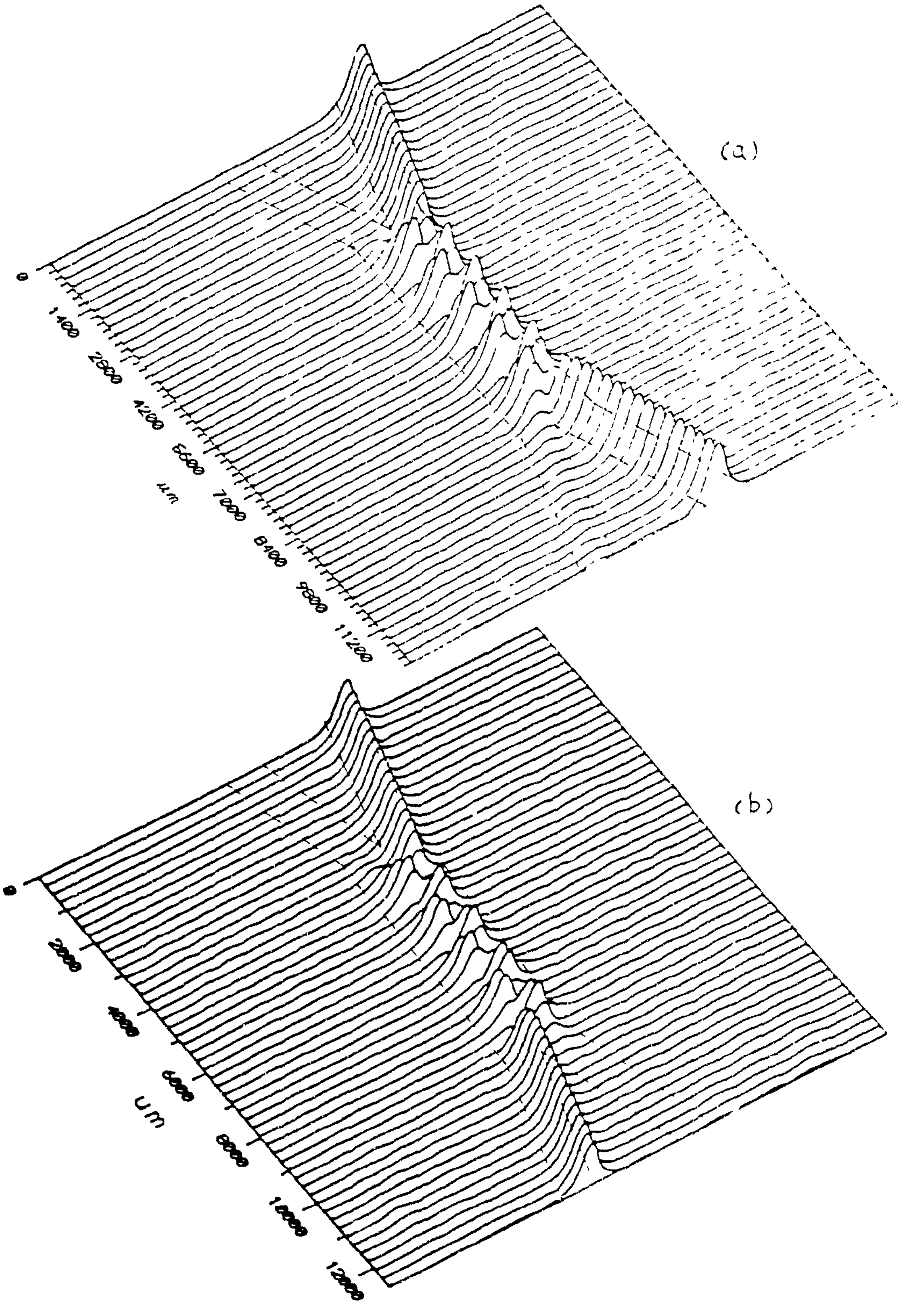

Fig. IV-7 Evolution of the optical field (TM modes) in a X-branch type WDM device, where the structure parameters are $\alpha=0.5^{\circ}$, $w=6.1\mu m$, $L=4188\mu m$. (a) $\lambda=1.31\mu m$, $D_e=29.52dB$, $L_r=14.13dB$; (b) $\lambda=1.55\mu m$, $D_e=33.38dB$, $L_r=12.32dB$. In both calculations, *2048* grid points and *200μm* window width are used.

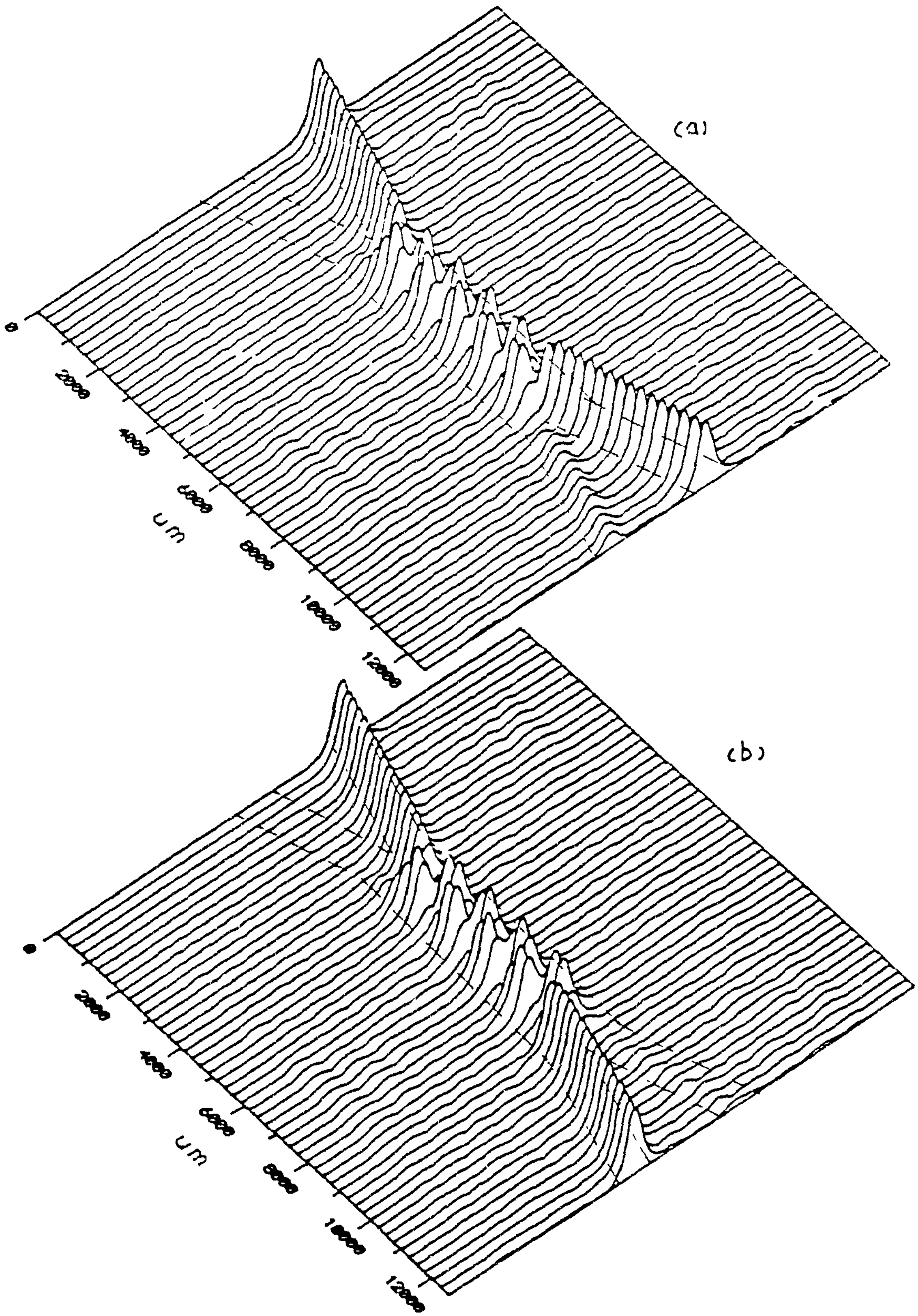

Fig IV-3 Evolution of the optical field (TM modes) in the structure as Fig. IV-7 with *0.2μm* width fabrication deviation. (a) $\lambda=1.31\mu m$, $D_e=12.06dB$, $L_r=12.78dB$; (b) $\lambda=1.55\mu m$, $D_e=23.66dB$, $L_r=12.10dB$ In both calculations, *2048* grid points and *200μm* window width are used.

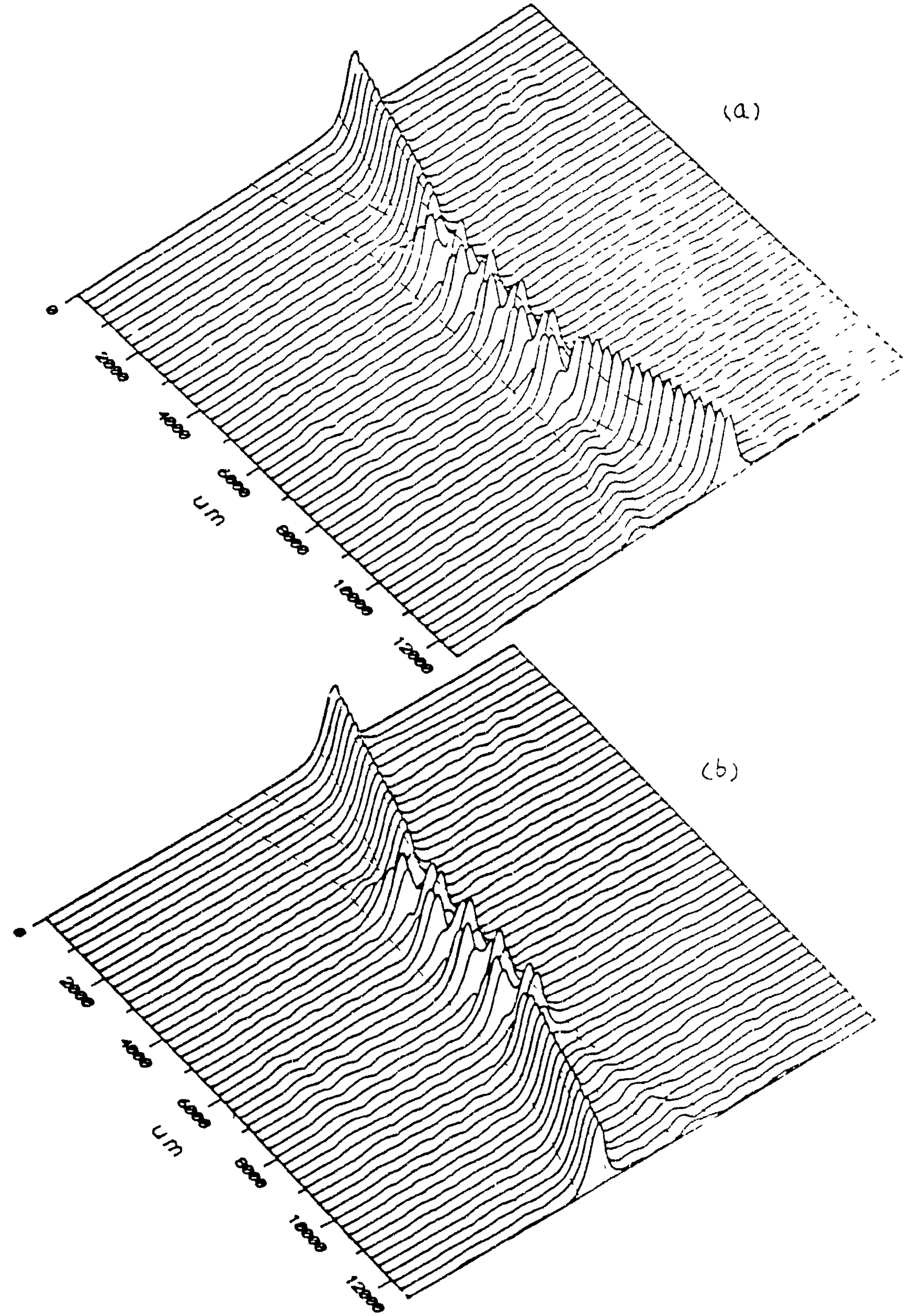

Fig. IV-9 Evolution of the optical field (TM modes) in the structure as Fig. IV-7 with *-2min* diffusion time fabrication deviation (a) $\lambda=1.31\mu m$, $D_e=24.47dB$, $L_r=13.94dB$; (b) $\lambda=1.55\mu m$, $D_e=21.72dB$, $L_r=11.70dB$. In both calculations, *2048* grid points and *200µm* window width are used.

CHAPTER V

CONCLUSIONS

Conclusively, the work presented in this thesis can be conveniently split up into two main aspects.

Chapter II can be possibly summarized as a fairly good discussion on some analytical techniques applicable to either slab or channel optical waveguides with the arbitrary index distributions. Since K^+-ion exchange technique provides very low index increment as $\Delta n_{sTE}=8.6\times10^{-3}$ and $\Delta n_{sTM}=10.0\times10^{-3}$ for TE and TM modes respectively, weakly guiding condition is widely satisfied by the integrated optics circuits on glass substrates This property allows us to design and analyze the waveguides and devices well by using the methods discussed in this thesis. Our analysis shows, by properly matching the field solutions at the dielectric discontinuities, the first-order WKB approximation not only can yield identical results with the ray optics approach, but also can be extended to studying the piecewise graded-index optical waveguide problems with accuracy. Furthermore, extending the transverse resonance method (TRM) to the inhomogeneous waveguide structures, we can analyze any slab optical waveguides with arbitrary index profiles exactly without considering the modal fields. Although channel optical waveguides possess more complicated geometrical structures, by introducing the lateral effective index profile, the effective index method can still be applied by combining with the WKB method and becomes a very favorable method as long as the modal fields are not necessary. Besides, it was also shown that, with the stationary and extreme properties, variational technique provides a very reliable and flexible approach to study arbitrary optical guiding structures even with a refractive index discontinuity on the surface.

The second part of this thesis deals with the practical design considerations for the X-branch type single mode wavelength division demultiplexer. This includes the device property analysis in Chapter III and function simulations by the BPM in Chapter IV As a zero-gap coupler, X-branch waveguide possesses maximum propagation constant difference between even and odd modes. Utilizing the wavelength dependence properties of the two-mode interference, the structure can perform as a compact dual channel wavelength demultiplexer Since the periodic like device transmission curve, a cascaded multichannel WDM-device can also be constructed.

Generally speaking, the X-branch waveguide properties mainly depend on the center two-mode section. To be a wavelength division demultiplexer, single X-branch waveguide gives a channel separation inversely proportional to the length of this region. Also, the narrower the waveguide width is in this region, the shorter the total device length becomes. Since the device length of the X-branch waveguide made by K^{+}-ion exchange technique is several thousand times of wavelength, the output crosstalk is quite sensitive to the waveguide width deviation and refractive index determination. Therefore, utilizing the double width configuration (for two-mode center region) can not only simplify the fabrication process, but also provide a better fabrication tolerance. Owing to glass being a low refractive index material, the beam propagation method analysis indicates that a smaller Y-branching angle (around 0.5°) is needed to reduce scattering loss and improve channel isolations. Besides, by adjusting the Y-branch angle, all the channel wavelengths can be shifted approximately in parallel.

Fabrication tolerance studies indicate that, for the single X-branch type demultiplexer, the output extinction ratio of the longer wavelength is more sensitive to the waveguide depth deviation By contrast, the counterpart of the shorter wavelength is more apparently influenced by the waveguide width error. Confirmed by the BPM simulation also, the numerical results show that, under the present state of art, it would still be challenging to make glass integrated optical devices which are based on the two-mode interference principle, especially for the two-wavelength device such as wavelength division demultiplexers. With the proposed cascaded structure by three X-branch waveguides, an adjustable single-mode demultiplexer with high stopband rejection becomes possible. Theoretical analysis shows that *30dB* extinction ratio for both wavelengths can be achieved by depositing claddings on the two-mode center waveguide regions.